AD-A053 211 NAVAL POSTGRADUATE SCHOOL MONTEREY CALIF F/G 20/4
ANALYSIS OF SUPERSONIC FLOW PAST OSCILLATING CASCADES USING LIN--ETC(U)
SEP 77 J A STRADA

UNCLASSIFIED NL

1 OF 2
AD A053211

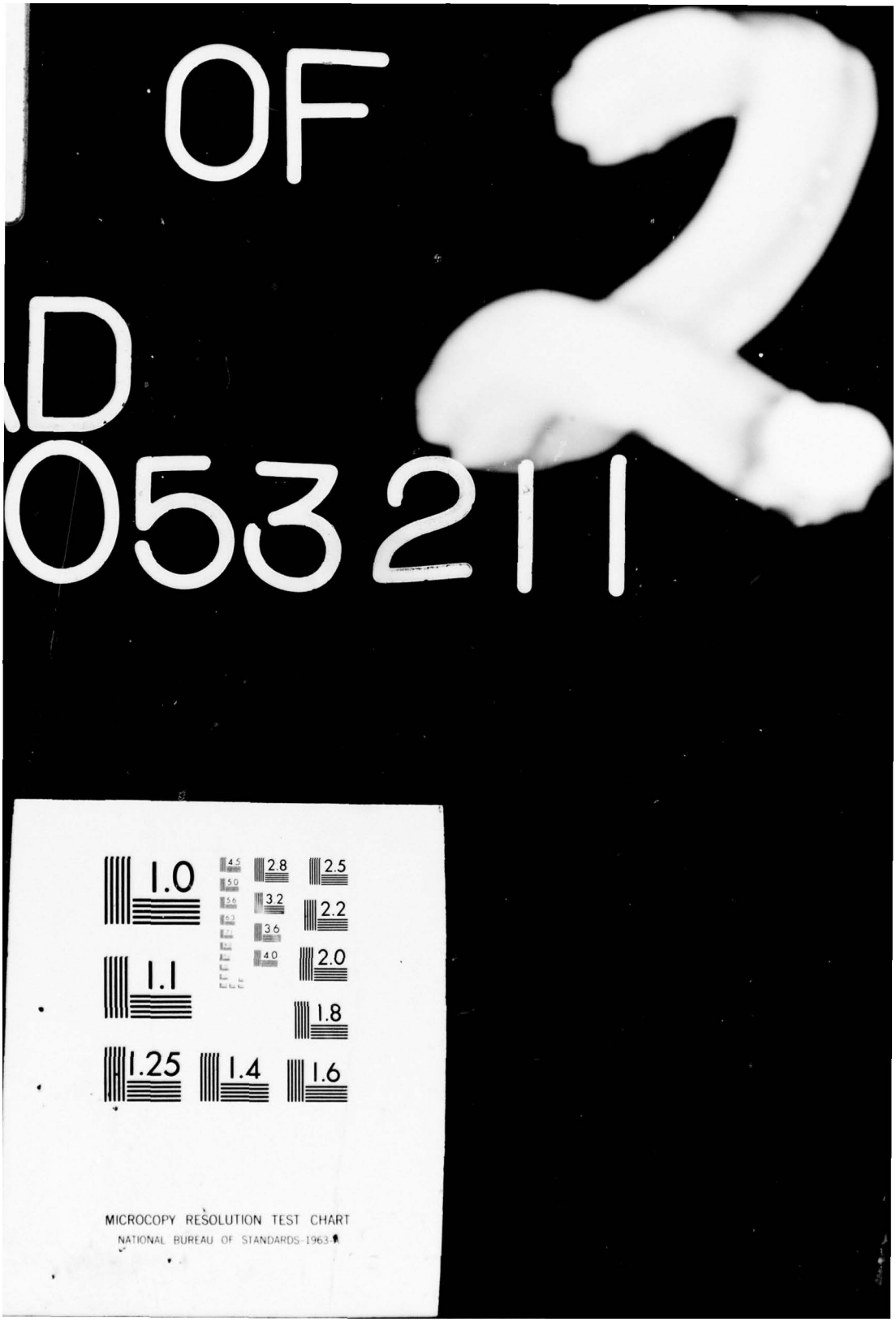
OF
AD
053211
1.0
1.1
1.25
1.4
1.6
1.8
2.0
2.2
2.5
2.8
3.2
3.6
4.0
5.0
5.6
MICROCOPY RESOLUTION TEST CHART
NATIONAL BUREAU OF STANDARDS-1963-A

NAVAL POSTGRADUATE SCHOOL
Monterey, California

THESIS

ANALYSIS OF SUPERSONIC FLOW PAST OSCILLATING CASCADES USING LINEAR AND NONLINEAR METHODS

by

Joseph Anthony Strada

September 1977

Thesis Advisor: M.F. Platzer

UNCLASSIFIED

SECURITY CLASSIFICATION OF THIS PAGE (When Data Entered)

REPORT DOCUMENTATION PAGE		READ INSTRUCTIONS BEFORE COMPLETING FORM
1. REPORT NUMBER	2. GOVT ACCESSION NO.	3. RECIPIENT'S CATALOG NUMBER
4. TITLE (and Subtitle) (6) ANALYSIS OF SUPERSONIC FLOW PAST OSCILLATING CASCADES USING LINEAR AND NONLINEAR METHODS.		5. TYPE OF REPORT & PERIOD COVERED Doctor of Philosophy Thesis; September 1977
		6. PERFORMING ORG. REPORT NUMBER
7. AUTHOR(s) (10) Joseph Anthony Strada		8. CONTRACT OR GRANT NUMBER(s)
9. PERFORMING ORGANIZATION NAME AND ADDRESS Naval Postgraduate School Monterey, California 93940		10. PROGRAM ELEMENT, PROJECT, TASK AREA & WORK UNIT NUMBERS
11. CONTROLLING OFFICE NAME AND ADDRESS (11) Naval Postgraduate School Monterey, California 93940		12. REPORT DATE Sept[redacted]77
		13. NUMBER OF PAGES 156 (12) 158 p.
14. MONITORING AGENCY NAME & ADDRESS(if different from Controlling Office)		15. SECURITY CLASS. (of this report) Unclassified
		15a. DECLASSIFICATION/DOWNGRADING SCHEDULE

16. DISTRIBUTION STATEMENT (of this Report)

Approved for public release; distribution unlimited.

17. DISTRIBUTION STATEMENT (of the abstract entered in Block 20, if different from Report)

(9) Doctoral thesis

18. SUPPLEMENTARY NOTES

19. KEY WORDS (Continue on reverse side if necessary and identify by block number)

Unsteady supersonic cascade theory; linear theory; thickness effects; resonance; turbomachine fan and compressor blades.

20. ABSTRACT (Continue on reverse side if necessary and identify by block number)

This study presents two methods of analysis for the supersonic oscillating cascade with subsonic leading edge. A relatively straightforward solution is developed for the slowly oscillating finite and infinite flat-plate cascades which provides simple analytical expressions for the unsteady pressure distributions. Comparison with other solutions is generally excellent. Some additional linear topics including

(20. ABSTRACT Continued)

resonance and a unique inflow condition are also treated. In addition a nonlinear method of characteristics solution for finite cascades is described which permits analysis of blade thickness effects on flutter. At this time, only the inlet and passage flow computations have been completed and are compared with available experimental data.

Approved for public release; distribution unlimited

Analysis of Supersonic Flow Past Oscillating Cascades Using Linear and Nonlinear Methods

by

Joseph Anthony Strada
Lieutenant Commander, United States Navy
B.S., Villanova University, 1967
M.S.A.E., Naval Postgraduate School, 1976

Submitted in partial fulfillment of the
requirements for the degree of

DOCTOR OF PHILOSOPHY

from the
NAVAL POSTGRADUATE SCHOOL
September 1977

Author: Joseph A Strada

Approved by:

M.F. Platzer
Professor of Aeronautics
Thesis Advisor

L.V. Schmidt
Professor of Aeronautics

D.J. Collins
Professor of Aeronautics

F.D. Faulkner
Distinguished Professor of Mathematics

A.E. Fuhs
Distinguished Professor of Mechanical Engineering

Approved by: Chairman, Department of Aeronautics

Approved by: Academic Dean

ABSTRACT

This study presents two methods of analysis for the supersonic oscillating cascade with subsonic leading edge. A relatively straightforward solution is developed for the slowly oscillating finite and infinite flat-plate cascades which provides simple analytical expressions for the unsteady pressure distributions. Comparison with other solutions is generally excellent. Some additional linear topics including resonance and a unique inflow condition are also treated. In addition a nonlinear method of characteristics solution for finite cascades is described which permits analysis of blade thickness effects on flutter. At this time, only the inlet and passage flow computations have been completed and are compared with available experimental data.

TABLE OF CONTENTS

LIST OF SYMBOLS

a_∞	flowfield speed of sound (2.2.8)
b	dimensionless pitch axis location (2.2.19)
c	blade chord (2.1.1)
C_p	pressure coefficient (2.2.15)
C_{po}	steady pressure coefficient (3.6.1)
C_{p1}	isolated (linear) blade pressure coefficient (2.3.9); unsteady pressure coefficient (3.9.1)
d	vertical blade spacing in percent chord (figure 2.2.2)
F	describing function for the surface of an arbitrary body (2.2.16)
F_h	describing function for a plunging flat plate (2.2.18)
F_α	describing function for a pitching flat plate (2.2.19)
F1R,F1I	unsteady, straight-mesh, perturbation potential (3.6.2)
F2R,F2I	unsteady, curved-mesh, perturbation potential (3.9.1)
g	Sauer function (2.3.2); complex shock displacement function (3.4.11)
h	Sauer function (2.3.2); flowfield enthalpy (3.4.5)
h_o	maximum plunging amplitude (2.2.18)
i	$(-1)^{1/2}$ (2.2.18)
k	dimensionless reduced frequency of oscillation (2.1.1)
M	freestream Mach number (2.2.12)
M_N	Mach number component normal to shock (3.4.26)

m	horizontal Mach line separation in percent chord (figure 2.2.2)
m_i, n_i, p_i	shock equation coefficients (3.4.29-36,38-41)
P	flowfield pressure (2.2.1)
S	flowfield entropy (2.2.2)
s	$x - \beta y$ (2.3.1)
$\bar{s}$	$x + \beta y$ (2.3.1)
σ	cascade solidity (2.2.30)
t	time (2.2.2); dimensionless after (2.2.23)
U	freestream velocity (2.1.1)
U11R,U11I V11R,V11I	unsteady, dimensionless, straight-mesh velocity perturbations (3.6.2)
U12R,U12I V12R,V12I	unsteady, dimensionless, curved-mesh velocity perturbations (3.8.1)
u_o, v_o	steady, dimensionless, velocity components (3.3.8,9)
u_1, v_1	unsteady, dimensionless, velocity components (3.3.10)
$\bar{V}$	flowfield velocity (2.2.4)
V_s	shock velocity relative to fluid (3.4.6)
V_n/V_t	velocity components normal/tangent to shock (3.4.17,18)
x,y	space variables; dimensionless after (2.2.24)
x_o, y_o	blade leading-edge coordinates (3.4.11)
XB,YB	blade spacing parameters (3.5.2,3)
α	Mach angle (2.7.5)
α_o	maximum pitching amplitude (2.2.19)
α, β	characteristic families (3.3.12)
β^2	$M^2 - 1$ (2.2.28)

γ	ratio of specific heats (3.4.4)
γ_0	local, steady shock angle (3.4.10)
γ'	small, unsteady perturbation from the steady shock angle (3.4.10)
η	dimensionless space variable (figure 2.5.1)
θ	cascade stagger angle (2.2.29)
θ_0	unique-inflow-condition stagger angle (2.7.6)
λ, μ	state variables (3.3.8,9)
μ	interblade phase angle (2.5.6)
ξ	dimensionless space variable (figure 2.5.1)
ρ	flowfield density (2.2.4)
σ	$\xi - \beta\eta$ (2.5.1)
$\bar{\sigma}$	$\xi + \beta\eta$ (2.5.1)
τ	midchord thickness ratio (3.2.1)
ϕ	perturbation potential (2.2.3); dimensionless after (2.2.24)
ϕ_0	steady perturbation potential (3.3.1)
ϕ_1	isolated-blade perturbation potential (2.3.2); unsteady perturbation potential (3.3.1)
ω	dimensional frequency of oscillation (2.1.1)

ACKNOWLEDGEMENT

This dissertation could not have been written without the assistance of many fine people to whom I am sincerely grateful: Professor M.F. Platzer for his guidance, encouragement and friendship; Dr. W.R. Chadwick whom I knew as a friend and instructor; Professors D.J. Collins and R.D. Zucker who introduced me to gas dynamics; many professors in the Departments of Aeronautics and Mathematics for sharing their time and knowledge; Drs. J.J. Adamczyk, M. Kurosaka, and J.J. Verdon all of whom provided unpublished results of their work for use in this thesis; Drs. S. Fleeter and R.E. Riffel for providing additional details of their experimental work; Commander Brad Hall USN (Retired) who made my Doctoral studies a reality; and most of all my wife for her constant support and encouragement.

1. INTRODUCTION

1.1 General. Unsteady flow in turbomachines can be broadly divided into two categories: circumferential asymmetry in the flow through the turbomachine and flow perturbation due to the self-excited oscillatory motion (flutter) of the internal blading [1]. As shown in figure 1.1.1, taken from [2], at least four types of flutter may occur in a compressor rotor. The two stalled-flutter phenomena are encountered when compressor or fan blading is subjected to incidence angles near or exceeding the stall angle, and so are off-design phenomena. Subsonic stalled flutter has long plagued the engine designer [3]. Choke flutter and supersonic unstalled flutter are low-incidence instabilities occurring when the flow over the blade is, respectively, transonic along most of the chord, or supersonic over the outer span portions [3]. Supersonic unstalled flutter (hereafter referred to simply as supersonic flutter), which has appeared only recently as a significant problem in turbomachinery, is the subject of this investigation. Primarily a concern in compressors and fans [1], it is an instability born of the recent technological advances aimed at increasing the thrust-to-weight ratios of turbomachines: increased tip speeds, composite blades, lighter discs and blades, and the elimination of part-span shrouds [2,3]. Some insight into the nature of supersonic flutter is gained by a consideration of its characteristics:

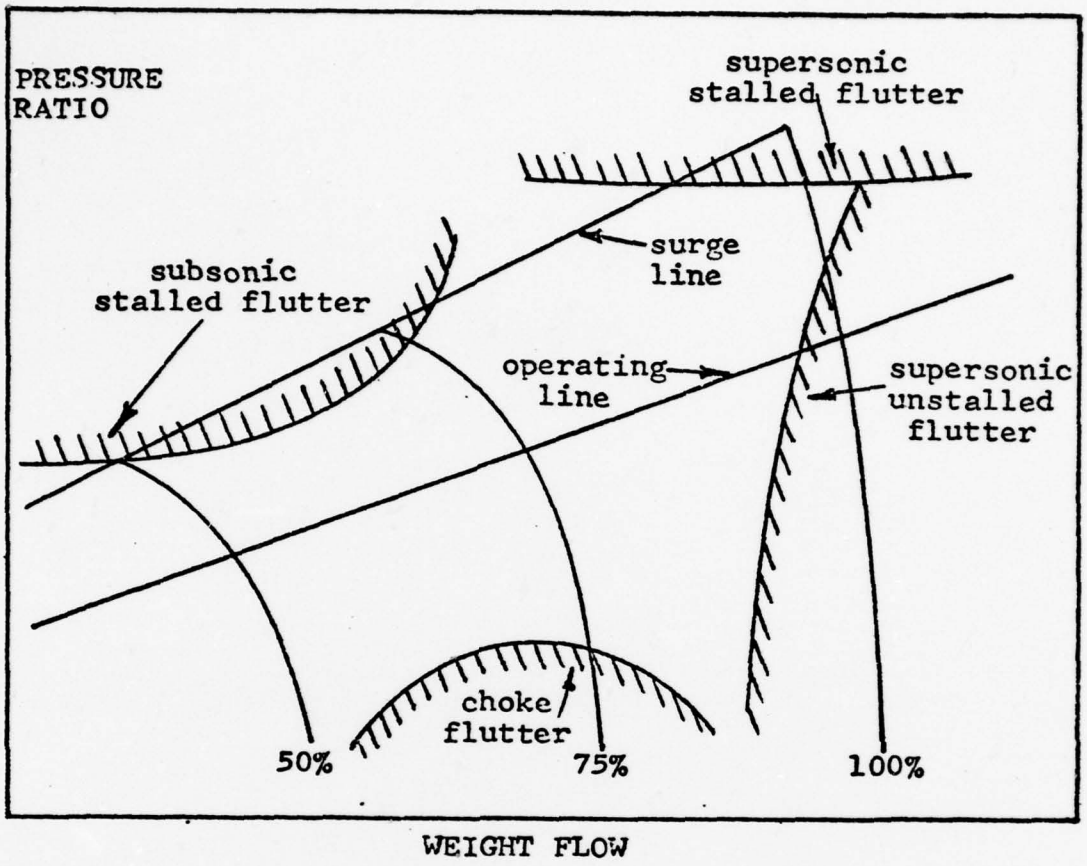

Figure 1.1.1 Compressor map showing boundaries for four types of flutter.

1. Its flutter boundary imposes a high-speed limit on compressor operation [2].

2. It is a low-incidence, attached-flow instability that can occur at the design condition (figure 1.1.1).

3. Flutter amplitude decreases with increasing back pressure on the rotor [2]. (For this reason the present analysis considers the most critical case of zero pressure rise across the rotor.)

4. At the flutter condition all the blades are observed to flutter at the same frequency with a constant interblade phase angle [2].

5. Both single-degree-of-freedom torsional flutter (pitch) and two-degree-of-freedom torsional-flexural flutter (pitch and plunge) can occur [3,4].[1]

6. The flutter boundaries are significantly affected by airfoil shape [4,5].

7. The primary flutter mechanism is an inviscid phenomenon. If the unsteady aerodynamic force lags the blade motion by a phase angle which is sufficient to ensure positive work over the entire cycle, then flutter can occur [3,4].

It is clear that reliable techniques for predicting the unsteady pressure distribution on a fluttering blade are required if one hopes to predict and avoid the onset of flutter. With this end in mind the cascade has been extensively employed as a theoretical abstraction of a compressor rotor. The unsteady flow is considered in an annulus of differential radial height within which equispaced airfoils are radially disposed. Unwrapping such an annulus gives rise to the two-dimensional approximation of plane flow through a cascade of airfoils [1]. The cascade is termed linear if the airfoils are flat plates of zero thickness. As seen in figure 1.1.2, a rotor does not require a supersonic axial flow to have a supersonic velocity component relative to, and parallel to, the blade axis. Indeed this

---

[1] R.A. Arnoldi *et al.* in "Supersonic Chordwise Bending Flutter in Cascades," Pratt & Whitney Report No. PWA-5271 of 31 May 1975 show that chordwise bending can also occur.

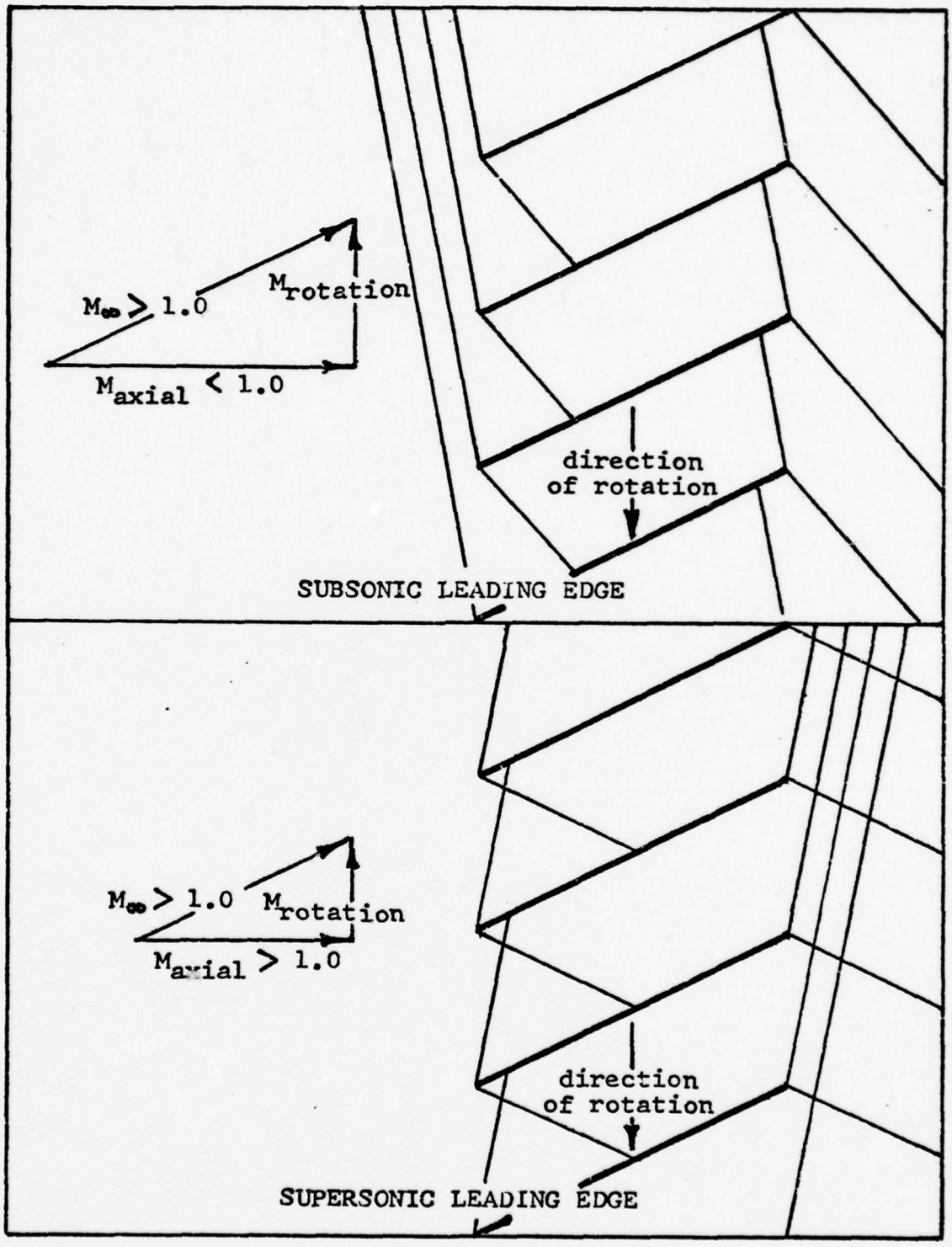

Figure 1.1.2 Supersonic cascade classification.

distinction provides a convenient method of classifying supersonic cascades. If the axial velocity is subsonic, the cascade is said to have a subsonic leading edge; in the other case it has a supersonic leading edge [6]. The physical significance of this distinction is clear from figure 1.1.2. In the supersonic-leading-edge cascade each blade influences only its immediate neighbors. When the cascade has a subsonic leading edge, however, disturbances generated by the upstream portions of each blade affect the flow around each subsequent blade in the cascade; furthermore the flowfield at the underside of each blade is influenced by the wake disturbances of all preceding blades. Since the supersonic-leading-edge cascade has been thoroughly investigated [7,8,9, 10], the more difficult subsonic-leading-edge case, which is also the more interesting in practice, is considered in the present study. Another cascade classification is frequently employed: if each blade is assumed to be preceded and followed by infinitely many others, the cascade is said to be infinite; if there is an identifiable first blade – a necessary prerequisite for many numerical solutions – the cascade is termed finite.

A considerable amount of effort has been expended in attempting to predict – numerically and analytically – the unsteady pressure distribution over a blade in an oscillating supersonic cascade with subsonic leading edge. A brief discussion of some of the more noteworthy advances follows.

1.2 The Linear Subsonic-Leading-Edge Cascade. Verdon and McCune [11] formulated a linear boundary value problem for the subsonic-leading-edge configuration, solving it for velocity potential. This permitted calculation of the pressure along the entire upper surface of an arbitrary blade and along the lower surface from the leading edge to the point of impingement of the trailing-edge Mach wave from the preceding blade. In a more recent paper Verdon [12] formulated a second boundary value problem, in which pressure is the basic dependent variable, which permitted determination of the pressure along the entire lower surface as well. Nagashima and Whitehead [13] and Goldstein [14] obtained solutions by replacing the cascade blades with doublet distributions. Kurosaka [6] introduced what he terms the passage approach in applying Laplace transform techniques to a slowly-oscillating cascade, obtaining closed-form analytical expressions for the pressure distributions of certain configurations. He recently [15] extended his solution to include arbitrary frequencies of oscillation. In assuming that a space periodicity of the flow exists from one blade passage to the next, Kurosaka claims that he avoids complications arising from the breakdown of linear acoustic theory in the far field [4]. Platzer and Brix [16] and Platzer and Bell [17] employed the method of characteristics to solve directly for the perturbation velocities and pressures everywhere in the flowfield. Their computer program has been thoroughly checked against existing

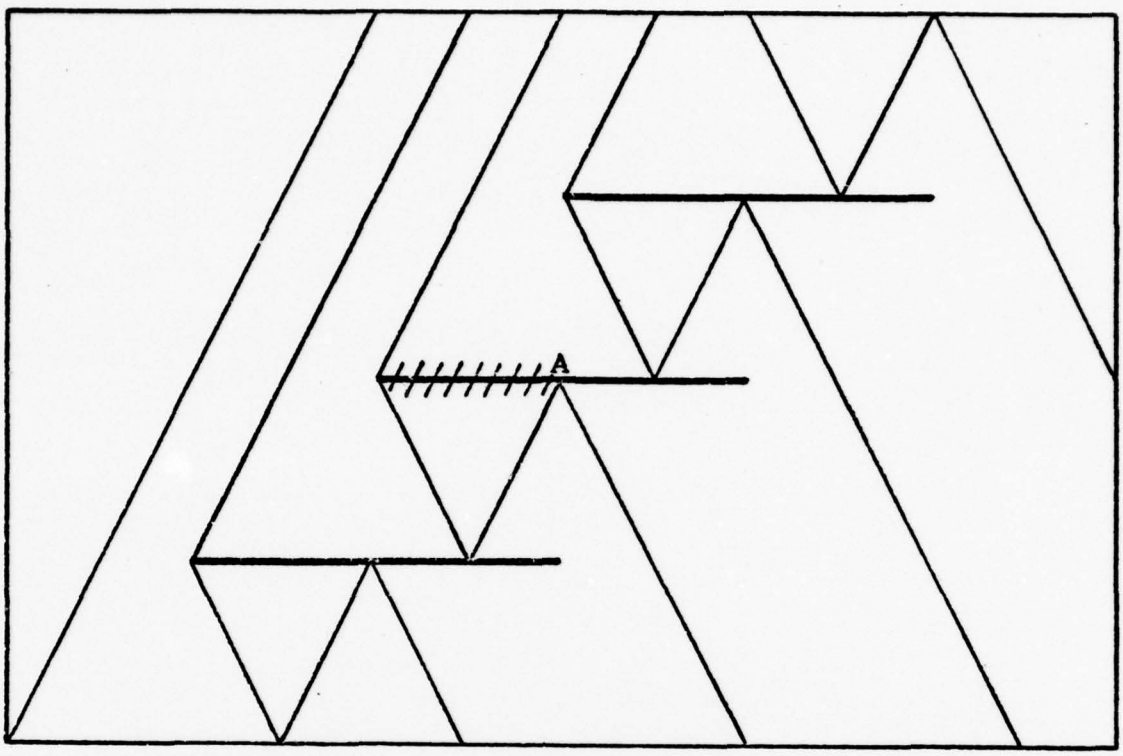

Figure 1.2.1 Limits of applicability of Chadwick's solution.

solutions [11,12,13] and is extensively employed in the present study as a method of comparison for both the analytical and numerical solutions presented. Chadwick [5] used Sauer's solution [18] of the unsteady potential equation, accurate to a first order in frequency of oscillation, to determine the pressure distribution on a given blade from the leading edge to the point of the first reflection (point A in figure 1.2.1) of disturbances from the preceding blade. He obtained exact analytical agreement with Kurosaka [6] over that portion of the blade for the single-degree-of-freedom pitching cascade. Chadwick's technique has the decided advantage of being much simpler than that of Kurosaka, easily

yielding closed-form expressions for any cascade, and raising the question as to whether the method could be extended to the entire blade for the cases of both pitch and plunge. Finally, Adamczyk [19], in a yet-unpublished work, employs the Wiener-Hopf method to obtain the pressure distribution for the linear cascade with subsonic leading edge.

1.3 The Nonlinear Subsonic-Leading-Edge Cascade. Attempts to deal analytically or numerically with an oscillating cascade of blades having thickness are not nearly so numerous as their linear counterparts. Carrier [20] provided an exact theory for a single oscillating wedge. VanDyke [21,22] also treated the isolated wedge as well as an oscillating airfoil of arbitrary profile. Teipel [23,24] employed an ingenious method-of-characteristics approach to numerically obtain the unsteady pressures on a single oscillating profile of arbitrary shape, obtaining good agreement with the single-blade solutions of Carrier and VanDyke. Teipel's method assumes potential flow with negligible entropy changes across leading-edge and trailing-edge shocks. Kurosaka and Edelfelt [4] have obtained numerical results for an isolated, oscillating, parabolic-arc airfoil and are presently working to extend their solution to a cascade of such airfoils. Chadwick [5] employed Teipel's method to obtain the unsteady pressure distribution over the preinterference zone of an arbitrary blade in a cascade of wedges. His results indicate

that nonlinear thickness effects significantly alter the unsteady pressure profile of an arbitrary blade.

1.4 The Present Investigation. The present work has two major parts: The first is analytical and treats the linear cascade while the second is numerical, dealing with a nonlinear configuration.

In the linear effort a closed-form analytical solution for the pressure-difference distribution along a blade in a slowly-oscillating cascade is obtained. The solution technique is that developed by Chadwick [5] in the pre-interference zone (figure 1.2.1) of a pitching cascade, in which Sauer's solution of the unsteady linearized potential equation is employed. In the present work Chadwick's solution is extended through all reflection zones and into the blade's wake. In addition, the solution is obtained for two degrees of freedom (pitch and plunge). Two standard configurations — Verdon's cascades A and B [12] — are considered, one from a finite-cascade approach and the other as an infinite cascade in which Kurosaka's passage approach is employed. Extensive comparisons are made with existing solutions [6,12,19,17]; and several special topics, including cascade resonance and a unique inflow condition, are briefly treated.

The nonlinear effort is an evaluation of the feasibility of extending Teipel's unsteady method of characteristics to a cascade of airfoils with arbitrary profiles. Teipel

[23,24] represents the nonlinear flowfield by a harmonic, unsteady, velocity potential superimposed on a steady one, and discontinuities in the flowfield variables across the shockwaves emanating from the airfoil are determined from the isentropic Rankine-Hugoniot relations. These concepts, coupled with the characteristic grid and compatibility relations derived by Teipel, permit determination of the steady and unsteady preinterference pressures acting on the second blade of a cascade of parabolic-arc airfoils. The numerical results are compared with experimental data from tests conducted with a pitching cascade by Fleeter and Riffel [25] and with linear theory. An improved method for determining the jump conditions across the bow shock is presented and the computational procedure is carefully outlined to facilitate extension of the technique to the entire flowfield of a completely general cascade.

1.5 Some Comments on Notation. In the linear portion of this investigation it is the unsteady, dimensionless, pressure-difference distribution along a particular cascade blade that is sought. This pressure difference is a complex quantity given the symbol ΔC_p and represents an amplitude function of distance along the blade. The harmonic oscillation factor e^{ikt} is always implicitly understood. In addition it is desirable to obtain an expression for ΔC_p at the instant that the blade in question achieves

maximum up displacement, referred to as the initial position. This expression is obtained by multiplying through by the factor $e^{-i\mu}$ and so it is indicated by the sumbol $\Delta C_p e^{-i\mu}$.

In the nonlinear portion of this study only the local pressures – C_p upper and lower – are sought. They are also complex quantities and it is convenient to express them as a magnitude and phase angle relative to the motion of the blade under study; the symbols $|C_p|$ and $\angle C_p$, respectively, are employed.

2. THE LINEAR LOW-FREQUENCY CASCADE

2.1 General. A cascade of flat plates with chord c oscillating harmonically with frequency ω in a steady, uniform flow U is said to oscillate at a dimensionless reduced frequency of oscillation k defined by

$$k = \frac{\omega c}{U} \qquad (2.1.1)$$

If k^2 is small when compared with k, then the cascade is termed a low-frequency or slowly-oscillating cascade. Although low-frequency flutter is not common, it is worthy of investigation for several reasons, the major one being that it is the only case for which one can hope to attain a relatively simple, closed-form expression for the unsteady pressures on a given blade. Such expressions provide insight into the flutter phenomenon, as evidenced by the identification of a unique inflow condition in a subsequent chapter of this study. Also, the low-frequency cascade provides an important limiting case for any general-frequency solution, numerical or analytical.

2.2 Problem Formulation.

2.2.1 The Linearized Potential Equation. The flow variables in the cascade flowfield are assumed to be composed of a freestream component and a much smaller

perturbation component

$$P = P_\infty + P' \tag{2.2.1}$$

The cascade is assumed immersed in a perfect gas, each particle of which maintains constant entropy as it moves through the flowfield

$$\frac{DS}{Dt} = 0 \tag{2.2.2}$$

In addition the flow is assumed inviscid and irrotational, guaranteeing the existence of a velocity potential

$$\bar{V} = \nabla\phi \tag{2.2.3}$$

The continuity and momentum equations for the flow are, respectively

$$\frac{D\rho}{Dt} + \rho\,\nabla\cdot\bar{V} = 0 \tag{2.2.4}$$

$$\frac{D\bar{V}}{Dt} + \frac{\nabla P}{\rho} = \bar{0} \tag{2.2.5}$$

Introducing the velocity potential and integrating (2.2.5) produces, after linearization

$$\frac{\partial\phi}{\partial t} + U\frac{\partial\phi}{\partial x} + \frac{P - P_\infty}{\rho_\infty} = 0 \tag{2.2.6}$$

Using the equation for the freestream speed of sound

$$a_\infty^2 = \gamma\frac{P_\infty}{\rho_\infty} \tag{2.2.7}$$

the continuity equation can be linearized to give

$$\frac{\partial^2\phi}{\partial x^2} + \frac{\partial^2\phi}{\partial y^2} + \frac{1}{\rho_\infty a_\infty^2}\left[\frac{\partial P}{\partial t} + U\frac{\partial P}{\partial x}\right] = 0 \tag{2.2.8}$$

From (2.2.6) one obtains

$$\frac{\partial P}{\partial t} = -\rho_\infty \left[\frac{\partial^2 \phi}{\partial t^2} + U \frac{\partial^2 \phi}{\partial x \partial t}\right] \quad (2.2.9)$$

and

$$\frac{\partial P}{\partial x} = -\rho_\infty \left[\frac{\partial^2 \phi}{\partial x \partial t} + U \frac{\partial^2 \phi}{\partial x^2}\right] \quad (2.2.10)$$

Substitution of (2.2.9) and (2.2.10) into (2.2.8) then produces the linearized unsteady potential equation in two dimensions

$$\frac{1}{a_\infty^2}\frac{\partial^2 \phi}{\partial t^2} + 2\frac{M}{a_\infty}\frac{\partial^2 \phi}{\partial x \partial t} = (1-M^2)\frac{\partial^2 \phi}{\partial x^2} + \frac{\partial^2 \phi}{\partial y^2} \quad (2.2.11)$$

where M is the freestream Mach number

$$M = \frac{U}{a_\infty} \quad (2.2.12)$$

2.2.2 The Linearized Pressure Coefficient. A generalized form of Bernoulli's equation follows directly from the momentum equation (2.2.5)

$$\frac{\partial \phi}{\partial t} + \frac{|\bar{V}|^2}{2} + \int_{P_\infty}^{P} \frac{dP}{\rho} = \text{CONST.} \qquad (2.2.13)$$

Introducing the perturbation quantities in the form of (2.2.1) and ignoring the products of perturbation quantities one obtains

$$\frac{\partial \phi}{\partial t} + U\frac{\partial \phi}{\partial x} + \frac{P-P_\infty}{\rho_\infty} = 0 \qquad (2.2.14)$$

where the prime notation has again been dropped. Thus, the dimensionless pressure coefficient is given by

$$C_p = \frac{P-P_\infty}{\frac{1}{2}\rho_\infty U^2} = -\frac{2}{U^2}\left(\frac{\partial \phi}{\partial t} + U\frac{\partial \phi}{\partial x}\right) \qquad (2.2.15)$$

2.2.3 The Linearized Boundary Conditions. The surface of a body placed in the flow can be described as a function of space and time

$$F(\bar{r}, t) = 0 \qquad (2.2.16)$$

where $\bar{r}$ is the position vector of points on the surface. The condition that the flow at the body surface be everywhere tangent to the surface can be expressed by

$$\frac{DF}{Dt} = 0 \qquad (2.2.17)$$

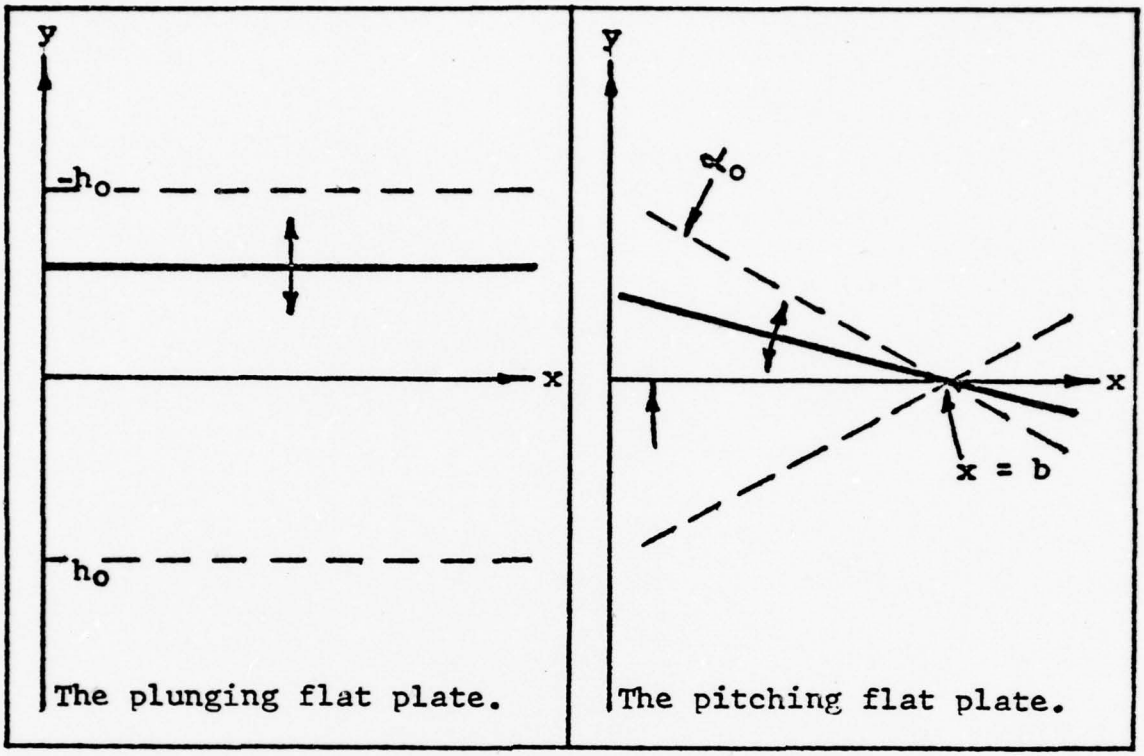

Figure 2.2.1 Two-degree-of-freedom oscillation.

at the surface. If the body is a flat plate oscillating harmonically in plunge and/or pitch, as shown in figure 2.2.1, then the describing functions are respectively

$$F_h(x,y,t) = y + h_o e^{i\omega t} = 0 \qquad (2.2.18)$$

$$F_\alpha(x,y,t) = y + \alpha_o(x-b) e^{i\omega t} = 0 \qquad (2.2.19)$$

where h_o and α_o are the maximum displacements and b is the pitch axis location on the x axis. Applying the generalized flow tangency condition (2.2.17) to (2.2.18) and (2.2.19) yields the boundary conditions for plunge and

pitch respecitvely

$$\frac{\partial \phi}{\partial y} = -h_o i\omega e^{i\omega t} \quad \text{at } y=0 \qquad (2.2.20)$$

$$\frac{\partial \phi}{\partial y} = -\alpha_o\left[U + i\omega(x-b)\right]e^{i\omega t} \quad \text{at } y=0 \qquad (2.2.21)$$

2.2.4 Nondimensionalization. It is convenient to introduce nondimensional variables into the governing equations to simplify and generalize them. The distance variables (x,y,b) are normalized by chordlength c , velocity potential by the product Uc and time by the quantity c/U . It is also convenient to set

$$h_o = c \qquad \alpha_o = 1 \text{ RADIAN} \qquad (2.2.22)$$

and to separate the velocity potential into a complex amplitude and phase angle

$$\phi(x,y,t) = \phi(x,y)e^{ikt} \qquad (2.2.23)$$

Thus the potential equation (2.2.11), pressure coefficient (2.2.15) and boundary conditions (2.2.20,21) become

$$\beta^2\frac{\partial^2\phi}{\partial x^2} - \frac{\partial^2\phi}{\partial y^2} - k^2M^2\phi + 2ikM^2\frac{\partial\phi}{\partial x} = 0 \qquad (2.2.24)$$

$$C_p = -2\left(\frac{\partial\phi}{\partial x} - ik\phi\right) \qquad (2.2.25)$$

$$\frac{\partial \phi}{\partial y} = -ik \quad \text{at} \quad y=0 \qquad (2.2.26)$$

$$\frac{\partial \phi}{\partial y} = -[1 + ik(x-b)] \quad \text{at} \quad y=0 \qquad (2.2.27)$$

where,

$$\beta^2 = M^2 - 1 \qquad (2.2.28)$$

and C_p and ϕ are complex amplitude functions of x and y only with the factor e^{ikt} omitted.

2.2.5 Cascade Geometry. The physical parameters chosen to describe the cascade are the vertical distance between the blades d and the horizontal distance between the leading-edge Mach waves m. Both parameters are normalized by chordlength. The cascade can also be described by solidity σ and stagger angle Θ, which are shown in figure 2.2.2. These parameters are related as follows

$$\text{TAN}\,\Theta = \frac{d}{m + \beta d} \qquad (2.2.29)$$

$$\sigma = \frac{\sin\Theta}{d} \qquad (2.2.30)$$

where β is given by (2.2.28). The linear cascades employed in this study are Verdon's cascades A and B [12], which have become standards in the field and are depicted in figure 2.2.2.

2.3 The Isolated Airfoil. Consider a single flat plate oscillating with two degrees of freedom as shown in figure 2.2.1, and define

$$s = x - \beta y \qquad \bar{s} = x + \beta y \tag{2.3.1}$$

Then s is constant along any left-running (upper surface) Mach wave, while $\bar{s}$ is constant along right-running (lower surface) waves. Sauer [18] showed that the potential equation (2.2.24) has the following left-running and right-running solutions, respectively, for a slowly-oscillating airfoil

$$\phi_1^u(x,y) = g_u(s) + k\left[h_u(s) - \frac{iM^2}{\beta} y\, g_u(s)\right] \tag{2.3.2}$$

$$\phi_1^L(x,y) = g_L(\bar{s}) + k\left[h_L(\bar{s}) + \frac{iM^2}{\beta} y\, g_L(\bar{s})\right] \tag{2.3.3}$$

where the g and h functions are determined from the boundary conditions (2.2.26,27). Requiring that the velocity potential be continuous across the leading-edge Mach waves, one has

$$g_u(0) = h_u(0) = g_L(0) = h_L(0) = 0 \tag{2.3.4}$$

Enforcing flow tangency at the upper surface of the airfoil yields, for plunge and pitch respectively

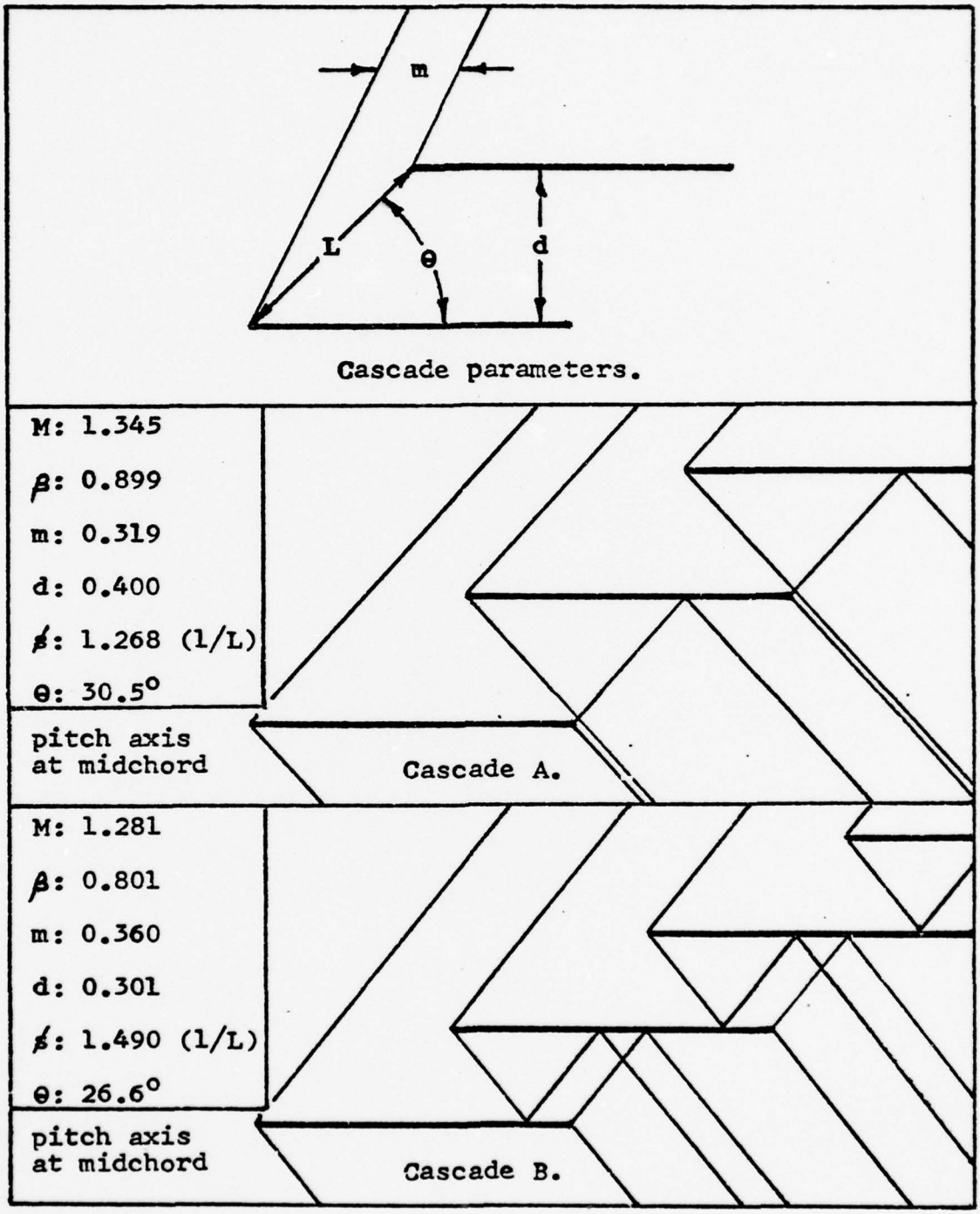

Figure 2.2.2 Cascade geometry.

PL: $g_u(s) = 0 \qquad h_u(s) = \frac{i}{\beta} s$ (2.3.5)

PI: $g_u(s) = \frac{s}{\beta} \qquad h_u(s) = -\frac{i}{\beta^3}\left(\frac{s^2}{2} + b\beta^2 s\right)$ (2.3.6)

And so on the upper surface

PL: $\phi_1^u(x,y) = \frac{ik}{\beta} s$ (2.3.7)

PI: $\phi_1^u(x,y) = \frac{s}{\beta} - \frac{ik}{\beta^3}\left[\frac{s^2}{2} + s(b\beta^2 + \beta M^2 y)\right]$ (2.3.8)

Thus the upper-surface pressure coefficient follows from (2.2.25)

PL: $C_{p_1}^u = -\frac{2ik}{\beta}$ (2.3.9)

PI: $C_{p_1}^u = -\frac{2}{\beta} + \frac{2ik}{\beta^3}\left[s(1-\beta^2) + b\beta^2\right]$ (2.3.10)

where the subscript indicates the single airfoil. Similarly, for the lower surface

$$C_{p_1}^l = -C_{p_1}^u \qquad (2.3.11)$$

2.4 Continuity of the Velocity Potential Across a Mach Wave. Consider two reflection zones separated by the Mach wave $s = s_o$, as shown in figure 2.4.1, and let the variables z and $\bar{z}$ respectively measure distance tangent and normal to the Mach wave. The velocity potential in zone II is simply

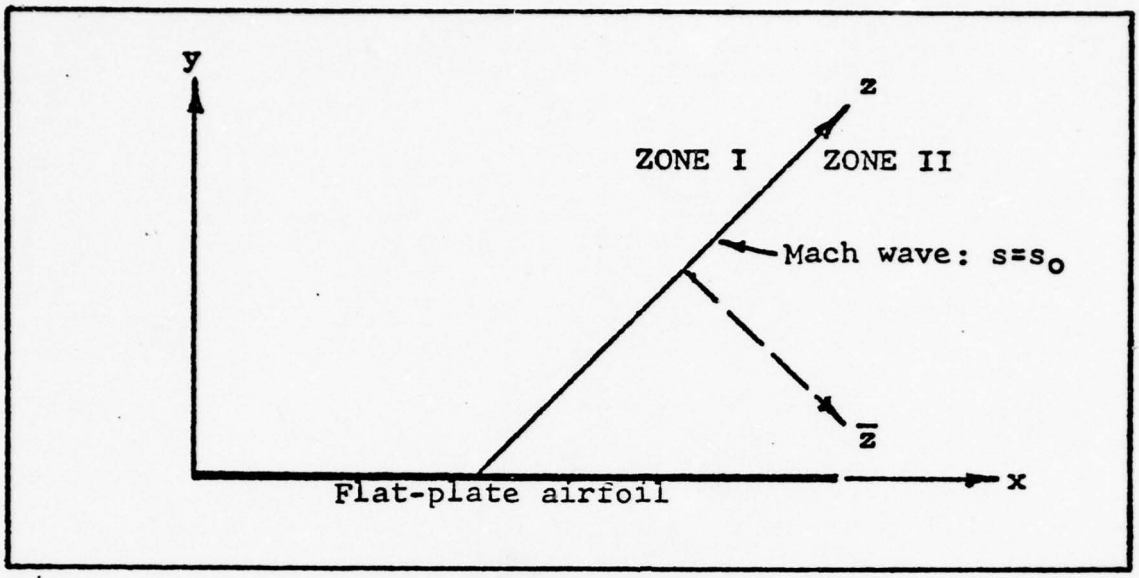

Figure 2.4.1 Variation of the velocity potential along the boundaries of reflection zones.

that in zone I plus an additional disturbance

$$\phi^{II} = \phi^{I} + \phi_d \qquad (2.4.1)$$

Since the tangential velocity component remains unchanged across the wave, (2.4.1) implies that ϕ_d is a function of $\bar{z}$ alone, along the Mach wave

$$\phi_d = \phi_d(\bar{z}) \quad \text{for} \quad s = s_o \qquad (2.4.2)$$

But since $\bar{z}$ is itself constant along the Mach wave, then ϕ_d must have the form

$$\phi_d = \text{CONST.} \quad \text{for} \quad s = s_o \qquad (2.4.3)$$

That the constant is zero follows from the physical constraint that the velocities remain finite in the wave itself, and so

$$\phi^{I}(\xi_0) = \phi^{II}(\xi_0) \qquad (2.4.4)$$

which is in agreement with the conclusion reached by Landahl [26].

2.5 The Finite Two-Degree-of-Freedom Cascade. As an elementary means of introducing the method of analysis, the pressure-difference distribution is found for the second blade of a finite version of cascade A. This analysis also affords the opportunity to compare the finite-cascade results obtained with numerical finite-cascade data [17] and analytical results [6] of existing solutions. It is emphasized that the pitch results through equation (2.5.27) were first obtained by Chadwick [5]. The reflection zones referred to are pictured in figure 2.5.1, and the pressure results are given in terms of the isolated-blade pressure coefficients (2.3.9,10). Before proceeding with the analysis, some additional variables are introduced for blade two

$$\sigma = \xi - \beta\eta \qquad \bar{\sigma} = \xi + \beta\eta \qquad (2.5.1)$$

which are related to those of blade one by the translation relations

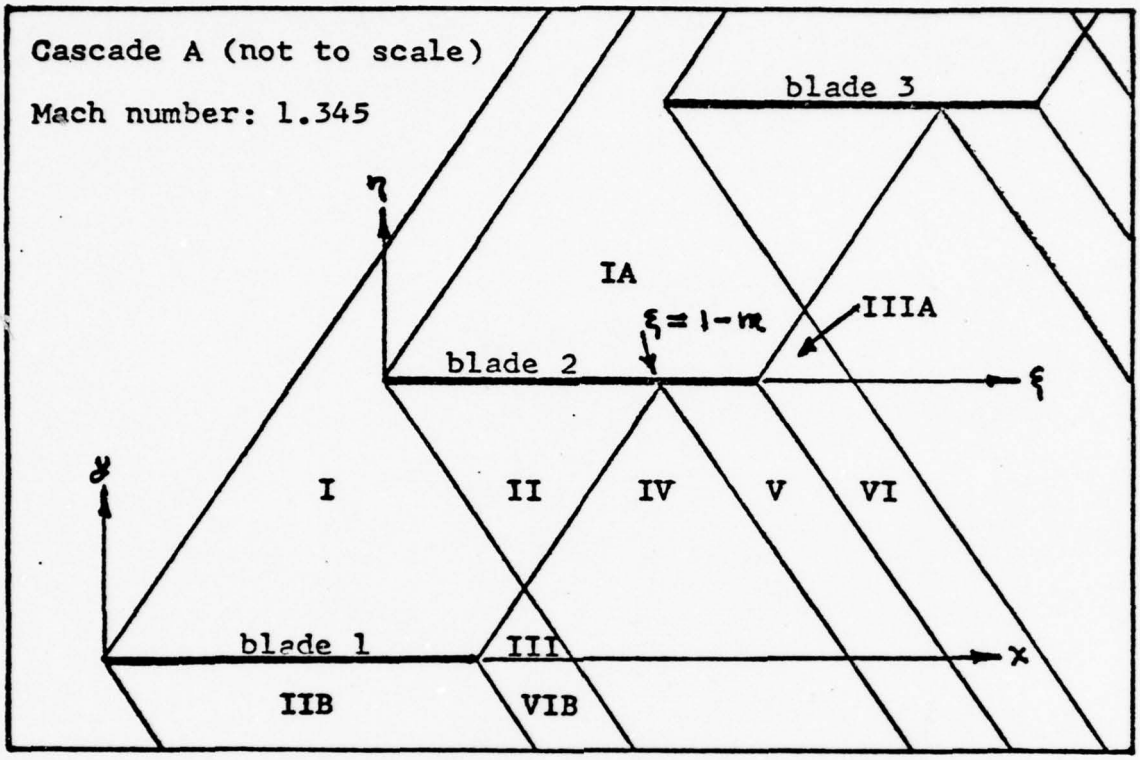

Figure 2.5.1 The finite-cascade reflection zones.

$$x = \xi + m + \beta d \qquad y = \eta + d \qquad (2.5.2)$$

$$s = \sigma + m \qquad \bar{s} = \bar{\sigma} + m + 2\beta d \qquad (2.5.3)$$

2.5.1 Zones I and IA. In zones I and IA Sauer's single-blade solution applies

$$\phi_1^{I}(x,y) = g_1(s) + k\left[h_1(s) - \frac{iM^2}{\beta} y\, g_1(s)\right] \qquad (2.5.4)$$

$$\phi_2^{IA}(\xi,\eta) = g_{1A}(\sigma) + k\left[h_{1A}(\sigma) - \frac{iM^2}{\beta} \eta\, g_{1A}(\sigma)\right] \qquad (2.5.5)$$

and in zone IA the boundary conditions take the form

PL: $$\frac{\partial \phi_2^{IA}}{\partial \eta} = -ik e^{i\mu} \quad \text{at } \eta = 0 \qquad (2.5.6)$$

PI: $$\frac{\partial \phi_2^{IA}}{\partial \eta} = -\left[1 + ik(\sigma - b)\right] e^{i\mu} \quad \text{at } \eta = 0 \qquad (2.5.7)$$

where μ is the interblade phase angle by which the second blade leads the first. Applying the boundary condition at the upper surface of each blade and using that

$$g_1(0) = h_1(0) = 0 \qquad (2.5.8)$$

gives, for plunge and pitch

PL: $$g_1(s) = 0 \qquad g_{1A}(\sigma) = A \qquad (2.5.9)$$

PI: $$g_1(s) = \frac{s}{\beta} \qquad g_{1A}(\sigma) = \frac{\sigma}{\beta} e^{i\mu} + B \qquad (2.5.10)$$

PL: $$h_1(s) = \frac{i}{\beta} s \qquad h_{1A}(\sigma) = \frac{i}{\beta} \sigma e^{i\mu} + C \qquad (2.5.11)$$

PI: $$h_1(s) = -\frac{i}{\beta^3}\left(\frac{s^2}{2} + b\beta^2 s\right)$$
$$h_{1A}(\sigma) = -\frac{i}{\beta^3}\left[\left(\frac{\sigma^2}{2} + b\beta^2\sigma\right)e^{i\mu} + \beta C M^2 \sigma\right] + D \qquad (2.5.12)$$

where A, B, C and D are constants of integration. By enforcing continuity of the velocity potential across the leading-edge Mach wave of blade two, the constants are evaluated and the velocity potentials determined in terms of the isolated blade potential ϕ_1^{μ} (2.3.7,8)

PL: $\phi_1^I = \phi_1^U \qquad \phi_2^{IA} = \phi_1^U e^{i\mu} + \frac{ik}{\beta} m$ (2.5.13)

PI: $$\phi_1^I = \phi_1^U$$
$$\phi_2^{IA} = \phi_1^U e^{i\mu} + \frac{m}{\beta} - \frac{ik}{\beta^3}(mM^2\sigma + \beta m M^2 \eta + \mathcal{C}) \qquad (2.5.14)$$

where $\mathcal{C}$ is a constant that need not be evaluated because it becomes the coefficient of a term in k^2 when the pressure coefficients are formed.[1] Thus, on the upper surface of the second blade, in terms of the isolated-blade pressure coefficient $C_{P_1}^U$ (2.3.9,10)

PL: $$C_{P_2}^{U\,IA} = C_{P_1}^U e^{i\mu} \qquad (2.5.15)$$

PI: $$C_{P_2}^{U\,IA} = C_{P_1}^U e^{i\mu} + \frac{2ik}{\beta^3} m \qquad (2.5.16)$$

2.5.2 Zones IIB and VIB. In zone IIB the velocity potential is that of the isolated blade (2.3.3)

$$\phi_1^{IIB} = \phi_1^L \qquad (2.5.17)$$

while in VIB the potential acquires an additional

---

[1]The symbol $\mathcal{C}$ is used throughout section 2 to indicate a constant which need not be determined.

right-running disturbance

$$\phi_1^{IIB} = \phi_1^{IB} + g_6(S) + k\left[h_6(S) + \frac{iM^2}{\beta} g g_6(S)\right] \qquad (2.5.18)$$

2.5.3 Zone II. In zone II a right-running reflection occurs and, using the translation relations (2.5.2,3) to shift to the blade-two coordinate system, one has

PL:
$$\phi_2^{II} = \phi_1^{I} + g_2(\bar{\sigma}) + k\left[\frac{im}{\beta} + h_2(\bar{\sigma}) + \frac{iM^2}{\beta}\eta g_2(\bar{\sigma})\right] \qquad (2.5.19)$$

PI:
$$\phi_2^{II} = \phi_1^{I} + \frac{m}{\beta} - \frac{ik}{\beta^3}\left[\sigma(m+\beta d M^2) + \beta m M^2 \eta + \phi\right] + g_2(\bar{\sigma}) + k\left[h_2(\bar{\sigma}) + \frac{iM^2}{\beta}\eta\, g_2(\bar{\sigma})\right] \qquad (2.5.20)$$

where

$$g_2(0) = h_2(0) = 0 \qquad (2.5.21)$$

Applying the flow tangency condition at the lower surface of blade two and using the Sauer functions to construct the velocity potentials yields

PL:
$$\phi_2^{II} = \phi_1^{I} + \frac{ik}{\beta}\left[\bar{\sigma}(1-e^{i\mu}) + m\right] \qquad (2.5.22)$$

PI:
$$\phi_2^{II} = \phi_1^{I} + \frac{m}{\beta} + \frac{\bar{\sigma}}{\beta}(1-e^{i\mu}) - \frac{ik}{\beta^3}\left\{\frac{\bar{\sigma}^2}{2}(1-e^{i\mu}) + \bar{\sigma}\left[-\beta^2 m + \beta d M^2 + (b\beta^2 - \beta M^2\eta)(1-e^{i\mu})\right] + \sigma(m+\beta d M^2) + \beta m M^2 \eta + \phi\right\} \qquad (2.5.23)$$

And the pressure coefficients follow from the potentials

PL: $$C_{P_2}^{L,II} = C_{P_1}^{U}(2 - e^{i\mu}) \tag{2.5.24}$$

PI: $$C_{P_2}^{L,II} = C_{P_1}^{U}(2 - e^{i\mu}) + \frac{2ik}{\beta^2}(m - 2\beta^2 m + 2\beta d M^2) \tag{2.5.25}$$

Thus the pressure difference can be computed through zone II, and by multiplying by the factor $e^{-i\mu}$ the pressure-difference amplitude is obtained at the moment the second blade reaches maximum displacement

PL: $$\Delta C_p e^{-i\mu} = -2C_{P_1}^{U}(1 - e^{-i\mu}) \qquad 0 \le \xi < 1 - m \tag{2.5.26}$$

PI: $$\Delta C_p e^{-i\mu} = -2C_{P_1}^{U}(1 - e^{-i\mu}) + \frac{4ik}{\beta^2}(\beta d M^2 - \beta^2 m)\, e^{-i\mu} \qquad 0 \le \xi < 1 - m \tag{2.5.27}$$

2.5.4 Zone III. In zone III a left-running wake disturbance is experienced, and after applying the translation relations

PL: $$\phi_1^{III} = \phi_2^{II} + g_3(s) + k\left[h_3(s) - \frac{iM^2}{\beta}\gamma g_3(s) + \phi\right] \tag{2.5.28}$$

PI: $$\begin{aligned}\phi_1^{III} = \phi_2^{II} - \frac{m}{\beta} - \frac{ik}{\beta^2}\Big\{&\bar{s}(-m - 2\beta d + \beta d M^2)(1 - e^{i\mu}) \\ &- s(m + \beta d M^2) + \gamma\left[-\beta m M^2 + (2\beta^2 d M^2 + \beta m M^2)(1 - e^{i\mu})\right] \\ &+ \phi\Big\} + g_3(s) + k\left[h_3(s) - \frac{iM^2}{\beta}\gamma g_3(s)\right]\end{aligned} \tag{2.5.29}$$

where

$$g_3(1) = h_3(1) = 0 \qquad (2.5.30)$$

Since zones III and VIB are separated by the wake of the blade rather than the blade itself, the wake boundary conditions are used between the two zones. The first of these demands pressure equilibrium across the wake

$$C_{P_1}^{III} = C_{P_1}^{VIB} \qquad \text{at } y=0 \qquad (2.5.31)$$

which leads to the equations

$$g_3'(s) - g_6'(\bar{s}) = ST\,(C_{P_1}^{v}) \qquad (2.5.32)$$

$$h_3'(s) - h_6'(\bar{s}) + i\left[g_3(s) - g_6(\bar{s})\right] = FR\,(C_{P_1}^{v}) \qquad (2.5.33)$$

where the right-hand sides of (2.5.32,33) refer to the steady and frequency terms respectively of C_{pl}^{u} (2.3.9,10). The second wake condition requires continuity of the normal velocity component through the wake

$$\frac{\partial \phi^{III}}{\partial y} = \frac{\partial \phi^{VIB}}{\partial y} \qquad \text{at } y=0 \qquad (2.5.34)$$

which leads to the equations

$$g_3'(s) + g_6'(\bar{s}) = 0 \qquad (2.5.35)$$

$$h_3'(s) + h_6'(\bar{s}) + \frac{iM^2}{\beta^2}\left[g_3(s) + g_6(\bar{s})\right] = 0 \qquad (2.5.36)$$

Equations (2.5.32,33,35,36) are solved for the zone-III disturbances

PL: $$g_3(s) = 0 \qquad h_3'(0) = -\frac{i}{\beta} \qquad (2.5.37)$$

PI: $$g_3(s) = -\frac{1}{\beta}(s-1) \qquad h_3'(s) = \frac{i}{\beta^3}(s - \beta^2 + b\beta^2) \qquad (2.5.38)$$

2.5.5 Zone V. In zone V an unknown disturbance is added

$$\phi_2^{\text{V}} = \phi_2^{\text{II}} + g_3(\sigma) + g_5(\bar{\sigma}) + k\Big\{h_3(\sigma) + h_5(\bar{\sigma}) + \frac{iM^2}{\beta}\eta\left[-g_3(\sigma) + g_5(\bar{\sigma})\right] - \frac{iM^2}{\beta} d\, g_3(\sigma)\Big\} \qquad (2.5.39)$$

which is determined by enforcing flow tangency at the lower surface of blade two in zone V

PL: $$g_5(\bar{\sigma}) = 0 \qquad h_5'(\bar{\sigma}) = -\frac{i}{\beta} \qquad (2.5.40)$$

PI: $$g_5(\bar{\sigma}) = -\frac{1}{\beta}(\bar{\sigma} - 1 + m)$$
$$h_5'(\bar{\sigma}) = \frac{i}{\beta^3}(\bar{\sigma} - \beta^2 + m + b\beta^2 + \beta d M^2) \qquad (2.5.41)$$

which leads directly to the pressure difference for the last portion of the blade

PL: $$\Delta C_p e^{-i\mu} = -2C_{p_1}^u \qquad 1-m < \xi \leq 1 \qquad (2.5.42)$$

PI: $$\Delta C_p e^{-i\mu} = -2C_{p_1}^u - \frac{4ik}{\beta^3}\left(m - \frac{\beta d M^2}{2}\right) e^{-i\mu} \qquad 1-m < \xi \leq 1 \qquad (2.5.43)$$

2.5.6 Results and Conclusions. The finite results for the second blade are compared with four existing solutions in figures 2.5.2 and 2.5.3 for three interblade phase angles: Kurosaka's solution [6] is a closed-form, analytical, infinite-cascade solution; Platzer's [16,17] is a numerical, method-of-characteristics solution for the finite cascade; and Adamczyk's [19] and Verdon's [12] solutions are numerical, infinite-cascade results. It is interesting to note that the finite results agree exactly with Kurosaka's infinite solution over the entire blade for the plunge case and through zone II for the pitch case. Over the zone-V portion of the pitching blade – the portion exposed to the wake disturbances from blade one – the two solutions agree numerically, as seen in figure 2.5.3, but are not analytically the same. In fact, Kurosaka's solution is singular for $\mu = 0$ (in-phase oscillation of the blades) over the last portion of the blade, while equation (2.5.43) behaves well for that case. All five solutions were found to be in excellent agreement for interblade phase angles larger than 15°, but for small angles considerable disagreement is evident, as seen in figure 2.5.2.

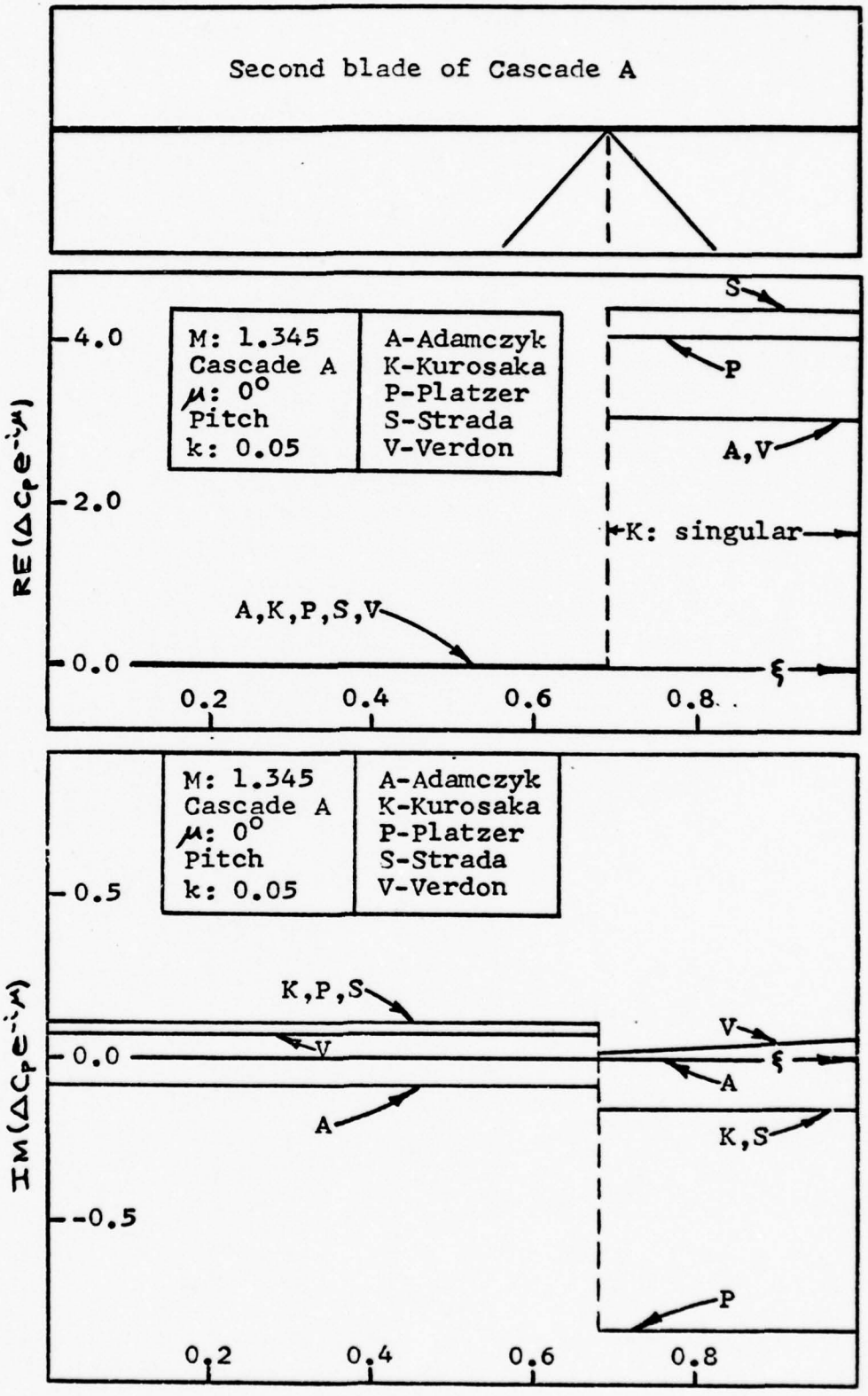

Figure 2.5.2 Comparison of the finite-cascade solution with existing solutions.

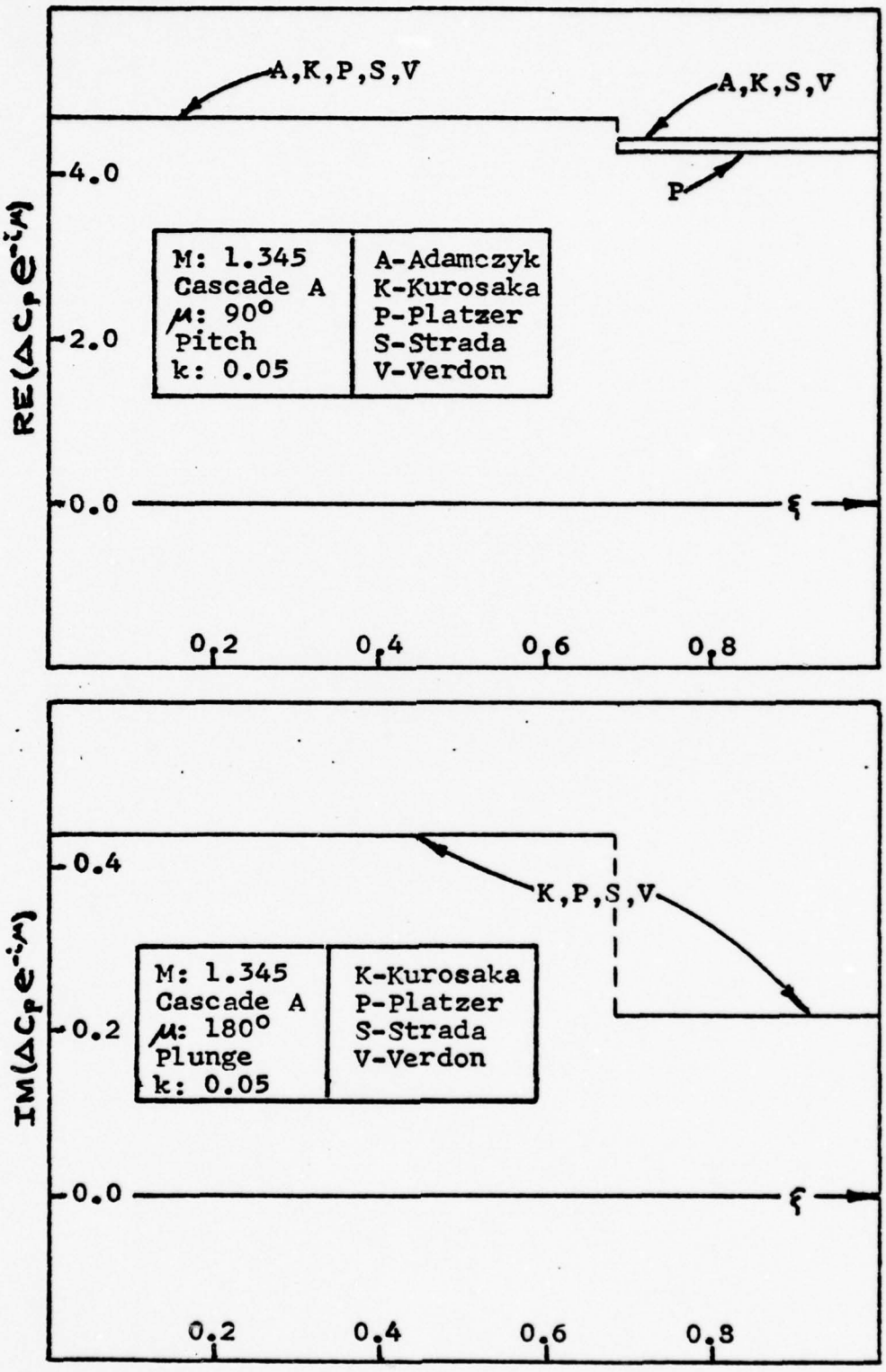

Figure 2.5.3 Comparison of the finite-cascade solutions with existing solutions.

Chadwick [5] compared his finite and infinite results for the pitch case over the in-flow portion of the blade and noted that although the finite and infinite pressure-difference (ΔC_p) distributions are the same, the local pressure distributions (C_p^U, C_p^L) may in fact differ. The author found this phenomenon occuring over the remaining portion of the pitching blade also. Figure 2.5.4 shows that the local pressure distributions for the present finite solution and Verdon's infinite solution do not agree as well as the pressure-difference distributions. Some conclusions can be drawn from the analysis at this point:

1. For low frequencies of oscillation the finite cascade rapidly approaches the infinite-cascade solution, achieving good agreement with the pressure-difference distribution of the latter at the second blade.

2. For small interblade phase angles, the present solution agrees with Kurosaka's Laplace transform solution for the infinite cascade but considerable differences with the other published solutions are noted.

3. Although the present finite-cascade solution and Verdon's infinite-cascade solution for the pressure-difference distributions are in agreement for large interblade phase angles, the local pressure distributions resulting from the two solutions are seen to disagree.

2.6 <u>The Infinite Two-Degree-of-Freedom Cascade.</u> In order to demonstrate the applicability of the above analysis to

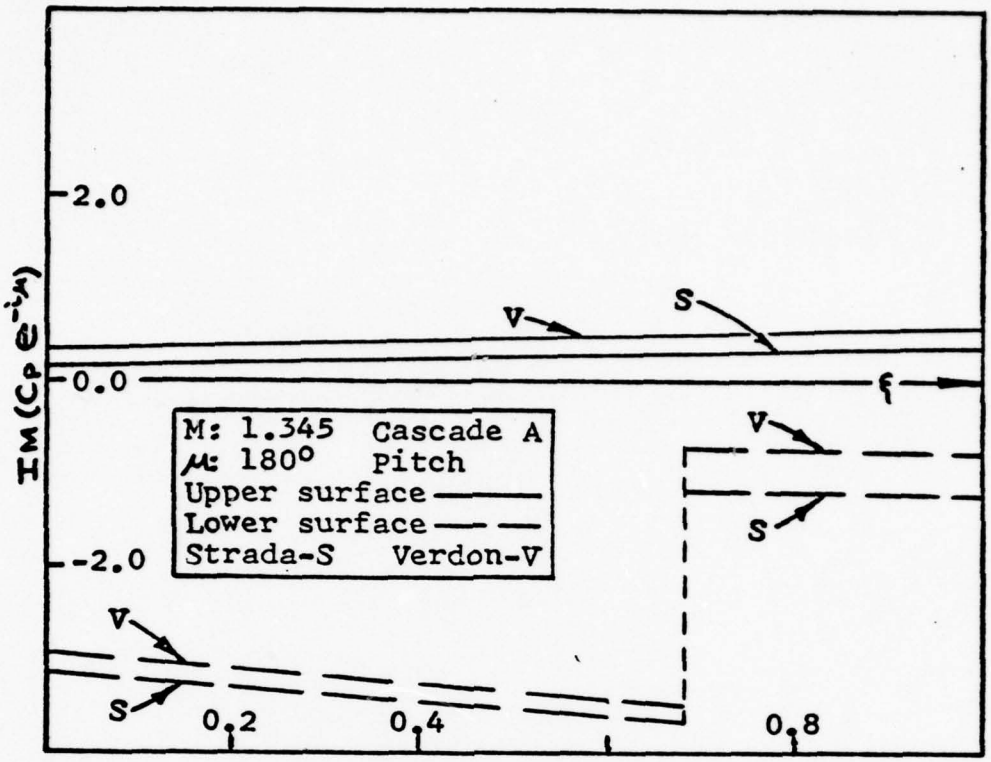

Figure 2.5.4 Comparison of the finite and infinite local pressure distributions.

the infinite cascade, it is applied to an infinite version of Cascade B. Since the advantage of an identifiable first blade is lost, a condition specifying the space periodicity of the flowfields between the blades is derived. The pitch results through equation (2.6.17) were first obtained by Chadwick [5], and the reflection zones referred to in the solution are depicted in figure 2.6.1.

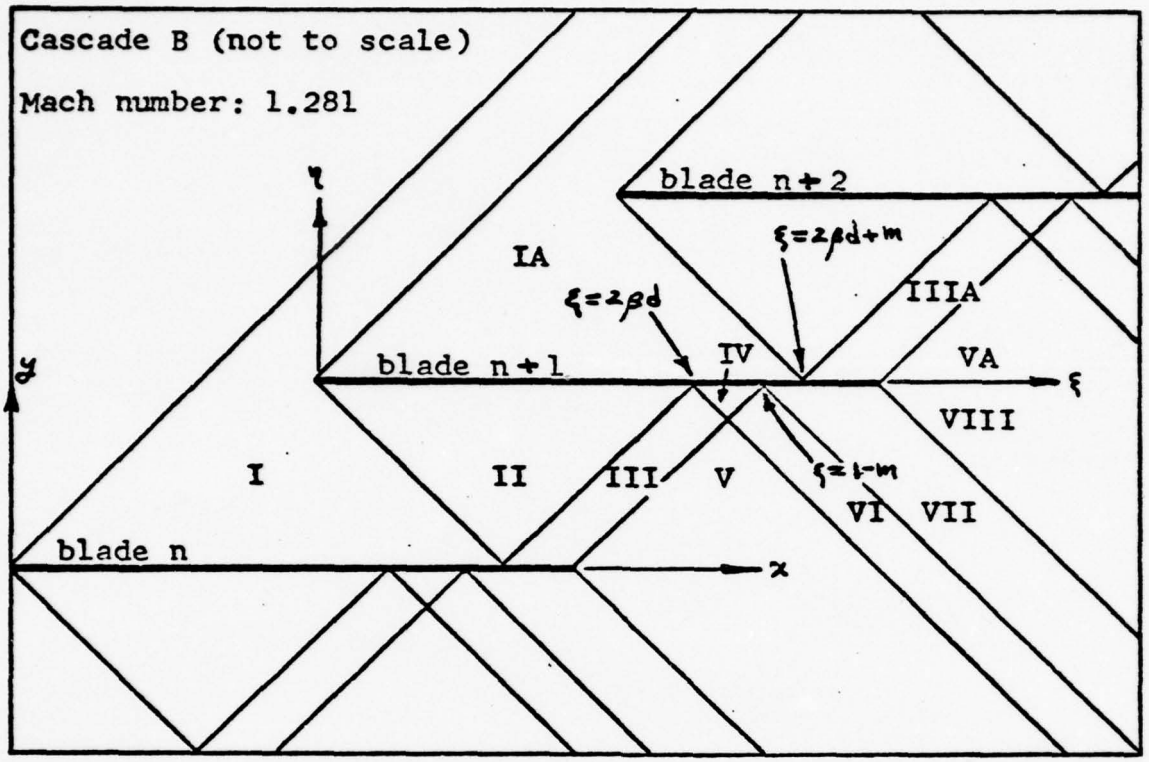

Figure 2.6.1 The infinite-cascade reflection zones.

2.6.1 <u>The Flow Periodicity Condition.</u> The periodicity of the flow from blade passage to blade passage was first identified by Kurosaka [6] and is the heart of his passage approach to the infinite cascade. An alternate derivation follows.

Consider the corresponding zones I and IA, and assume that the potentials are the same there except for a complex factor K

$$\phi_n^{I}(x,y) = K\ \phi_{n+1}^{IA}(\xi,\eta) \qquad (2.6.1)$$

Since each potential must satisfy the boundary condition of its corresponding blade

$$\frac{\partial \phi_n^I}{\partial y} = -ik \quad \text{at } y=0 \tag{2.6.2}$$

$$\frac{\partial \phi_{n+1}^{IA}}{\partial \eta} = -ik e^{i\mu} \quad \text{at } \eta = 0 \tag{2.6.3}$$

it is clear that

$$\kappa = e^{-i\mu} \tag{2.6.4}$$

and so

$$\phi_n^I(x,y) = \phi_{n+1}^{IA}(\xi,\eta)\, e^{-i\mu} \tag{2.6.5}$$

The same result follows for any pair of corresponding zones on adjacent blades – for pitch and plunge – and is termed the flow periodicity condition.

2.6.2. Zones I and IA. The analysis in zones I and IA proceeds much as in the finite case (section 2.5.1). The velocity potentials have the form

$$\phi_n^I = g_1(s) + k\left[h_1(s) - \frac{iM^2}{\beta} y\, g_1(s)\right] \tag{2.6.6}$$

$$\phi_{n+1}^{IA} = g_{1A}(\sigma) + k\left[h_{1A}(\sigma) - \frac{iM^2}{\beta}\eta\, g_{1A}(\sigma)\right] \tag{2.6.7}$$

and the boundary conditions yield

PL: $$g_1(s) = A \qquad g_{1A}(\sigma) = B \tag{2.6.8}$$

PI: $$g_1(s) = \frac{s}{\beta} + C \qquad g_{1A}(\sigma) = \frac{\sigma}{\beta} e^{i\mu} + D \tag{2.6.9}$$

PL: $$h_1(s) = \frac{i}{\beta} s - \frac{iM^2}{\beta^2} A s + E$$
$$h_{1A}(\sigma) = \frac{i}{\beta} \sigma e^{i\mu} - \frac{iM^2}{\beta^2} B\sigma + F \tag{2.6.10}$$

PI: $$h_1(s) = -\frac{i}{\beta^3}\left(\frac{s^2}{2} + b\beta^2 s + \beta M^2 C s\right) + G$$
$$h_{1A}(\sigma) = -\frac{i}{\beta^3}\left[\left(\frac{\sigma^2}{2} + b\beta^2\sigma\right) e^{i\mu} + \beta M^2 D\sigma\right] + H \tag{2.6.11}$$

The constants A through D are evaluated using, respectively, continuity of the velocity potential across the leading-edge Mach wave of the (n+1)st blade and the flow periodicity condition

$$\phi_1(s=m) = \phi_{1A}(\sigma=0) \tag{2.6.12}$$

$$\phi_n^I = \phi_{n+1}^{IA} e^{-i\mu} \tag{2.6.13}$$

The pressure coefficients, in terms of those of the isolated blade (2.3.9,10), follow

PL: $$C_{Pn}^{UI} = C_{P_1}^{U} \tag{2.6.14}$$

PI: $$C_{Pn}^{UI} = C_{P_1}^{U} - \frac{2iR}{\beta^3}\frac{m}{(1-e^{i\mu})} \tag{2.6.15}$$

2.6.3 Zones II through IV. Finding the additional reflections through zone IV is accomplished by routine use of the flow tangency condition (2.2.26,27), and so only the pressure results for the (n+1)st blade are given below

$$\text{PL:}\quad \Delta C_p e^{-i\mu} = -2 C_{p_1}^u (1 - e^{-i\mu}) \qquad 0 \le \xi < 2\beta d \tag{2.6.16}$$

$$\text{PI:}\quad \Delta C_p e^{-i\mu} = -2 C_{p_1}^u (1 - e^{-i\mu}) + \frac{4ik}{\beta^3}(\beta d M^2 - \beta^2 m) e^{-i\mu} \qquad 0 \le \xi < 2\beta d \tag{2.6.17}$$

$$\text{PL:}\quad \Delta C_p e^{-i\mu} = -4 C_{p_1}^u (1 - e^{-i\mu}) \qquad 2\beta d < \xi < 1 - m \tag{2.6.18}$$

$$\text{PI:}\quad \Delta C_p e^{-i\mu} = -4 C_{p_1}^u (1 - e^{-i\mu}) + \frac{8ik}{\beta^3}\left[(\beta d M^2 - \beta^2 m) e^{-i\mu} - 2\beta^3 d (1 - e^{-i\mu})\right] \qquad 2\beta d < \xi < 1 - m \tag{2.6.19}$$

2.6.4 Zones V, VI, and VII. In the first three zones above the wake of the nth blade

$$\phi_n^{V} = \phi_n^{III} + g_5(s) + k\left[h_5(s) - \frac{iM^2}{\beta} y\, g_5(s)\right] \tag{2.6.20}$$

$$\phi_{n+1}^{VII} = \phi_n^{V} + g_4(\bar{\sigma}) + k\left[h_4(\bar{\sigma}) + \frac{iM^2}{\beta}\eta\, g_4(\bar{\sigma})\right] \tag{2.6.21}$$

$$\phi_{n+1}^{VIII} = \phi_{n+1}^{VII} + g_7(\bar{\sigma}) + k\left[h_7(\bar{\sigma}) + \frac{iM^2}{\beta}\eta\, g_7(\bar{\sigma})\right] \tag{2.6.22}$$

where the g_4 and h_4 Sauer functions are known from the analysis in zone IV and

$$g_5(1) = h_5(1) = 0 \tag{2.6.23}$$

$$g_7(1-m) = h_7(1-m) = 0 \tag{2.6.24}$$

2.6.5 Zones VA and VIII. In the zones straddling the wake of the (n+1)st blade, using flow periodicity and results from zones IV and V

$$\phi^{VA}_{n+1} = \phi^{IIIA}_{n+1} + g_{5A}(\sigma) + k\left[h_{5A}(\sigma) - \frac{iM^2}{\beta}\eta\, g_{5A}(\sigma)\right] \tag{2.6.25}$$

$$\begin{aligned}\phi^{VIII}_{n+1} = \phi^{IV}_{n+1} &+ g_5(\sigma)e^{-i\mu} + g_7(\bar{\sigma}) + g_8(\bar{\sigma}) \\ &+ k\left\{h_5(\sigma)e^{-i\mu} + h_7(\bar{\sigma}) + h_8(\bar{\sigma})\right. \\ &\left. - \frac{iM^2}{\beta}\eta\left[g_5(\sigma)e^{-i\mu} - g_7(\bar{\sigma}) - g_8(\bar{\sigma})\right] - \frac{iM^2}{\beta}d\, g_5(\sigma)e^{-i\mu}\right\}\end{aligned} \tag{2.6.26}$$

where

$$\begin{aligned}g_{5A}(\sigma) + k\left[h_{5A}(\sigma) - \frac{iM^2}{\beta}\eta\, g_{5A}(\sigma)\right] &= \\ \left\{g_5(s) + k\left[h_5(s) - \frac{iM^2}{\beta}y\, g_5(s)\right]\right\}e^{i\mu}&\end{aligned} \tag{2.6.27}$$

$$g_8(1) = h_8(1) = 0 \tag{2.6.28}$$

The wake boundary conditions – pressure equilibrium and normal velocity continuity – are enforced between zones VA and VIII

$$C_{P_{n+1}}^{IX_A} = C_{P_{n+1}}^{VIII} \quad \text{at } \eta = 0 \tag{2.6.29}$$

$$\frac{\partial \phi_{n+1}^{IX_A}}{\partial \eta} = \frac{\partial \phi_{n+1}^{VIII}}{\partial \eta} \quad \text{at } \eta = 0 \tag{2.6.30}$$

giving rise to two equations in three unknown Sauer functions

$$g_5'(1-e^{-i\mu}) - g_7' - g_8' = ST\left[-\tfrac{1}{2}(C_{P_{n+1}}^{L\,IV} - C_{P_{n+1}}^{U\,III_A})\right] \tag{2.6.31}$$

$$g_5'(1-e^{-i\mu}) + g_7' + g_8' = 0 \tag{2.6.32}$$

$$\begin{aligned} &h_5'(1-e^{-i\mu}) - h_7' - h_8' + \frac{iM^2}{\beta} d\, g_5' e^{-i\mu} \\ &+ i\left[g_5(1-e^{-i\mu}) - g_7 - g_8\right] = FR\left[-\tfrac{1}{2}(C_{P_{n+1}}^{L\,IV} - C_{P_{n+1}}^{U\,III_A})\right] \end{aligned} \tag{2.6.33}$$

$$h_5'(1-e^{-i\mu}) + h_7' + h_8' + \frac{iM^2}{\beta^2}\left[g_5(1-e^{-i\mu}) + g_7 + g_8 + \beta d\, g_5' e^{-i\mu}\right] = 0 \tag{2.6.34}$$

where the right-hand sides of (2.6.31,33) indicate the steady and frequency terms, respectively, of the enclosed quantity. The third equation in the set comes from applying the boundary condition to ϕ_{n+1}^{VII} at the lower surface of the (n+1)st blade

$$g_5' e^{-i\mu} - g_7' = 0 \tag{2.6.35}$$

$$h_5' e^{-i\mu} - h_7' + \frac{iM^2}{\beta^2}(g_5 e^{-i\mu} - g_7 - \beta d\, g_5' e^{-i\mu}) = 0 \tag{2.6.36}$$

Solving equations (2.6.31) through (2.6.36) for the Sauer functions permits determination of the pressure difference over the last portion of the blade

PL: $$\Delta C_p e^{-i\mu} = -2C_{P_1}^u \qquad 1-m<\xi<2\beta d+m \qquad (2.6.37)$$

PI: $$\Delta C_p e^{-i\mu} = -2C_{P_1}^u + \frac{4ik}{\beta^3}\frac{m}{(1-e^{i\mu})} \qquad 1-m<\xi<2\beta d+m \qquad (2.6.38)$$

PL: $$\Delta C_p e^{-i\mu} = -2C_{P_1}^u (2-e^{i\mu}) \qquad 2\beta d+m<\xi\leq 1 \qquad (2.6.39)$$

PI: $$\Delta C_p e^{-i\mu} = -2C_{P_1}^u (2-e^{i\mu}) - \frac{2ik}{\beta^3}\left\{2(\beta d M^2-\beta^2 m) + \left[2\beta d M^2+(\beta^2-2)(m+2\beta d)\right](1-e^{i\mu}) - \frac{2m}{(1-e^{i\mu})}\right\} \qquad 2\beta d+m<\xi\leq 1 \qquad (2.6.40)$$

2.6.6 Results and Conclusions. Figure 2.6.2 shows that, as with the finite-cascade solution, there is considerable disagreement among the several existing solutions for small interblade phase angles, but even for those angles the present solution and Kurosaka's are in agreement. The pressure-difference expressions derived above for the infinite cascade agree exactly with those of Kurosaka [6] over the entire plunging blade and up to $\xi = 2\beta d + m$ for the pitching one. Over the last portion of the pitching blade the two solutions are slightly different analytically but are in

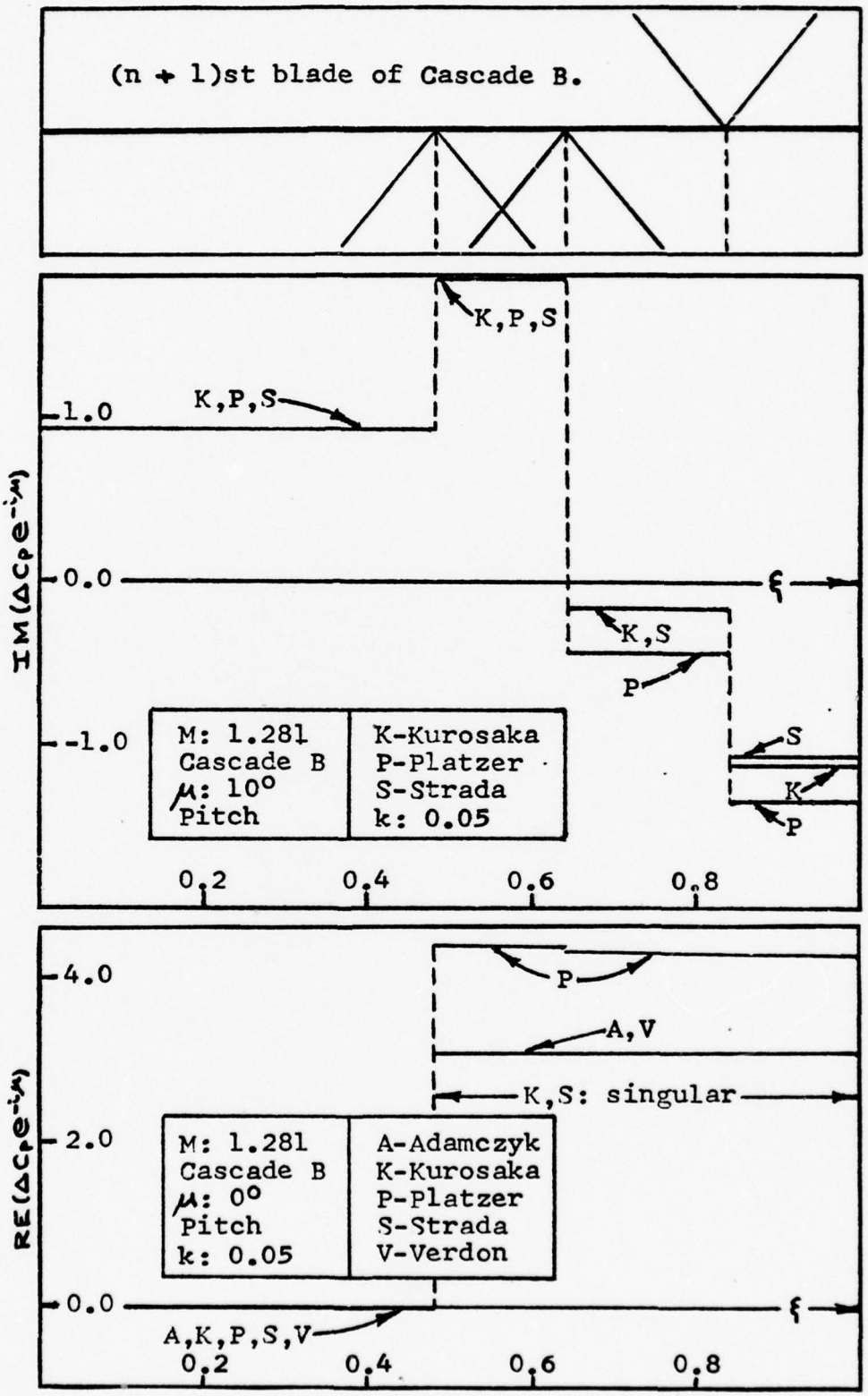

Figure 2.6.2 Comparison of the infinite-cascade solution with existing solutions.

numerical agreement as seen in figures 2.6.3 and 2.6.4; the analytical discrepancy could not be resolved. All of the solutions are in accord for the larger phase angles. Continuing with the conclusions begun in section 2.5.6, it can be added that:

4. For interblade phase angles larger than 15° the present method of analysis yields closed-form pressure-difference expressions which are in agreement with existing solutions for the slowly-oscillating cascade.

2.7 Limiting Cases of the Finite and Infinite-Cascade Solutions.

2.7.1 The Steady Cascade. All terms of the plunge solutions are frequency terms; therefore if k is set to zero, the pressure-difference distribution goes to zero for the entire blade, which is, of course, what should happen for a stationary flat plate aligned with the flow.

If k is set to zero in the pitching case, then one obtains for the isolated airfoil

$$C_{p_1}^{v} = -\frac{2}{\beta} \tag{2.7.1}$$

and so both the finite (2.5.27) and infinite (2.6.17) solutions becomes

$$\Delta C_p = \frac{4}{(M^2-1)^{1/2}} \tag{2.7.2}$$

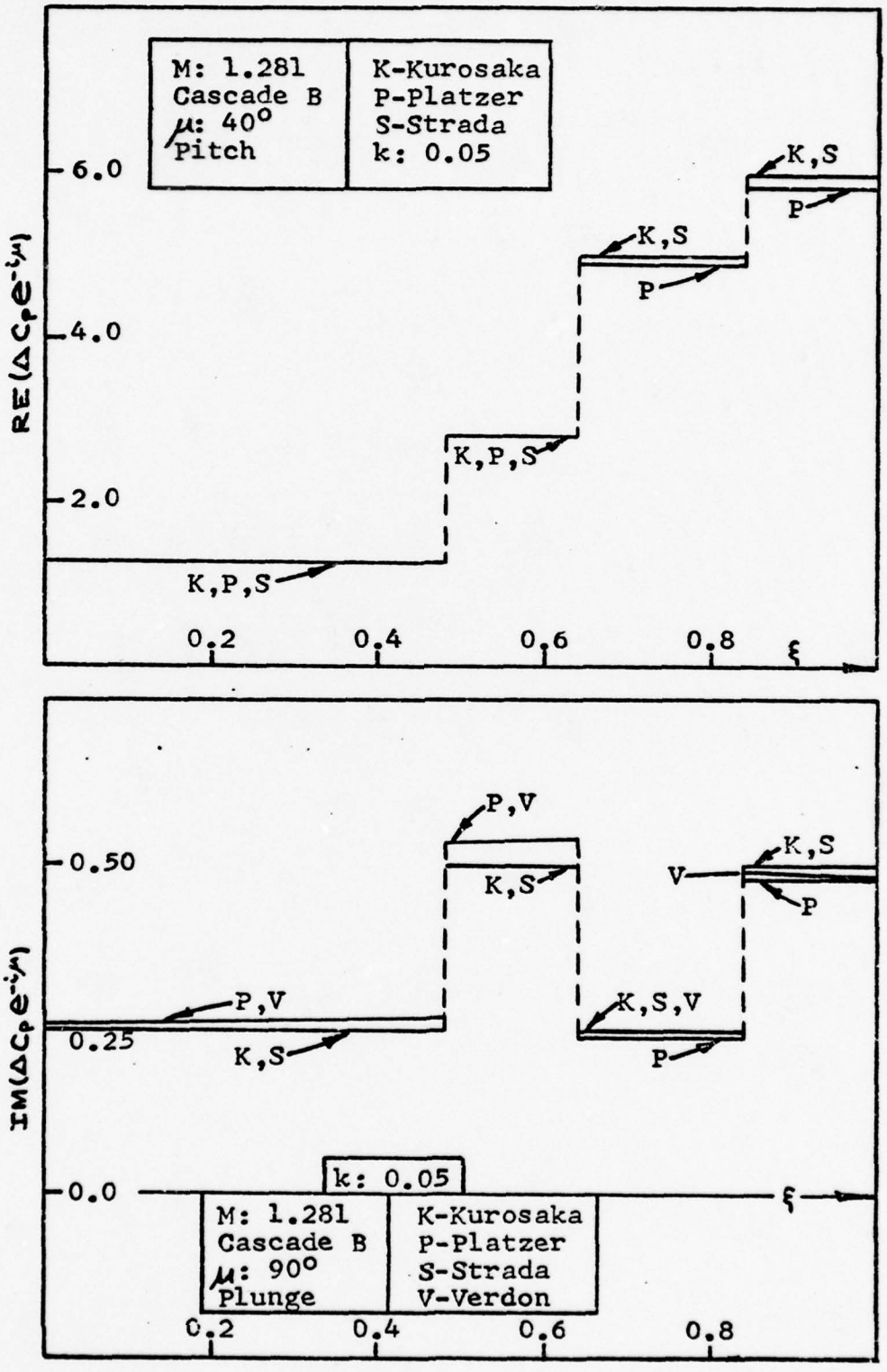

Figure 2.6.3 Comparison of the infinite-cascade solution with existing solutions.

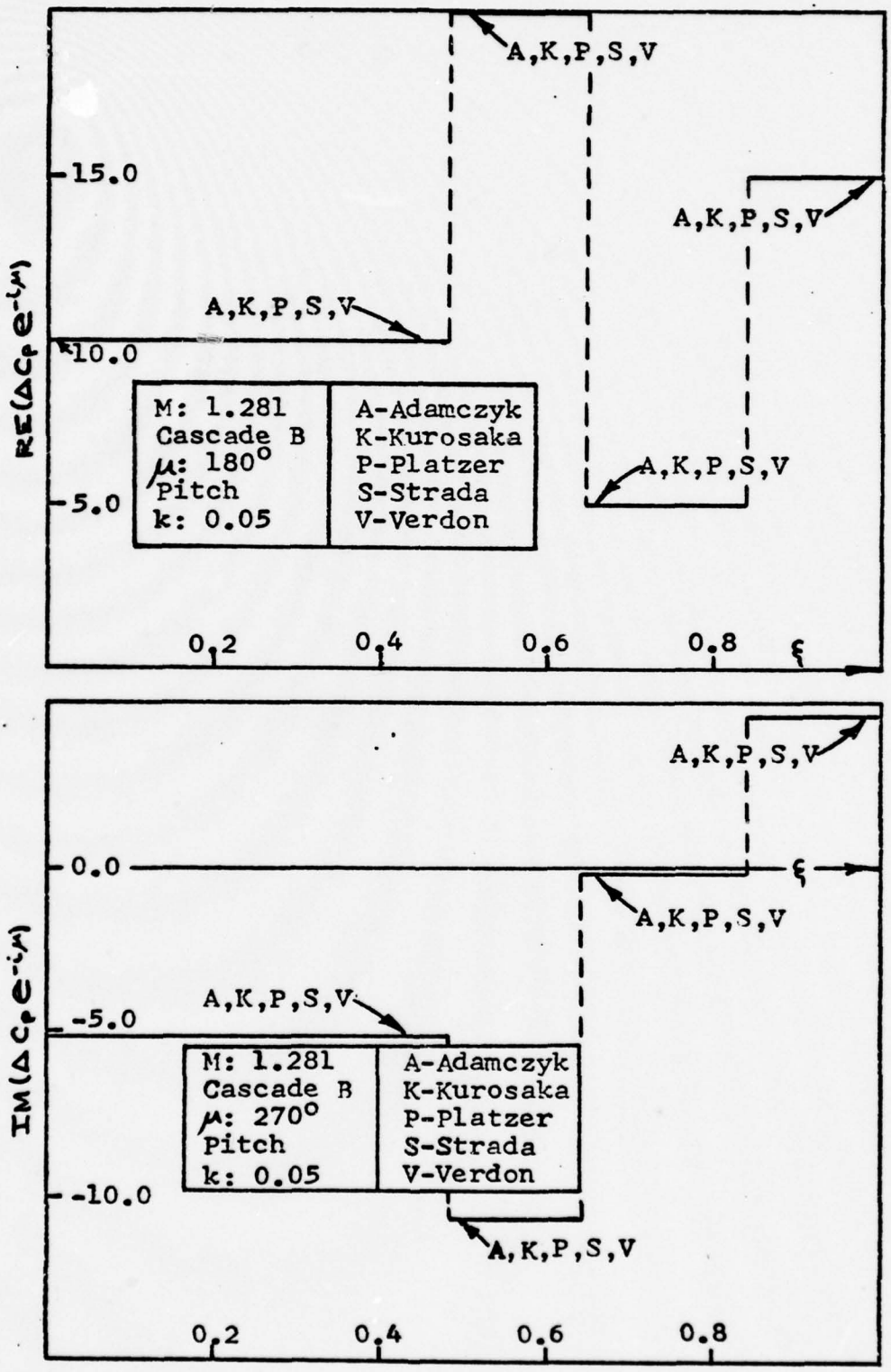

Figure 2.6.4 Comparison of the infinite-cascade solution with existing solutions.

where the phase-angle term has been ignored because it is meaningless in the steady case. Equation (2.7.2) is the classical Ackeret solution [27] for a flat plate at an angle of attack equal to one radian, which is the maximum up-pitch position.

2.7.2 The Single-Blade "Cascade". If either cascade is "squeezed" down to a single blade by setting the spacing parameters m and d to zero, then the solutions (2.5.26,27) and (2.6.16,17) reduce to those of the isolated blade

$$\Delta C_p = -2\, C_{p_1}^{\upsilon} \qquad (2.7.3)$$

where the phase term has again been ignored.

2.7.3 The Infinitely-Spaced Cascade. The isolated-blade solution is again recovered from equations (2.5.27) and (2.6.17) as the cascade spacing is allowed to get large. If the spacing parameters m and d approach infinity in such a way that the terms $\beta d M^2$ and $\beta^2 m$ remain equal, then equation (2.7.3) again results. The significance of these two terms is discussed further in the next section.

2.8 The Unique Inflow Condition. A consideration of the infinitely-spaced cascade in section 2.7.3 leads one[1] to

---

[1]The author is grateful to Professor M. F. Platzer for first asking this question.

ask: For which cascades does the relationship

$$\beta_d M^2 = \beta^2 m \qquad (2.7.4)$$

hold? As seen from equation (2.5.27), for such a cascade the pressure-difference over the inflow portion of the blade is merely that of the isolated pitching blade times the factor $(1 - e^{-iM})$.

Let α be the Mach angle defined by

$$\alpha = \sin^{-1}\left(\frac{1}{M}\right) \qquad (2.7.5)$$

then it is not difficult to show that for any cascade having the stagger angle

$$\theta_o = \tan^{-1}\left(\frac{\sin 2\alpha}{2 + \sin 2\alpha}\right) \qquad (2.7.6)$$

equation (2.7.4) will also hold. Said another way, all members of an infinite family of pitching cascades with the stagger angle given by (2.7.6) – and with no restrictions on blade spacing – will have exactly the same inflow pressure distribution, i.e.

PI: $$\Delta C_p = -2 C_{p_1}^{u} (1 - e^{-iM}) \qquad (2.7.7)$$

This is termed, by the author, the unique inflow condition for the slowly-oscillating cascade. Figure 2.8.1 depicts

CASCADE	MACH NUMBER	STAGGER ANGLE(θ_o)	d	m	SOLIDITY(σ)
C	1.414	18.43°	0.2	0.4	1.58
D	1.414	18.43°	0.3	0.6	1.05
E	1.414	18.43°	0.4	0.8	0.791

Cascade geometries.

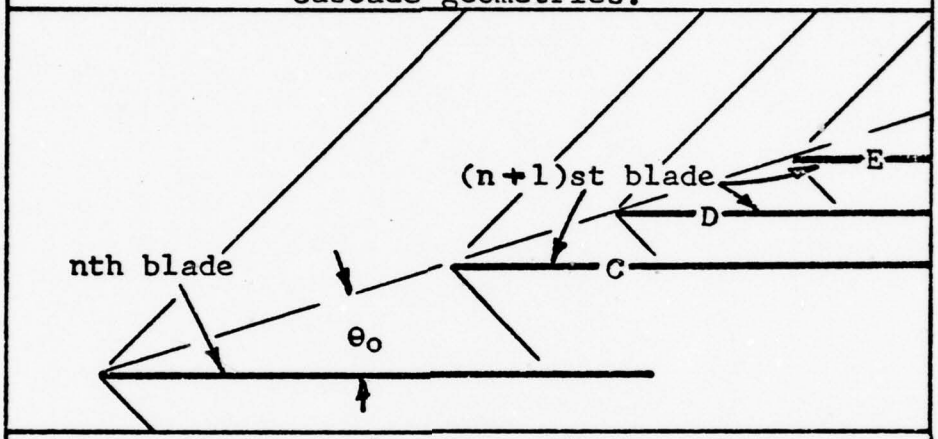

Blade spacing for each cascade.

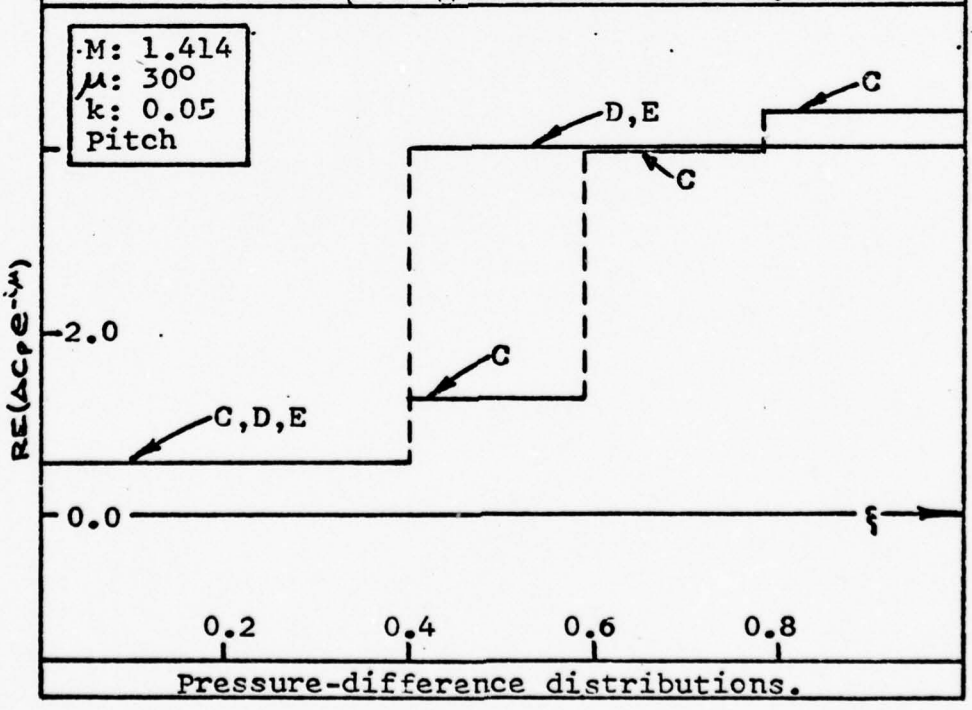

Pressure-difference distributions.

Figure 2.8.1 The unique inflow condition.

three different cascades, each with the same stagger angle, satisfying (2.7.6). The pressure distribution for each was obtained via Platzer's method-of-characteristics program. The unique inflow condition is evidenced by the exact agreement of the pressures for all three cascades over the first portion of the blade.

2.9 Some Comments on Resonance. For a given reference blade in an infinite cascade, resonance occurs when aerodynamic disturbance waves generated by upstream blade are in phase with the motion of the reference blade [12]. Samoylovich [28] shows that at the resonance condition the linear cascade experiences zero aerodynamic damping. The development that follows is based on Verdon's [12] excellent explanation of the resonance phenomenon and provides a means of delineating what he calls the subresonant and superresonant regions of the μ-k plane.

Referring to figure 2.9.1, also taken from [12], it is seen that the leading edge of each blade creates disturbances which propagate in all directions at the freestream speed of sound a_∞. These disturbances are swept downstream by the freestream flow U, and there are exactly two resultant waves which propagate along the cascade leading edge in the direction opposite to the direction of rotation and at velocities V_1 and V_2. From the law of cosines one has

$$\frac{V_i}{U} = \frac{M(m+\beta d) \mp [m(m+2\beta d)]^{1/2}}{M\left[(m+\beta d)^2 + d^2\right]^{1/2}} \qquad i = 1,2 \qquad (2.9.1)$$

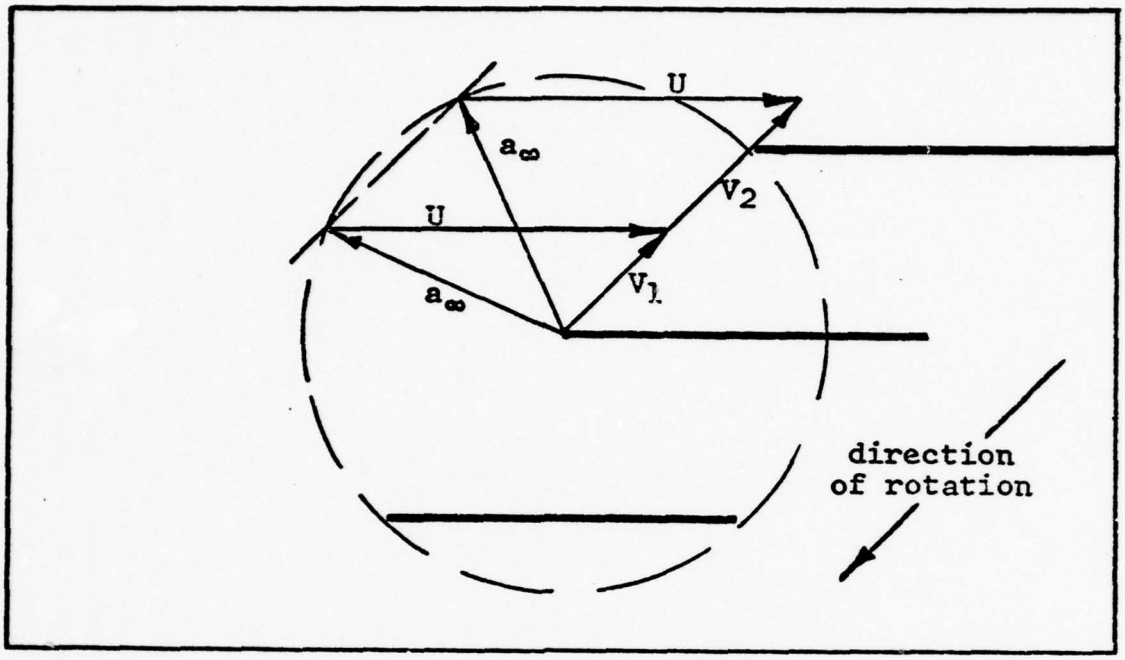

Figure 2.9.1 The backward-traveling waves causing resonance.

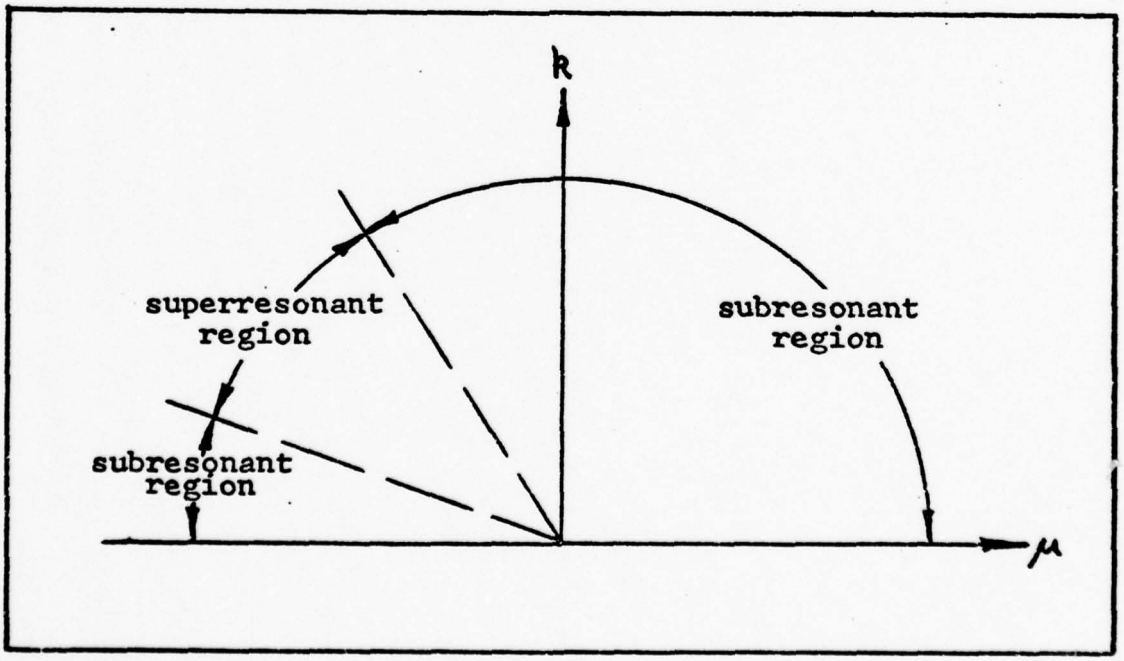

Figure 2.9.2 The subresonant and superresonant regions.

The times t_{1n}, t_{2n} required for a wave from an upstream blade (n = -1, -2, ...) to reach any given reference blade (n = 0) are

$$t_{1n,2n} = \frac{-nM}{\beta^2}\left\{M(m+\beta d) \pm \left[m(m+2\beta d)\right]^{1/2}\right\} \qquad (2.9.2)$$

The reference blade lags an upstream blade by

$$t_0 = \frac{n\mu}{k} \qquad n = -1, -2, \ldots \qquad (2.9.3)$$

and resonance occurs when the upstream waves are in phase with the reference-blade motion, i.e. when

$$t_0 = t_{1n,2n} \qquad (2.9.4)$$

or when

$$\mu_{1,2} = \frac{-kM}{\beta^2}\left\{M(m+\beta d) \pm \left[m(m+2\beta d)\right]^{1/2}\right\} \qquad (2.9.5)$$

For a fixed reduced frequency k the superresonant interblade phase angles lie between μ_1 and μ_2, as shown in figure 2.9.2, while the subresonant phase angles lie to either side. The superresonant region is important because Verdon is of the opinion that, in that region, neither a finite-cascade solution nor a passage-approach infinite-cascade solution will adequately approximate the true infinite-cascade solution. In an effort to shed some light

on the subject, some comparisons are presented in figures 2.9.3 through 2.9.6. For cascade A, with $k = 0.05$, the superresonant range of phase angles is approximately $-7°$ to $-2°$, and so $-5°$ was examined. Figures 2.9.3 and 2.9.4 show that Platzer's finite solution and the author's passage-approach infinite solution are in agreement with Verdon's solution. For cascade B, however, Verdon's solution is significantly different from the other two over the last portion of the blade for the superresonant phase angle $-3°$. Figures 2.9.5 and 2.9.6 show some high-frequency comparisons for the phase angle $-90°$, which is in the superresonant regions of both cascades A and B. In these two cases the two solutions — one finite and one infinite — are in accord.

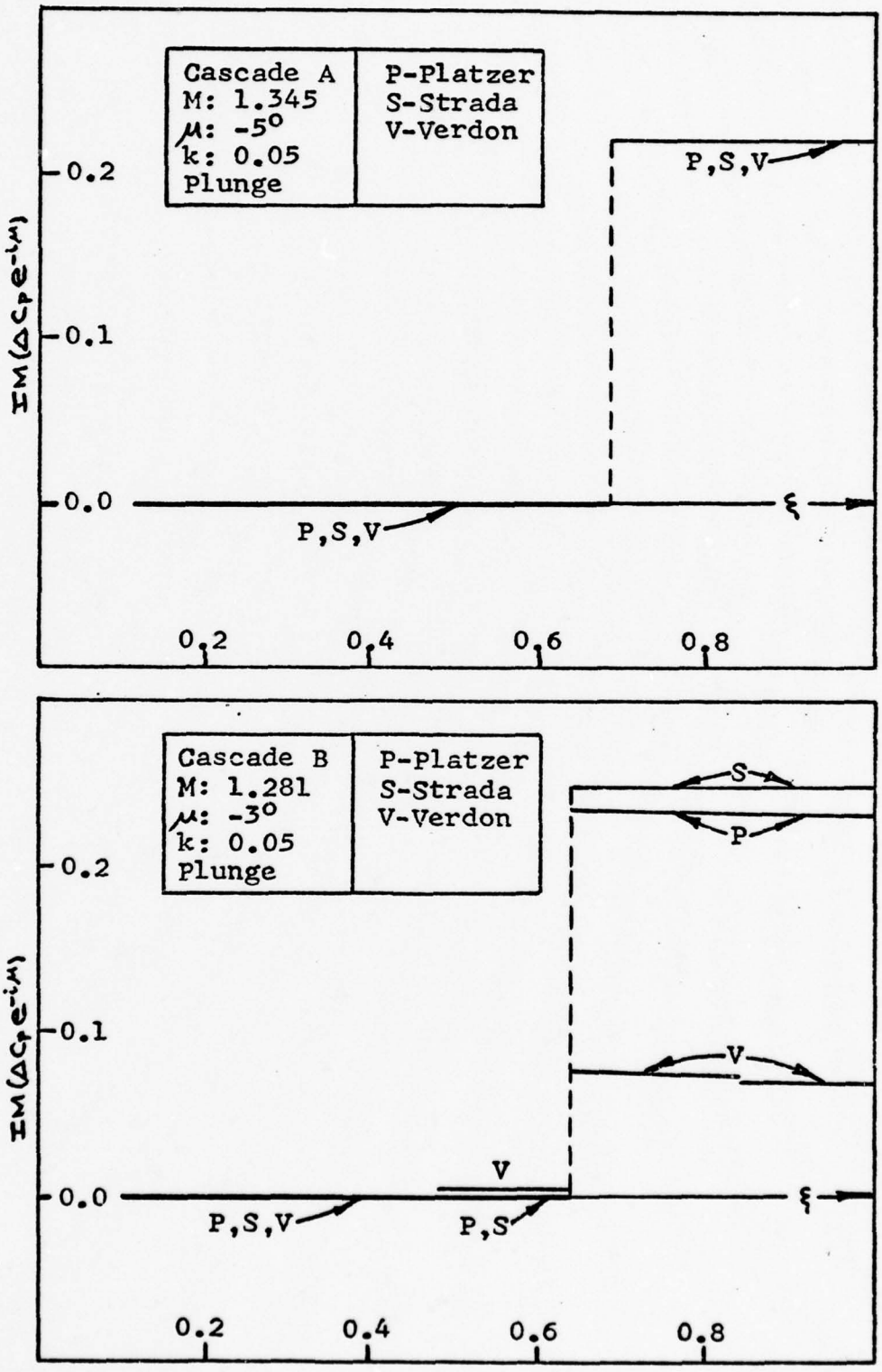

Figure 2.9.3 Low-frequency superresonant pressure distributions.

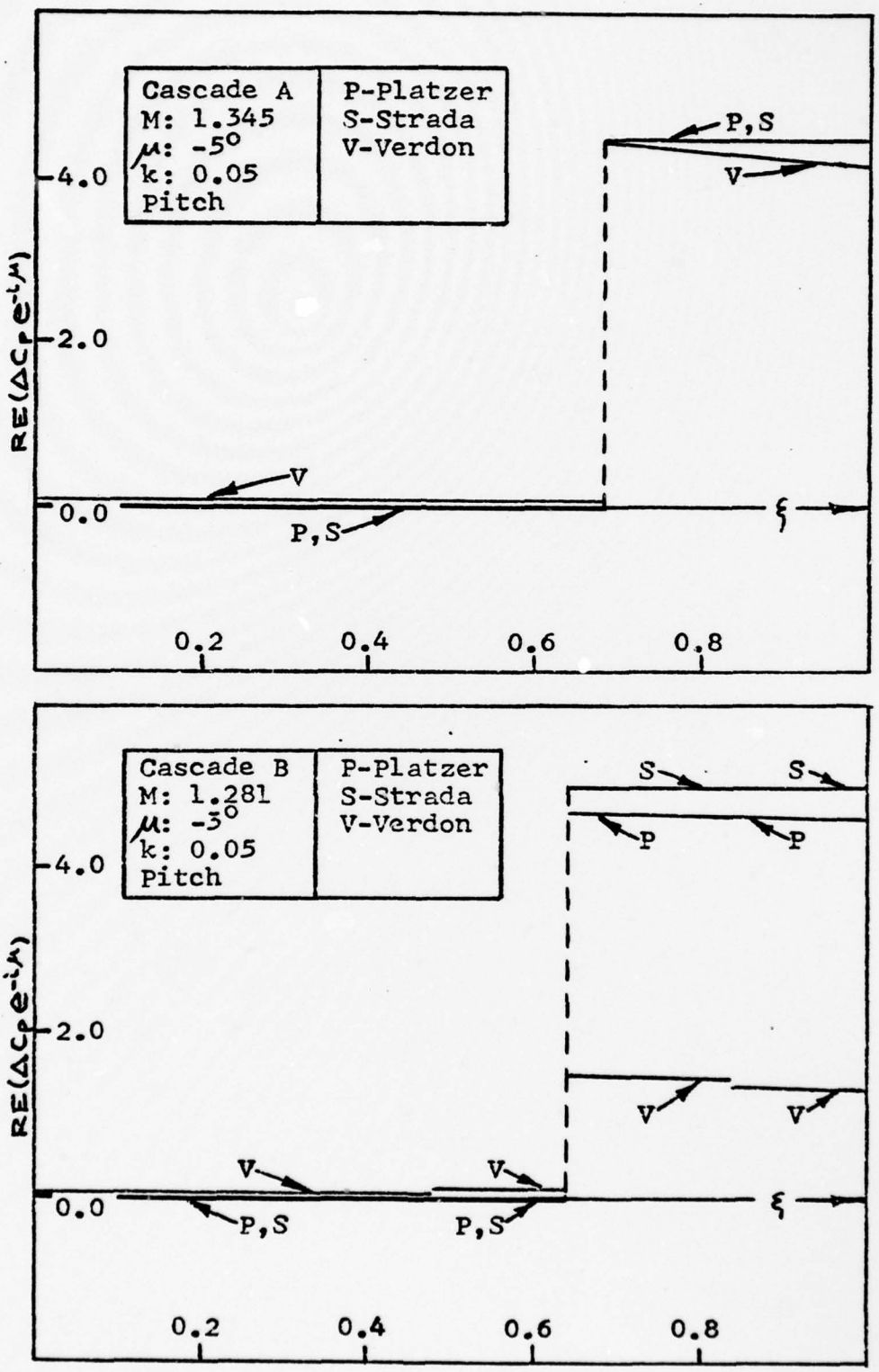

Figure 2.9.4 Low-frequency superresonant pressure distributions.

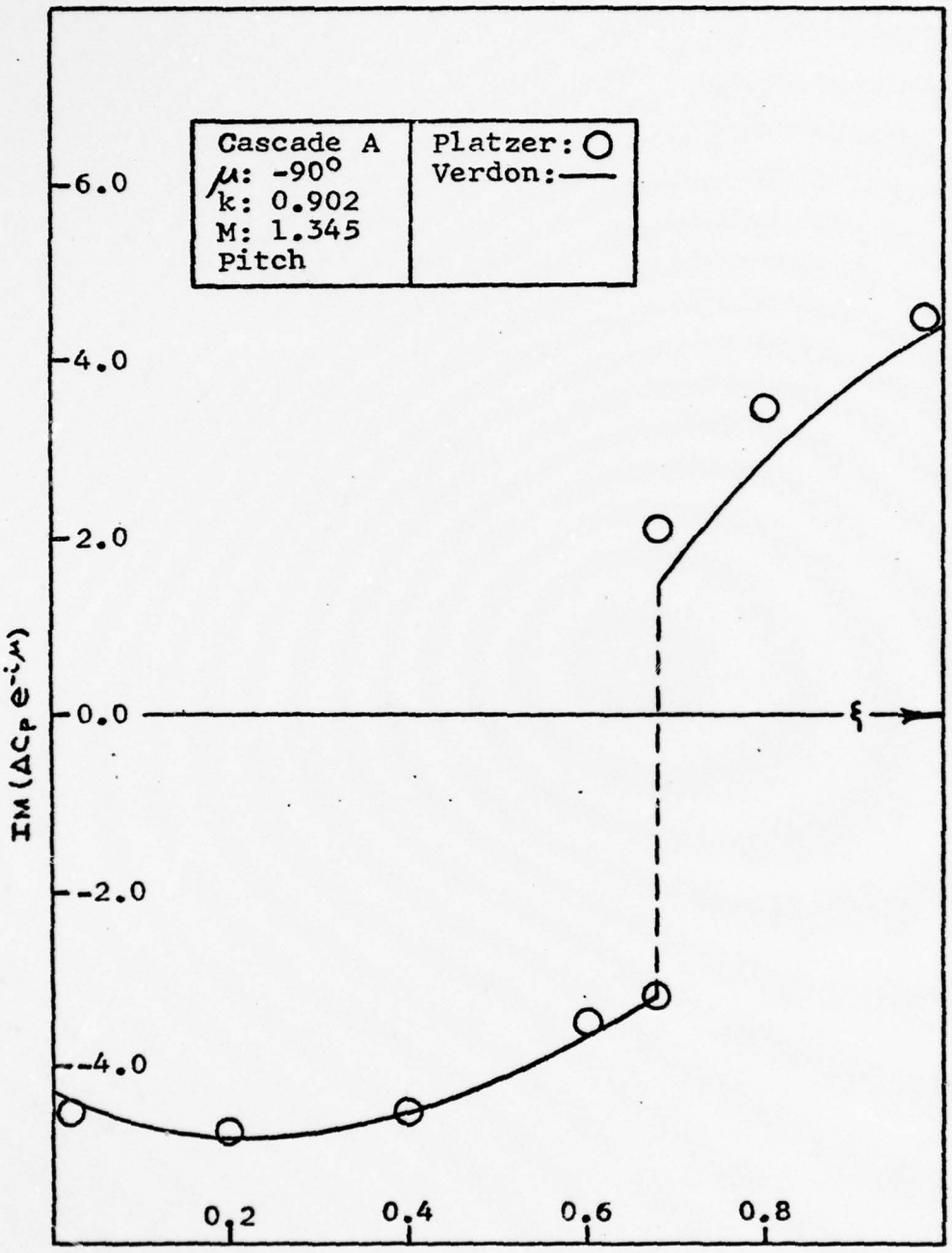

Figure 2.9.5 High-frequency superresonant pressure distributions.

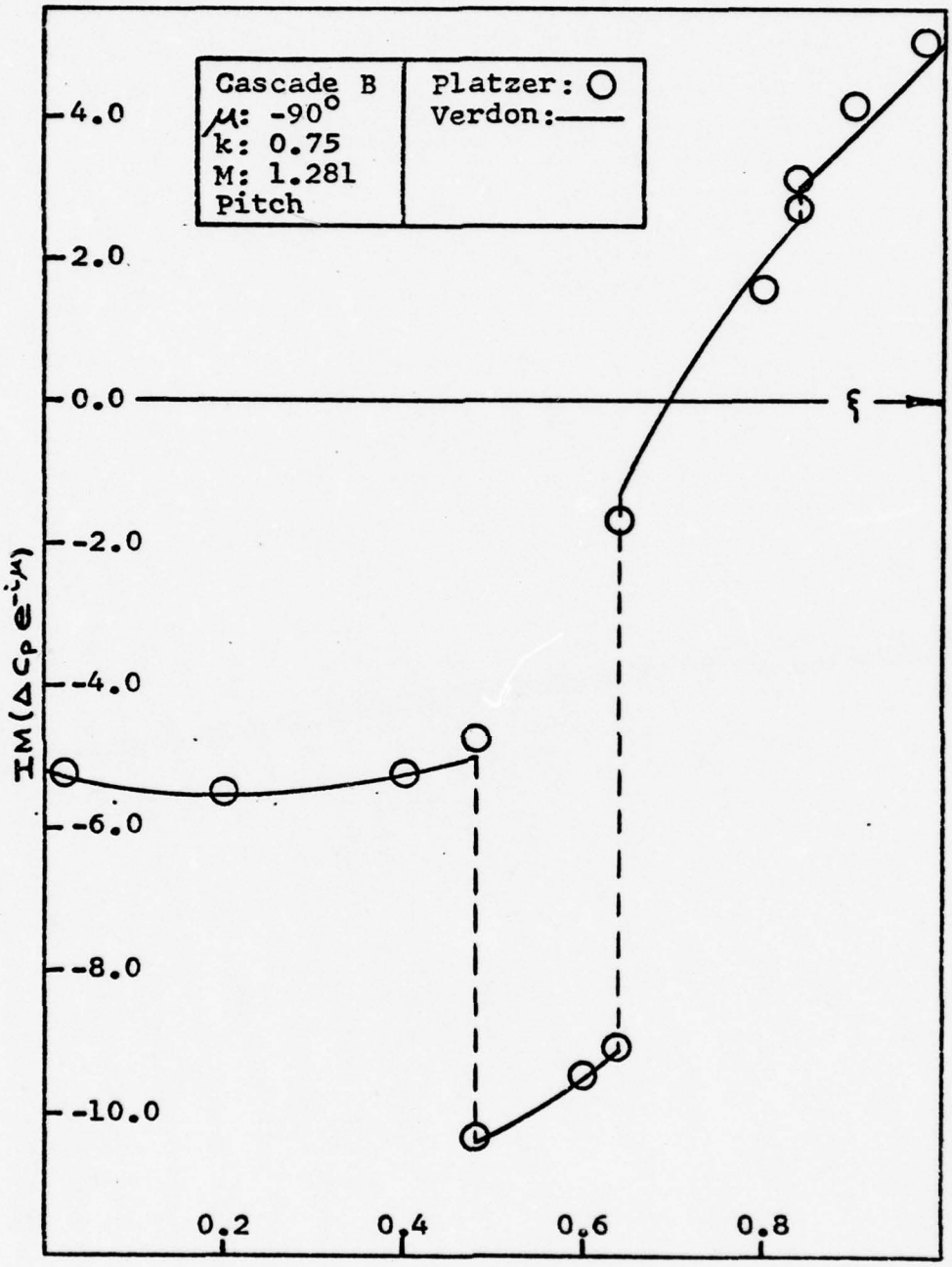

Figure 2.9.6 High-frequency superresonant pressure distributions.

3. THE NONLINEAR CASCADE

3.1 General. In two papers Teipel provides the numerical tools for the analysis of low supersonic flow past a single oscillating airfoil of finite thickness. In one paper [23] he presents an unsteady, nonlinear characteristics method to determine the continuous variation of flow variables. In the other [24] he treats the oscillating shock waves present in the nonlinear problem to permit determination of the discontinuous jumps in the flow variables across the shocks emanating from the single blade. Using these techniques as well as some computational and theoretical insight provided by Chadwick [5], who very ably translated and applied Teipel's work, the present study is aimed at finding the pressures, steady and unsteady, on the second blade of a parabolic-arc cascade. The cascade oscillates in pitch alone, and the pressures are sought over the entire upper blade surface and over the lower surface up to the point of impingement of the trailing-edge shock from the preceding blade (figure 3.2.2). These surface pressures are computed by means of a FORTRAN IV computer program prepared by the author for the IBM-360 computer. The program listing appears at the end of this work immediately after Appendix A. What follows is an orderly presentation of the theory underlying the computer program and the computational techniques used in implementing that theory. Wherever possible the text notation will coincide with that used in the program.

3.2 Cascade Geometry.

3.2.1 Blade Shape. The blade shape was chosen to approximate the blades in the test cascade employed by Fleeter and Riffel [25] who attempted to measure steady and unsteady pressures in a pitching cascade. The airfoil used in the computer model has a flat upper surface and a lower surface conforming to the parabolic arc given by

$$y = 4\tau x(x-1) \qquad (3.2.1)$$

where chordwise distance x and midchord thickness τ are normalized by chordlength. Figure 3.2.1 shows the computer model for $\tau = 0.03$ superimposed on Fleeter's test blade and lists the surface coordinates of the test blade in percent chord. The greatest discrepancy between the two shapes occurs on the aft portion of the blade in the region behind the lower-surface shock reflection; however, the lower-surface pressures are not computed in this region.

3.2.2 Blade Spacing. The blade spacing parameters are input variables for the program and are discussed in more detail in section 3.5.1. The physical spacing of the blades of the computer-model cascade – dubbed Cascade T – is shown in figure 3.2.2.

3.3 Teipel's Method of Characteristics. The underlying insight of Teipel's treatment of the unsteady problem is

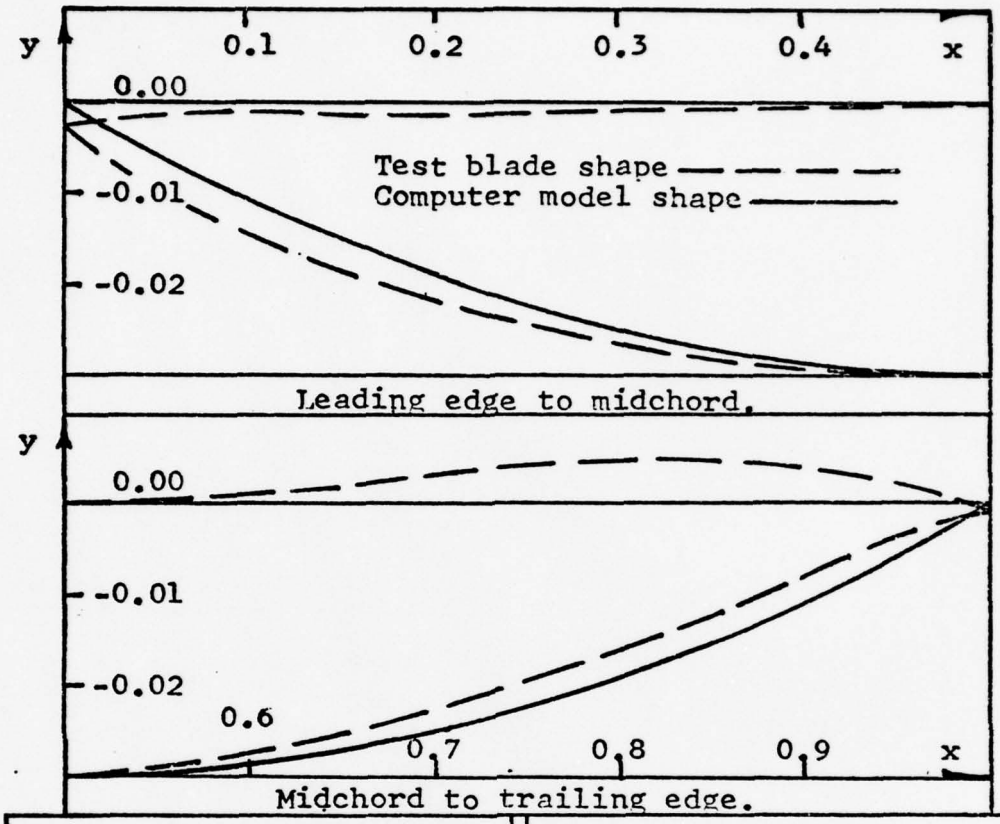

UPPER SURFACE				LOWER SURFACE			
x*	y*	x*	y*	x*	y*	x*	y*
0.00	-0.26	49.35	0.00	0.00	-0.26	50.51	-2.97
5.21	-0.14	55.65	0.10	6.29	-1.08	56.83	-2.84
11.53	-0.16	61.95	0.19	12.59	-1.65	63.15	-2.60
17.84	-0.16	68.25	0.29	18.90	-2.12	69.47	-2.27
24.14	-0.15	74.55	0.41	25.21	-2.49	75.78	-1.83
30.45	-0.13	80.88	0.50	31.53	-2.76	82.06	-1.37
36.75	-0.10	87.21	0.46	37.85	-2.93	88.36	-0.96
43.05	-0.04	93.53	0.26	44.18	-3.00	94.66	-0.62
		99.85	-0.10			99.86	-0.10

* Expressed in percent chord.

Surface coordinates.

Figure 3.2.1 Test blade shape and coordinates.

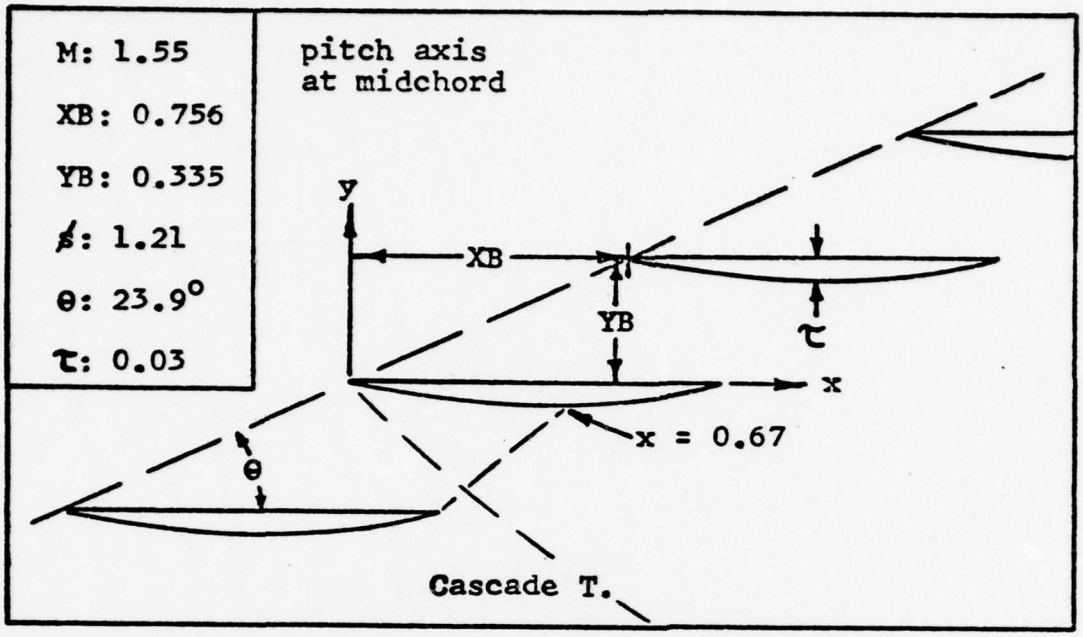

Figure 3.2.2 Geometry of the computer model.

his representation of the velocity potential as the sum of a steady component and a small-amplitude unsteady one

$$\phi(x,y,t) = \phi_0(x,y) + \phi_1(x,y)e^{ikt} \qquad (3.3.1)$$

as depicted in figure 3.3.1. When (3.3.1) is substituted into the transonic unsteady small-disturbance equation[1]

$$\left[\beta^2 + M^2(\gamma+1)\frac{\partial\phi}{\partial x}\right]\frac{\partial^2\phi}{\partial x^2} - \frac{\partial^2\phi}{\partial y^2} + 2M^2\frac{\partial^2\phi}{\partial x\,\partial t} + M^2\frac{\partial^2\phi}{\partial t^2} = 0 \qquad (3.3.2)$$

and into the unsteady boundary condition

---

[1]For a discussion of the limitations imposed by this equation see Teipel [23] and Chadwick [5].

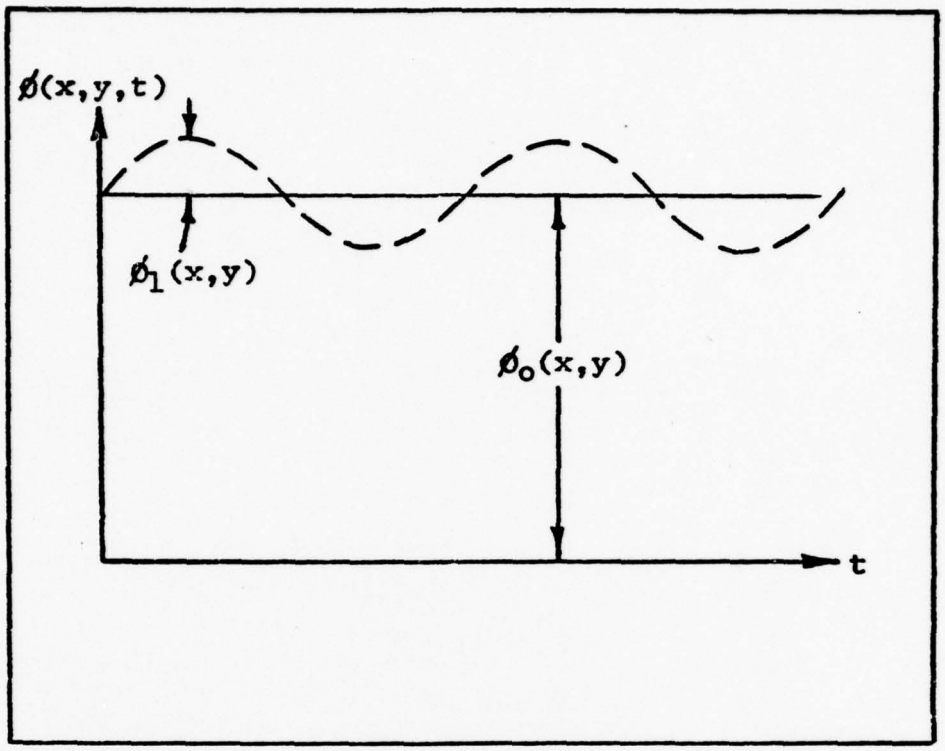

Figure 3.3.1 The total velocity potential.

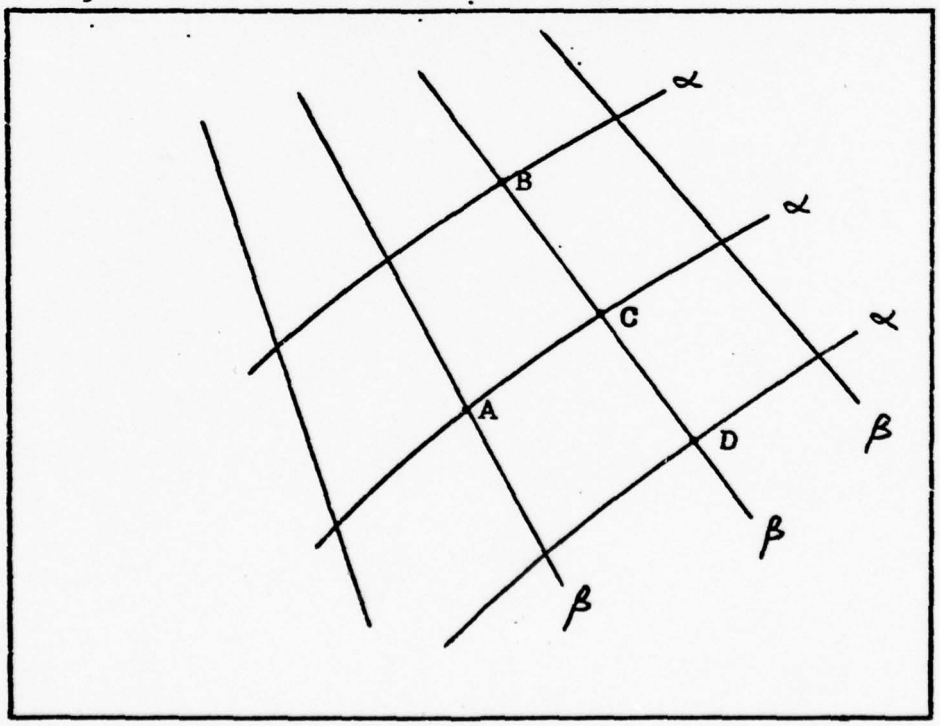

Figure 3.3.2 The characteristic grid.

$$\frac{\partial \phi}{\partial y} = \frac{\partial \bar{y}}{\partial x} + \frac{\partial \bar{y}}{\partial t} \qquad (3.3.3)$$

where $\bar{y}(x,t)$ describes the oscillating airfoil surface, one obtains two separate problems coupled by the steady velocity potential ϕ_o. One problem is nonlinear, steady and zero-angle-of-attack

$$\left[\beta^2 + M^2(\gamma+1)\frac{\partial \phi_o}{\partial x}\right]\frac{\partial^2 \phi_o}{\partial x^2} - \frac{\partial^2 \phi_o}{\partial y^2} = 0 \qquad (3.3.4)$$

$$\frac{\partial \phi_o}{\partial y} = \frac{\partial \bar{y}}{\partial x} \qquad (3.3.5)$$

and the other linear and unsteady

$$\left[\beta^2 + M^2(\gamma+1)\frac{\partial \phi_o}{\partial x}\right]\frac{\partial^2 \phi_1}{\partial x^2} - \frac{\partial^2 \phi_1}{\partial y^2} + \left[M^2(\gamma+1)\frac{\partial^2 \phi_o}{\partial x^2} + 2ikM^2\right]\frac{\partial \phi_1}{\partial x} - M^2k^2\phi_1 = 0 \qquad (3.3.6)$$

$$\frac{\partial \phi_1}{\partial y} = -\left[1 + ik(x-b)\right] \qquad (3.3.7)$$

where $\phi_1(x,y)$ is an amplitude function and the factor e^{ikt} is omitted. It is important to note that since the characteristic directions are determined by the coefficients of the highest derivatives, both problems will have the same characteristic directions. The state variables[1] for the two

---

[1] The symbol μ is used both for the steady state variable and the interblade phase angle, and it is normally clear from usage which meaning applies.

problems are essentially the steady and unsteady velocity components u_o, v_o, u_1 and v_1

STEADY: $$\lambda = \beta^2 + M^2(\gamma+1)u_o \tag{3.3.8}$$

$$\mu = 3/2\, M^2(\gamma+1)v_o \tag{3.3.9}$$

UNSTEADY: $$u_1, v_1 \tag{3.3.10}$$

where

$$\beta^2 = M^2 - 1 \tag{3.3.11}$$

The characteristic directions for both problems are

$$\left(\frac{dx}{dy}\right)_{\alpha,\beta} = \pm \frac{1}{\lambda^{1/2}} \tag{3.3.12}$$

where the upper sign refers to the left-running α characteristics and the lower to the right-running β characteristics.[1] The compatibility relations, however, are not the same for the two problems. They are

STEADY: $$\lambda^{3/2} \mp \mu = \text{CONST}_{\alpha,\beta} \tag{3.3.13}$$

---

[1]The symbol β is used both for the quantity $(M^2-1)^{\frac{1}{2}}$ and the right-running characteristic direction. It is normally clear from usage which meaning applies.

UNSTEADY:

$$du_1 \mp \frac{dv_1}{\lambda^{1/2}} + \frac{u_1}{2\lambda}\Delta_{\alpha,\beta} + \frac{2ikM^2}{\lambda}u_1\,dx - \frac{k^2M^2}{\lambda}\phi_1\,dx = 0 \qquad (3.3.14)$$

where

$$\Delta_\alpha = \left.\frac{\partial\lambda}{\partial x}\right)_\beta dx \qquad \Delta_\beta = d\lambda \qquad (3.3.15)$$

Equation (3.3.14) requires some additional comment. Note first that in addition to the state variables u_1 and v_1, ϕ_1 is also present in the unsteady compatibility relations. Since

$$d\phi_1 = \frac{\partial\phi_1}{\partial x}dx + \frac{\partial\phi_1}{\partial y}dy \qquad (3.3.16)$$

then ϕ_1 must be found by integration as one moves from one gridpoint to another. For the points A, B, and C shown in figure 3.3.2, for example

$$\alpha: \quad \phi_1^C = \phi_1^A + \int_A^C \left(u_1 + \frac{v_1}{\lambda^{1/2}}\right)dx \qquad (3.3.17)$$

$$\beta: \quad \phi_1^C = \phi_1^B + \int_B^C \left(u_1 - \frac{v_1}{\lambda^{1/2}}\right)dx \qquad (3.3.18)$$

In performing the actual computations an average of the two above expressions is employed.

The factor Δ_β in (3.3.14) is straightforward, representing the increment in λ along the β characteristic. At point C in figure 3.3.2 for example one could use the approximation

$$\Delta_\beta \doteq \lambda_c - \lambda_B \tag{3.3.19}$$

However Δ_α is a bit more complex, for while the increment dx is along the α characteristic, the quantity $\left.\frac{\partial \lambda}{\partial x}\right)_\beta$ represents the change in λ with respect to x along the crossing β characteristic at the point of interest. Again at point C one could employ

$$\Delta_\alpha \doteq \frac{\lambda_D - \lambda_B}{x_D - x_B}(x_c - x_A) \tag{3.3.20}$$

3.4 Teipel's Treatment of the Oscillating Shock Wave with Extension to the Present Cascade.[1]

3.4.1 The Isentropic Rankine-Hugoniot Pressure Relation.

Consider a normal shock moving through an undisturbed perfect gas at velocity V_s relative to the gas as shown in figure 3.4.1, where the hat notation indicates conditions behind the shock. The governing continuity, momentum and energy equations are

---

[1] Except for u_1, v_1, $\hat{u}_1$ and $\hat{v}_1$, the velocities appearing in sections 3.4.1 through 3.4.6 are dimensional, in a brief departure from the normalization of all velocities by the freestream velocity U.

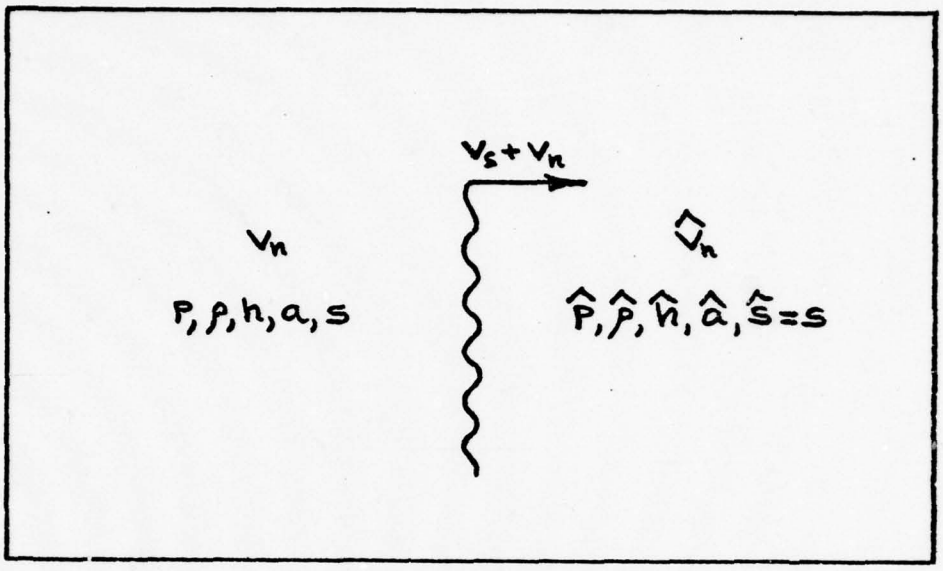

Figure 3.4.1 Jump conditions across a moving, normal shock.

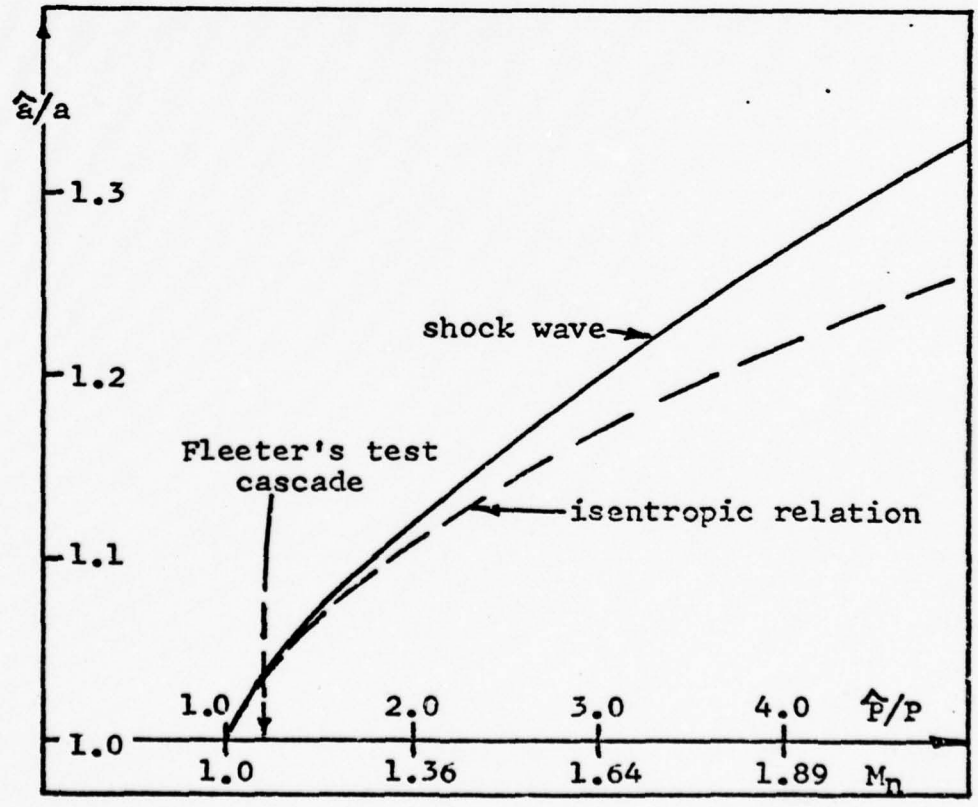

Figure 3.4.2 Consequences of the isentropic assumption.

$$\rho(-V_s) = \hat{\rho}(\hat{V}_n - V_s - V_n) \tag{3.4.1}$$

$$P + \rho V_s^2 = \hat{P} + \hat{\rho}(\hat{V}_n - V_s - V_n)^2 \tag{3.4.2}$$

$$h + \frac{V_s^2}{2} = \hat{h} + \frac{(\hat{V}_n - V_s - V_n)^2}{2} \tag{3.4.3}$$

Assuming constant specific heats, the speeds of sound are introduced, and the enthalpies are eliminated by

$$a^2 = \gamma \frac{P}{\rho} \qquad \hat{a}^2 = \gamma \frac{\hat{P}}{\hat{\rho}} \tag{3.4.4}$$

$$h = \frac{a^2}{\gamma - 1} \qquad \hat{h} = \frac{\hat{a}^2}{\gamma - 1} \tag{3.4.5}$$

and, after a good deal of manipulation, the change in the normal velocities across the shock is found in terms of the shock velocity and sound speed ahead of the shock

$$\frac{\hat{V}_n - V_n}{a} = \frac{2}{\gamma + 1}\left(\frac{V_s}{a} - \frac{a}{V_s}\right) \tag{3.4.6}$$

Equations (3.4.1) and (3.4.6) and the isentropic relation

$$\frac{\hat{P}}{P} = \left(\frac{\hat{a}}{a}\right)^{\frac{2\gamma}{\gamma - 1}} \tag{3.4.7}$$

yield the Rankine-Hugoniot pressure relation sought

$$\frac{\hat{P}}{P} = 1 + \frac{2\gamma}{\gamma + 1}\left[\left(\frac{V_s}{a}\right)^2 - 1\right] \tag{3.4.8}$$

Figure 3.4.2 is based on figure 8-3 of [29], and it shows that the isentropic approximation introduces no significant error for Fleeter's test cascade or its computer model.

3.4.2 The Blade-Two Shock Position. The leading-edge shock from the pitching blade oscillates out of phase with the blade. Let $\gamma_o(y)$ be the shock angle of the steady, leading-edge shock as shown in figure 3.4.3. Since the shock is curved, γ_o varies with distance y from the blade, and by convention

$$0 < \gamma_o < \frac{\pi}{2} \tag{3.4.9}$$

The shock angle at any point on the oscillating wave can be written as a small variation from the steady one[1]

$$\gamma = \gamma_o + \gamma' e^{ikt} \tag{3.4.10}$$

In order to locate the oscillating shock relative to the steady one, Teipel introduces the complex displacement function $g(y)$, also shown in figure 3.4.3, and so the x coordinate of a shock point is approximately

$$x = x_o + (y_o - y)\cot\gamma_o + g(y)e^{ikt} \tag{3.4.11}$$

---

[1]The symbol gamma used here and in figures 3.4.4 and 3.4.5 represents the total shock angle. All other uses of the unsubscripted, unsuperscripted gamma stand for the dimensionless ratio of specific heats.

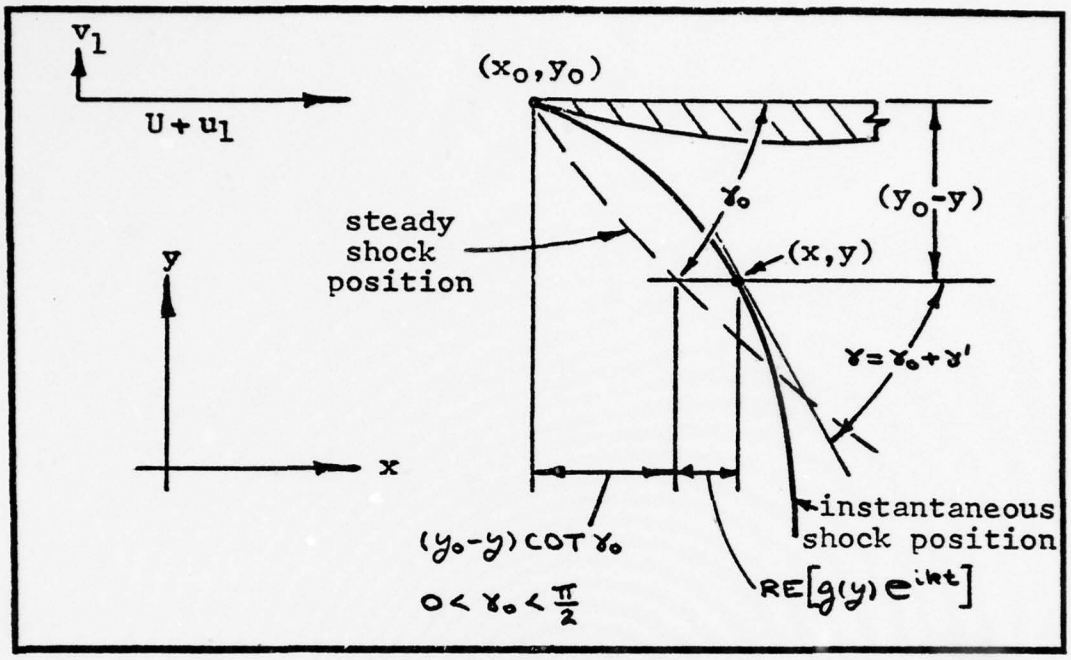

Figure 3.4.3 The oscillating leading-edge shock wave.

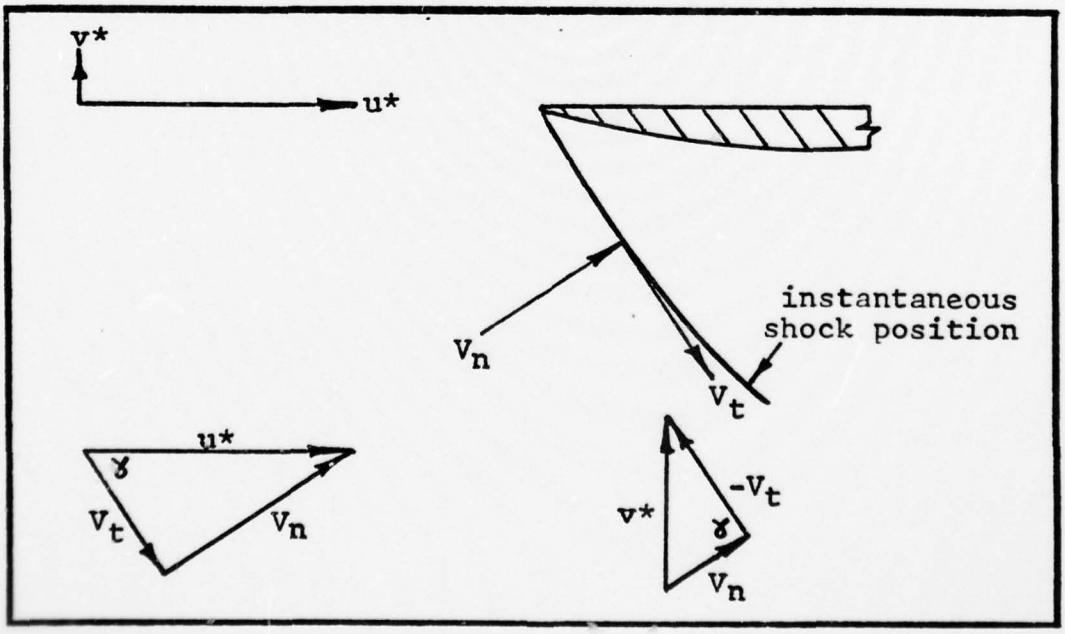

Figure 3.4.4 Velocity components and the oscillating shock wave.

where (x_o, y_o) are the steady coordinates of the blade's leading edge. Taking the total differential of (3.4.11) and noting that along the shock

$$\frac{\partial x}{\partial y} = -\cot \gamma \tag{3.4.12}$$

results in

$$\gamma' = \sin^2 \gamma_o \frac{d\varrho}{dy} e^{ikt} \tag{3.4.13}$$

thus relating shock angle and shock displacement.

3.4.3 The Velocity Components Upstream of the Blade-Two Shock Wave. Ahead of the shock the velocity components have both steady and unsteady parts

$$u^* = U + \bar{u}_o + \bar{u}_1 e^{ikt} \tag{3.4.14}$$

$$v^* = \bar{v}_o + \bar{v}_1 e^{ikt} \tag{3.4.15}$$

where the barred velocities are dimensional counterparts of the dimensionless quantities u_o, v_o, u_1 and v_1 already introduced in equations (3.3.8,9,10). However, the flat upper surfaces of the blades of cascade T are aligned with the flow in the steady position, and so, upstream of the shock

$$\bar{u}_o = \bar{v}_o = 0 \tag{3.4.16}$$

Referring to figure 3.4.4 one has for the normal and tangential velocity components ahead of the shock

$$V_n = U \sin\gamma_0 + U \cos\gamma_0 \gamma' + (\bar{u}_1 \sin\gamma_0 + \bar{v}_1 \cos\gamma_0) e^{ikt} \qquad (3.4.17)$$

$$V_t = U \cos\gamma_0 - U \sin\gamma_0 \gamma' + (\bar{u}_1 \cos\gamma_0 - \bar{v}_1 \sin\gamma_0) e^{ikt} \qquad (3.4.18)$$

3.4.4 The Blade-Two Shock-Motion-Induced Velocity. Relative to the gas ahead of it the shock is moving at the velocity

$$V_s = -V_n + V' \qquad (3.4.19)$$

where V' is a normal velocity induced by the motion of the shock, and is seen from figure 3.4.5 to be

$$V' = \frac{\partial x}{\partial t} \sin\gamma \qquad (3.4.20)$$

or, from (3.4.11)

$$V' = ikR \sin\gamma_0 \, g \, e^{ikt} \qquad (3.4.21)$$

3.4.5 The Velocity Jump Conditions Across the Blade-Two Shock. Using equation (3.4.13) to eliminate γ' from the expressions for the upstream velocity components (3.4.17,18), they become

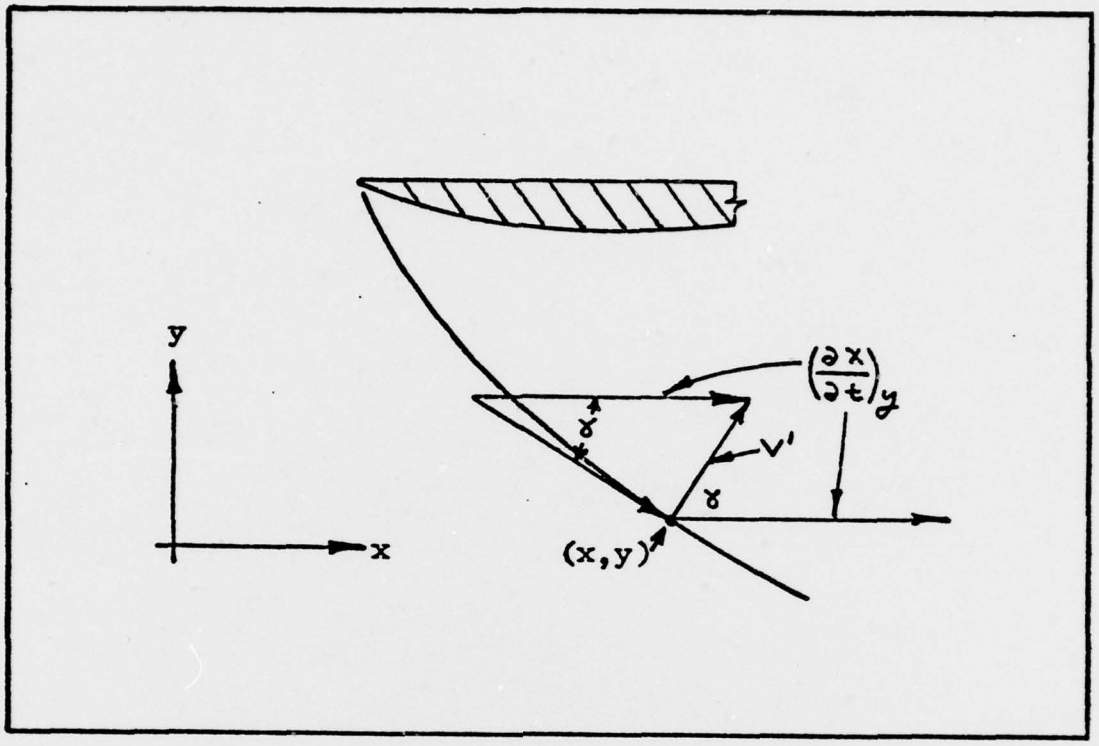

Figure 3.4.5 The shock-motion-induced velocity.

$$V_n = U \sin\gamma_o + (U \cos\gamma_o \sin^2\gamma_o \frac{dg}{dy} + \bar{u}_1 \sin\gamma_o + \bar{v}_1 \cos\gamma_o) e^{ikt} \quad (3.4.22)$$

$$V_t = U \cos\gamma_o + (-U \sin^3\gamma_o \frac{dg}{dy} + \bar{u}_1 \cos\gamma_o - \bar{v}_1 \sin\gamma_o) e^{ikt} \quad (3.4.23)$$

Note that each of the above velocities has three component parts. The first term in each expression arises from the steady shock position, the second arises from the oscillatory motion of the shock about that steady position, and the third and fourth terms arise from the unsteady disturbances ahead of the shock which are generated by the first blade's motion.

The components behind the shock are found by noting that the tangential component does not change

$$\hat{V}_t = V_t \tag{3.4.24}$$

and by using (3.4.6,19,21,22) to obtain

$$\begin{aligned}\hat{V}_n = {} & \frac{\gamma-1}{\gamma+1} U \sin\gamma_0 \left(1 + \frac{2}{\gamma-1}\frac{1}{M_N^2}\right) \\ & + \left[\frac{\gamma-1}{\gamma+1} U \cos\gamma_0 \sin^2\gamma_0 \left(1 - \frac{2}{\gamma-1}\frac{1}{M_N^2}\right)\frac{d\vartheta}{dy}\right. \\ & + \frac{2}{\gamma+1}\left(1+\frac{1}{M_N^2}\right)(ik \sin\gamma_0\, \vartheta) \\ & \left. + \frac{\gamma-1}{\gamma+1}\left(1-\frac{2}{\gamma-1}\frac{1}{M_N^2}\right)(\bar{u}_1 \sin\gamma_0 + \bar{v}_1 \cos\gamma_0)\right] e^{ikt}\end{aligned} \tag{3.4.25}$$

where

$$M_N = M \sin\gamma_0 \tag{3.4.26}$$

It is convenient to once again return to the dimensionless x-y velocity components $\hat{u}_1$ and $\hat{v}_1$, obtaining from the unsteady terms of (3.4.24,25)

$$\hat{u}_1 = m_1 \frac{d\vartheta}{dy} + i m_2 \vartheta + m_3 u_1 + m_4 v_1 \tag{3.4.27}$$

$$\hat{v}_1 = n_1 \frac{d\vartheta}{dy} + i n_2 \vartheta + n_3 u_1 + n_4 v_1 \tag{3.4.28}$$

where the factor e^{ikt} has been dropped and

$$m_1 = -\frac{2}{\gamma+1} \sin 2\gamma_o \sin^2 \gamma_o \tag{3.4.29}$$

$$m_2 = \frac{2}{\gamma+1} k\left(1+\frac{1}{M_N^2}\right) \sin^2 \gamma_o \tag{3.4.30}$$

$$m_3 = \cos^2 \gamma_o + \frac{\gamma-1}{\gamma+1} \sin^2 \gamma_o \left(1-\frac{2}{\gamma-1}\frac{1}{M_N^2}\right) \tag{3.4.31}$$

$$m_4 = -\frac{\sin 2\gamma_o}{2} + \frac{\gamma-1}{\gamma+1}\frac{\sin 2\gamma_o}{2}\left(1-\frac{2}{\gamma-1}\frac{1}{M_N^2}\right) \tag{3.4.32}$$

$$n_1 = -\frac{2}{\gamma+1}\left(\cos 2\gamma_o + \frac{1}{M_N^2}\right) \sin^2 \gamma_o \tag{3.4.33}$$

$$n_2 = \frac{2}{\gamma+1} k\left(1+\frac{1}{M_N^2}\right) \cot \gamma_o \sin^2 \gamma_o \tag{3.4.34}$$

$$n_3 = m_4 \tag{3.4.35}$$

$$n_4 = \sin^2 \gamma_o + \frac{\gamma-1}{\gamma+1} \cos^2 \gamma_o \left(1-\frac{2}{\gamma-1}\frac{1}{M_N^2}\right) \tag{3.4.36}$$

Note that the above coefficients are functions of the local shock angle γ_o and so are not constant along the shock.

If no unsteady disturbances exist upstream of the shock ($u_1 = v_1 = 0$) then (3.4.27,28) reduce to Teipel's single-blade results. If, in addition, the shock does not oscillate ($g = dg/dy = 0$), then $\hat{u}_1$ and $\hat{v}_1$ are identically zero indicating that there are no unsteady disturbances behind the shock. Equations (3.4.27,28) represent an extension of

Teipel's work from the single blade to the cascade, and they were first obtained by Chadwick for a cascade of wedges. It is noted for completeness that the above equations would apply equally well to an upper-surface shock wave if the signs of m_1, m_4, n_2 and n_3 were reversed.

3.4.6 The Pressure Jump Conditions Across the Blade-Two Shock. An additional extension of Teipel's work was accomplished by the author in order to develop a more accurate method of determining the flow-variable discontinuities than that employed by either Chadwick or Teipel. The improved method is treated in more detail in section 3.8, but it is based on the extension of the Rankine-Hugoniot pressure relation (3.4.8) to the cascade via equations (3.4.19,20,21), resulting in

$$\frac{\hat{p}}{P} = p_1 \frac{d\vartheta}{dy} + i\, p_2 g + p_3 u_1 + p_4 v_1 \qquad (3.4.37)$$

where

$$p_1 = \frac{2\gamma}{\gamma+1} M_N^2 \sin 2\gamma_0 \qquad (3.4.38)$$

$$p_2 = -\frac{4\gamma}{\gamma+1} M_N^2 k \qquad (3.4.39)$$

$$p_3 = \frac{4\gamma}{\gamma+1} M_N^2 \qquad (3.4.40)$$

$$p_4 = \frac{4\gamma}{\gamma+1} M_N^2 \cot \gamma_0 \qquad (3.4.41)$$

Equation (3.4.37) relates the pressure jump across the shock to the shock displacement and the upstream unsteady velocities. In the single-blade case u_1 and v_1 are zero, and Teipel's result is recovered.

3.4.7 The Boundary Conditions for the Shock Equations. In section 3.8, the flow variables behind the shock are obtained by the simultaneous solution of the difference equations resulting from (3.3.14) and the shock equations (3.4.27,28,37). In order to start the solution process, then, several quantities must initially be known at the point of intersection of the shock and blade, i.e. at (x_o, y_o). From figure 3.4.3 it is clear that

$$g(y_o) = 0 \qquad (3.4.42)$$

Also, immediately behind the shock the flow tangency condition for the second blade must hold

$$\hat{v}_1 = -\left[1 + ik(x_o - b)\right] e^{i\mu} \quad \text{at } (x_o, y_o) \qquad (3.4.43)$$

With v_1 known equation (3.4.28) provides

$$\frac{dg}{dy} = \frac{1}{n_1}(\hat{v}_1 - n_3 u_1 - n_4 v_1) \quad \text{at } (x_o, y_o) \qquad (3.4.44)$$

and (3.4.44) used with (3.4.27,37) gives the remaining boundary conditions

$$\hat{u}_1 = \frac{m_1}{n_1}\hat{v}_1 + \frac{m_3 n_1 - m_1 n_3}{n_1} u_1 + \frac{m_4 n_1 - m_1 n_4}{n_1} v_1 \quad \text{at } (x_0, y_0) \qquad (3.4.45)$$

$$\frac{\hat{p}}{p_\infty} = \frac{p}{p_\infty} + \frac{p_1}{n_1}\hat{v}_1 + \frac{p_3 n_1 - p_1 n_3}{n_1} u_1 + \frac{p_4 n_1 - p_1 n_4}{n_1} v_1 \quad \text{at } (x_0, y_0) \qquad (3.4.46)$$

Of course for equations (3.4.43) through (3.4.46) the hatted quantities are just behind the shock at (x_o, y_o). Equation (3.4.45) was derived by Chadwick while (3.4.46) is the author's result.

3.4.8 <u>The Velocity Potential Jump Conditions Across the Blade-Two Shock</u>. Landahl [26] shows that the total velocity potential (3.3.1) is continuous across the leading-edge shock, but this does not imply that either the steady or unsteady component is individually continuous. Teipel and Chadwick choose to assume that, at the first shock point

$$\phi_1(x_0, y_0) = \hat{\phi}_1(x_0, y_0) \qquad (3.4.47)$$

The author, on the other hand, chooses to find the initial velocity potential jump at the point (x_o, y_o). For a perfect gas with constant specific heats, it can be shown that

$$\hat{\phi}_1 = \frac{i}{k}\left(\hat{u}_1 + \frac{\hat{P}/P_\infty}{\gamma M^2}\right) \qquad (3.4.48)$$

and since $\hat{u}_1$ and $\hat{P}/P_\infty$ are known at (x_o, y_o) from equations (3.4.45,46), then so is $\hat{\phi}_1$. Figure 3.4.6 is a plot of computer data for cascade T, and it shows the discontinuity in ϕ_1 along the shock as a function of distance from the blade. Note that the initial discontinuity is small justifying Teipel's assumption (3.4.47), but equation (3.4.48) eliminates having to make that assumption at all.

3.5 Constructing the Characteristic Grid. Because the characteristic directions are the same for both the steady and unsteady problem, the characteristic grid can be constructed and employed to find both the steady and unsteady velocities. The grids above blade one (zone A) and above blade two (zone C) are composed of two families of straight, parallel characteristics. The mesh below blade two (zone B), however, is composed of one straight, divergent family (β) and one curved family (α).

3.5.1 The Straight Characteristic Grids Above Blades One and Two. Since the upper blade surfaces generate no steady disturbances, it is seen from (3.3.8) that, in zones A and C

$$\lambda_A = \lambda_C = M^2 - 1 = \beta^2 \qquad (3.5.1)$$

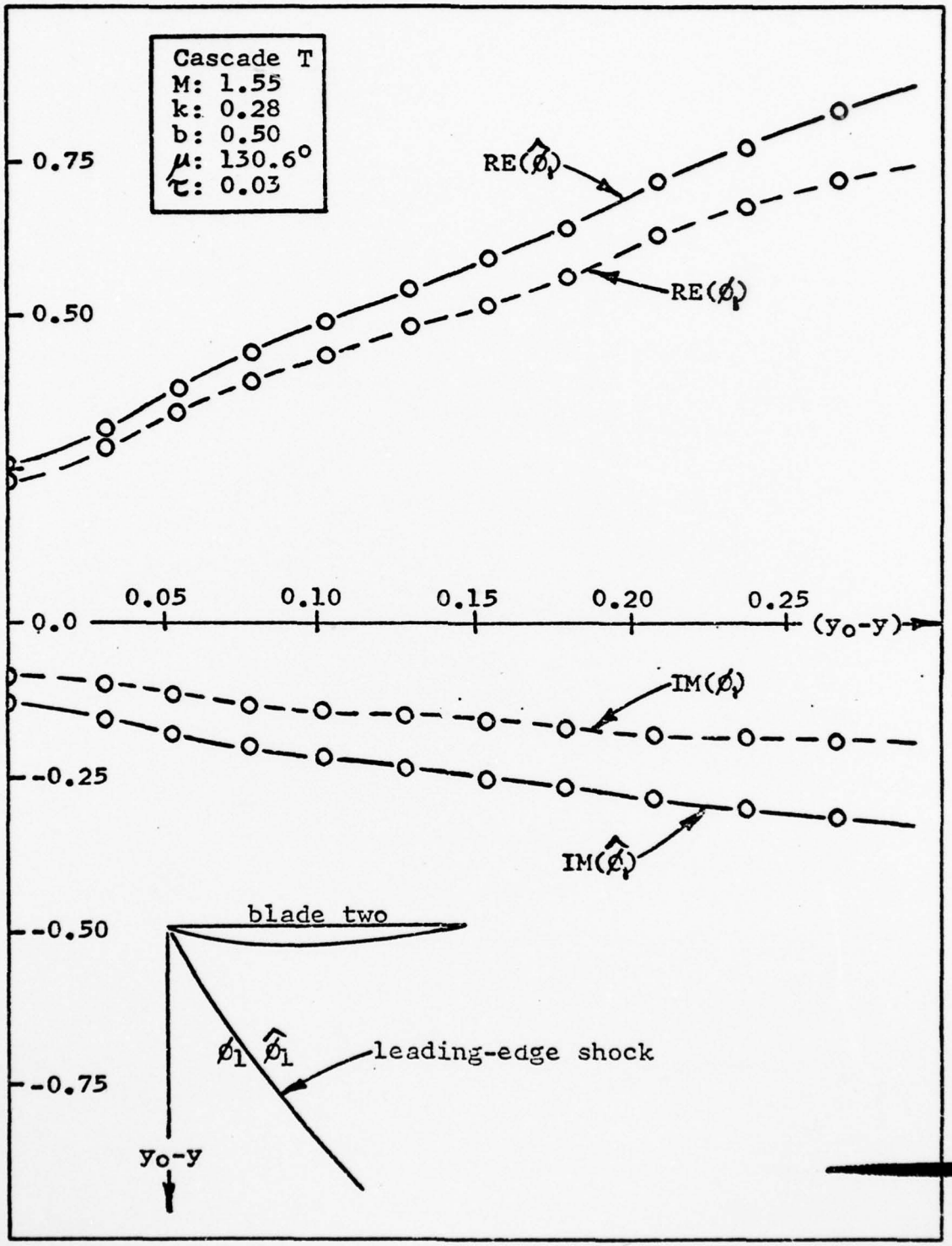

Figure 3.4.6 The discontinuous jump in the unsteady velocity potential across the leading-edge shock.

and so the characteristics in those zones are simply Mach waves (figure 3.5.1). Each blade has 21 equispaced upper-surface gridpoints, and the program requires that the leading edge of the second blade be positioned at one of the straight-mesh gridpoints. This is accomplished via the input parameters K and N which fix the cascade blade spacing according to

$$YB = 0.025 \frac{K}{\beta} \tag{3.5.2}$$

$$XB = YB\,\beta + 0.05\,N \tag{3.5.3}$$

For cascade T, K and N are 16 and 7 respectively. Figure 3.5.1 also shows the characteristic numbering convention employed in the program, so that a gridpoint may be located by two characteristic coordinates

$$(I_\alpha, J_\beta) \tag{3.5.4}$$

Note that the straight mesh is computed as if both blades were flat plates. The x-y coordinates of the straight mesh are referred to as X1, Y1 in the computer program.

3.5.2 The Curved Characteristic Grid Below Blade Two. In zone B (figure 3.5.2) the characteristic grid is non-linear and must be constructed iteratively. Figure 3.5.2 reveals the numbering convention employed for the curved mesh. The curved-mesh x-y coordinates are referred to as

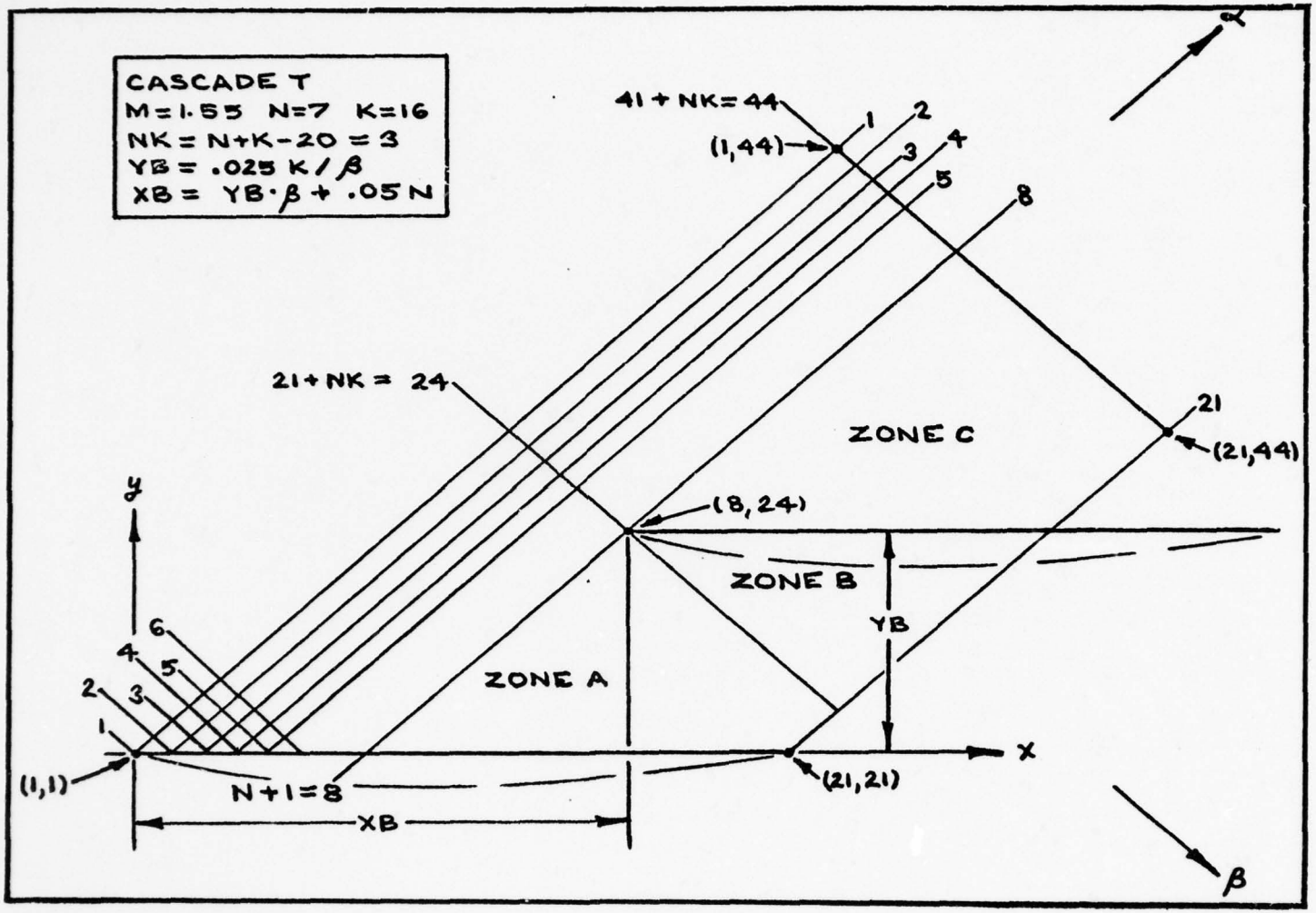

Figure 3.5.1 The straight characteristic grid.

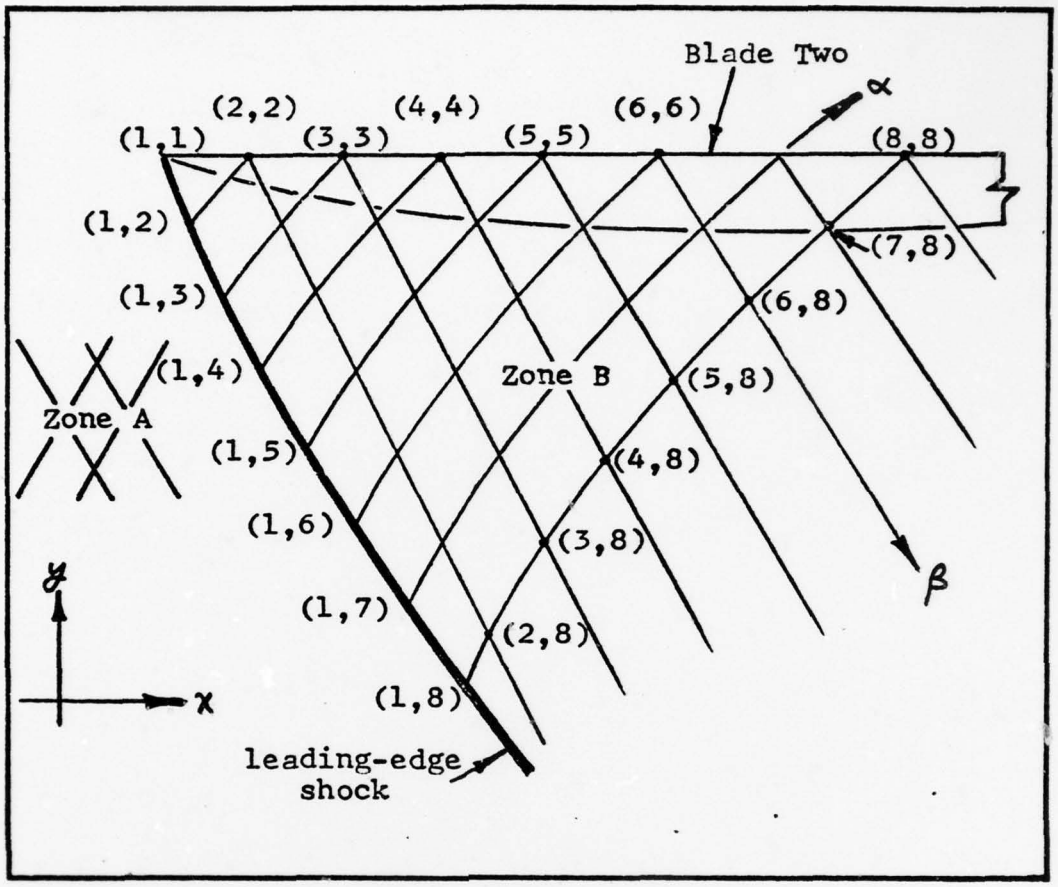

Figure 3.5.2 The curved characteristic grid.

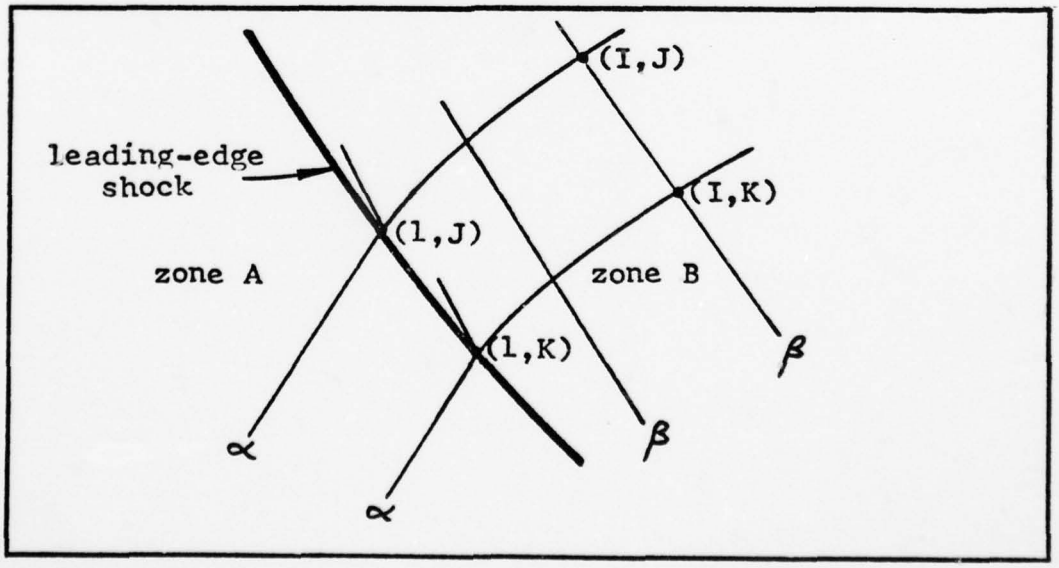

Figure 3.5.3 Characteristic lines through the shock.

AD-A053 211 NAVAL POSTGRADUATE SCHOOL MONTEREY CALIF F/G 20/4
ANALYSIS OF SUPERSONIC FLOW PAST OSCILLATING CASCADES USING LIN--ETC(U)
SEP 77 J A STRADA

UNCLASSIFIED NL

2 OF 2
AD
A053211

END
DATE
FILMED
6-78
DDC

2 OF 2

AD
A053211

X2,Y2 in the program to distinguish them from those of the straight mesh. Before proceeding with the grid consturction, some useful relations are obtained.

For an α characteristic passing through the shock from zone A to zone B (figure 3.5.3)

$$\lambda_A^{3/2} - \mu_A = \lambda_B^{3/2} - \mu_B \qquad (3.5.5)$$

and since μ_A is zero

$$\lambda_B = (\lambda_A^{3/2} + \mu_B)^{2/3} \qquad (3.5.6)$$

Now consider two points on the same β characteristic, also illustrated in figure 3.5.3. From the α compatibility relation

$$\lambda(I,J)^{3/2} - \mu(I,J) = \lambda_A^{3/2} \qquad (3.5.7)$$

$$\lambda(I,K)^{3/2} - \mu(I,K) = \lambda_A^{3/2} \qquad (3.5.8)$$

and from the β compatibility relation

$$\lambda(I,J)^{3/2} + \mu(I,J) = \lambda(I,K)^{3/2} + \mu(I,K) \qquad (3.5.9)$$

and so it must be that

$$\lambda(I,J) = \lambda(I,K) \qquad \mu(I,J) = \mu(I,K) \qquad (3.5.10)$$

which proves, in addition, that the β family is composed of straight lines.

The steady shock angle at any point along the shock is found by averaging the angles of the characteristic lines before and after the shock, i.e.

$$\gamma_o = \frac{1}{2}\left[\tan^{-1}(\lambda^{-1/2}) + \tan^{-1}(\hat{\lambda}^{-1/2})\right] \qquad (3.5.11)$$

Taking the tangent of (3.5.11) and applying the sum and double-angle trigonometric formulae leads to a quadratic equation in tan γ_o

$$(\lambda^{1/2} + \hat{\lambda}^{1/2})\tan^2\gamma_o + 2(\lambda^{1/2}\hat{\lambda}^{1/2} - 1)\tan\gamma_o - (\lambda^{1/2} + \hat{\lambda}^{1/2}) = 0 \qquad (3.5.12)$$

The solution of (3.5.12) is rather cumbersome and is adquately approximated by the simpler expression

$$\tan\gamma_o = \frac{2}{\lambda^{1/2} + \hat{\lambda}^{1/2}} \qquad (3.5.13)$$

In the computational implementation of (3.5.13), referring to figure 3.5.3 again, the characteristic angles at adjacent points behind the shock are first averaged together, and the result is averaged with the zone-A angle, i.e.

$$\tan\gamma_o = \frac{4}{2\lambda_A^{1/2} + \lambda(I,J)^{1/2} + \lambda(I,K)^{1/2}} \qquad (3.5.14)$$

3.5.2.1 Computing the Point (1,1). The X2-Y2 coordinates of (1,1) are of course those of the blade-two leading edge. $\mu(1,1)$ is found from the steady boundary condition (3.3.5) and equation (3.3.9) while $\lambda(1,1)$ follows from (3.5.6).

3.5.2.2 Computing the Points (1,2) and (2,2). The points (1,2) and (2,2) are established iteratively as follows. Program subroutines employed are indicated in parentheses, and figure 3.5.4 is provided for reference.

1. Establish the reference point XA on the blade, close to the leading edge

$$XA = X2(1,1) + 0.005$$

2. Compute μ at XA, which is equal to $\mu(1,2)$, using the steady boundary condition (3.3.5) and (3.3.9).

3. Compute λ at XA, which is equal to $\lambda(1,2)$, using equation (3.5.6).

4. (Subroutine SOLVE) Locate (1,2) at the intersection of a line through (XA, Y2(1,1)) with slope

$$\frac{-1}{\lambda(1,2)^{1/2}}$$

and a line through (X2(1,1), Y2(1,1)) with slope

$$\frac{-4}{2\lambda_A^{1/2} + \lambda(1,1)^{1/2} + \lambda(1,2)^{1/2}}$$

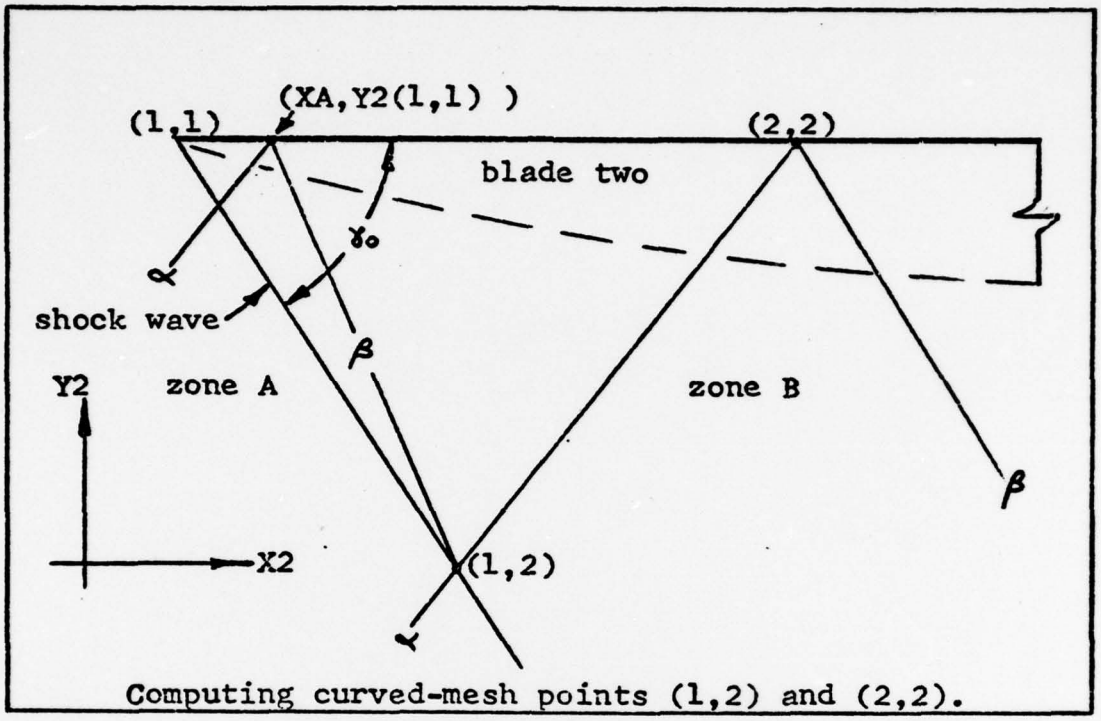

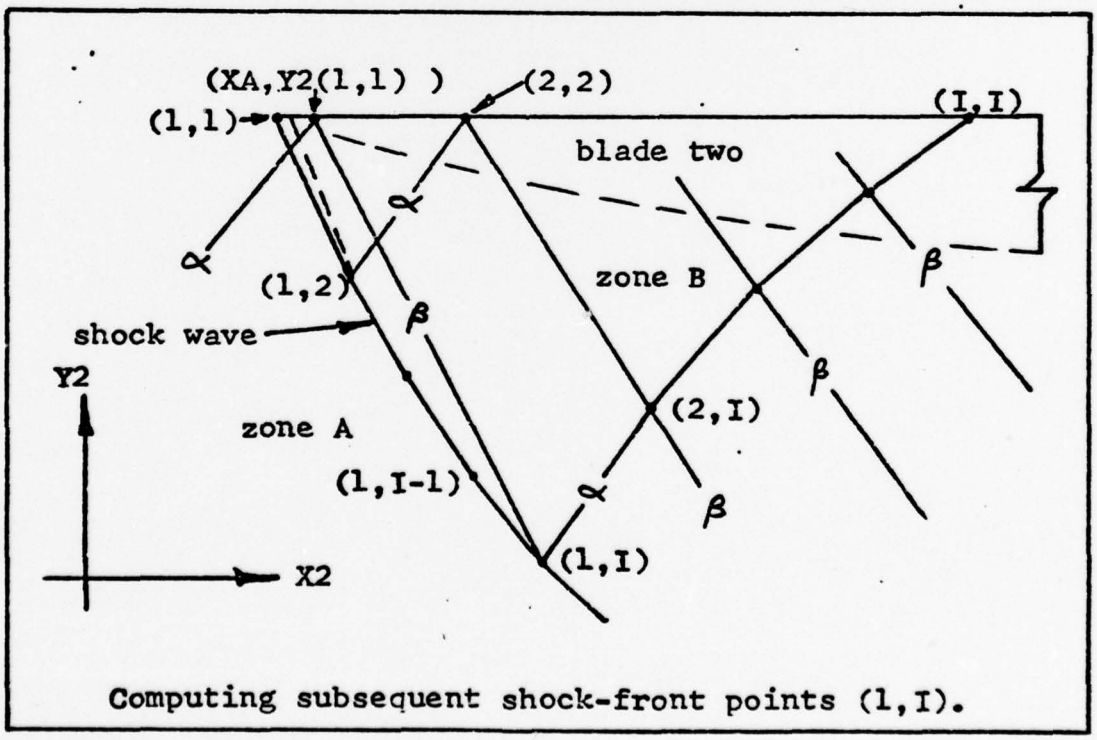

Figure 3.5.4 Computing the shock-front points.

5. (Subroutine ITER) Guess at the position of (2,2) on the blade

$$\overline{X2}(2,2) = X2(1,1)$$

6. (Subroutine ITER) Increment that guess

$$\overline{X2}(2,2) = \overline{X2}(2,2) + 0.001$$

7. (Subroutine ITER) Compute $\mu(2,2)$ from (3.3.5,9).

8. (Subroutine ITER) Compute $\lambda(2,2)$ from (3.5.6).

9. (Subroutine ITER) Solve for X2(2,2) from the slope of the α characteristic through (1,2) and (2,2)

$$\frac{X2(2,2) - X2(1,2)}{Y2(2,2) - Y2(1,2)} = \frac{2}{\lambda(1,2)^{1/2} + \lambda(2,2)^{1/2}}$$

10. (Subroutine ITER) Does $X2(2,2) = \overline{X2}(2,2)$?

YES: GO TO 11; NO: GO TO 6.

11. STOP.

3.5.2.3 <u>Computing Subsequent Shock Front Points</u>. Subsequent points (1,I) along the shock are also found iteratively. The technique follows, and figure 3.5.4 applies.

1. Relocate XA on the blade

$$XA = XA + DXA$$

where DXA is based on the first position of XA

$$DXA = \frac{X2(2,2) - XA}{15}$$

2. (Subroutine SHOKPT) Guess $\lambda(1,I)$

$$\lambda(1,I) = \lambda(1,I-1)$$

3. (Subroutine SHOKPT) Increment that guess.

$$\lambda(1,I) = \lambda(1,I) + 0.001$$

4. (Subroutine SHOKPT) Compute $\mu(1,I)$ using μ and λ at $(2,I)$, which are the same respectively as $\mu(2,2)$ and $\lambda(2,2)$

$$\mu(1,I) = \lambda(1,I)^{3/2} - \lambda(2,2)^{3/2} + \mu(2,2)$$

5. (Subroutine SOLVE) Locate $(1,I)$ at the intersection of a line through (XA, Y2(1,1)) with slope

$$\frac{-1}{\lambda(1,I)^{1/2}}$$

and a line through (X2(1,I-1), Y2(1,I-1)) with slope

$$\frac{-4}{2\lambda_A^{1/2} + \lambda(1,I-1)^{1/2} + \lambda(1,I)^{1/2}}$$

6. (Subroutine SHOKPT) Compute $\bar{\mu}(1,I)$ from the steady boundary condition (3.3.5) at XA and equation (3.3.9).

7. (Subroutine SHOKPT) Does $\mu(1,I) = \bar{\mu}(1,I)$? YES: GO TO 8; NO: GO TO 3.

8. STOP.

3.5.2.4 Computing the Curved-Mesh Interior Points. A point (I,J) interior to the curved mesh is located (figure 3.5.5) at the intersection of a line passing through (I-1,J) with slope

$$\frac{1}{\lambda(I-1,J)^{1/2}}$$

and a line through (I,I) with slope

$$\frac{-1}{\lambda(I,I)^{1/2}}$$

3.5.2.5 Computing Subsequent Blade-Surface Points. Subsequent points of the form (I,I) on the lower surface are computed in a manner exactly analagous to the computation of the point (2,2) as described in steps 5 through 11 of section 3.5.2.2.

3.6 Computing the Steady Velocities and Pressures. With μ and λ known throughout the grid, the steady velocities follow directly from (3.3.8,9). The steady pressures on

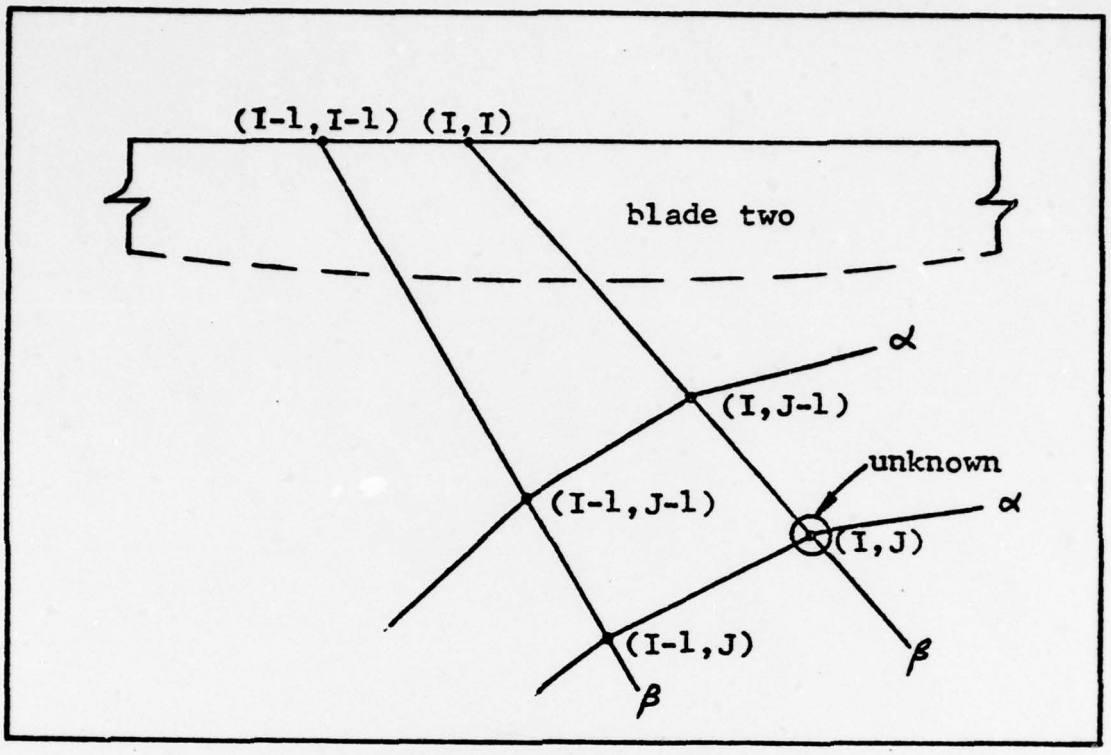

Figure 3.5.5 Computing the curved-mesh interior points.

the upper surface of blade two are zero and on the lower surface are given at the surface points (I,I) by

$$C_{p_0} = -2\, u_0(I,I) \qquad (3.6.1)$$

3.7 Computing the Unsteady Flow Variables at the Straight-Mesh Grid Points.

3.7.1 The Blade-One Upper-Surface Grid Points. In the straight mesh the unsteady velocities and velocity potential are designated by

$$u_1 = U11R + i\ U11I \qquad v_1 = V11R + i\ V11I$$

$$\phi_1 = F1R + i\ F1I \qquad (3.7.1)$$

The unsteady boundary condition for blade one (3.3.7) allows determination of the v_1 velocities

$$V1lR(I,I) = -1 \quad V1lI(I,I) = -k\left[X1(I,I) - b\right] \qquad (3.7.2)$$

Using the β compatibility relation (3.3.14) in difference form results in a system of linear equations for the unknowns U1lR(I,I), U1lI(I,I) . Figure 3.7.1 A applies, and the equations appear in matrix form in section A.1 of the appendix. The velocity potential is found by integration of the velocities, using equation (3.3.18); see section A.2 of appendix A.

3.7.2 The Straight-Mesh Field Points. As seen in figure 3.7.1 B, grid points not on the blade require use of both compatibility relations. The equations resulting for the unknown u_1 and v_1 velocities at each field point (I,J) are given in A.3 of the appendix. Equations (3.3.17,18) are averaged to find the velocity potential; see section A.4 of the appendix.

3.7.3 The Grid Points Immediately Upstream of the Shock. Figure 3.7.1 C shows that the shock points lie in the straight mesh and therefore the flow variables at each shock point — upstream of the shock — are found by means of an interpolation algorithm. The distances RI in figure 3.7.1 C are computed and any desired quantity Q(1,K) is found from the values of Q at the four surrounding points

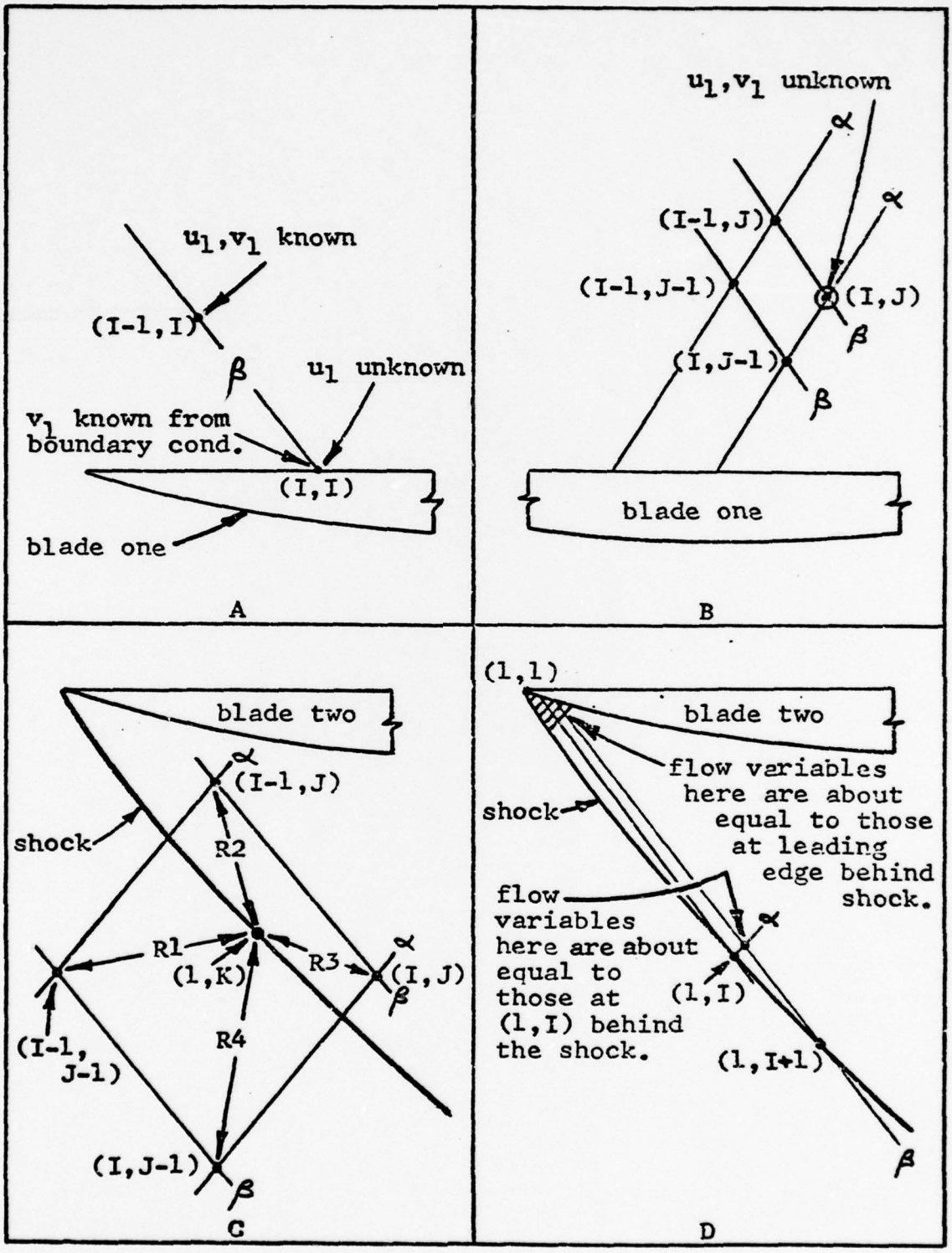

Figure 3.7.1 Computing the straight-mesh and curved-mesh grid points.

$$Q(I,K) = \frac{RR1\ Q(I-1,J-1)+RR2\ Q(I-1,J)+RR3\ Q(I,J)+RR4\ Q(I,J-1)}{RD} \qquad (3.7.3)$$

where

$$RRJ = \prod_{I \neq J} RI \qquad RD = \sum_{J=1}^{4} RRJ \qquad (3.7.4)$$

3.8 Determining the Jumps in the Flow Variables Across the Blade-Two Shock. It is in the determination of the jump conditions that the author employs a technique — alluded to in section 3.4.8 — that is different from the method used by Teipel in the single-blade case. The essence of Teipel's approach is to:

1. Assume that the velocity potential does not change across the shock at the first point (3.4.47).

2. Use the shock velocity equations (3.4.27,28), with boundary conditions (3.4.42,43,45), in conjunction with the β compatibility relation (3.3.14), to solve for $\hat{u}_1$, $\hat{v}_1$ (behind the shock) and g at each shock point.

3. Use equation (3.3.18) behind the shock to recover $\hat{\phi}_1$ at each shock point.

In contrast, the method employed in the present study is to:

1. Use (3.4.46,48) to determine $\hat{\phi}_1$ behind the shock at the first shock point.

2. Use the shock velocity equations (3.4.27,28), the shock pressure equation (3.4.37), the β compatibility relation (3.3.14) and the boundary conditions (3.4.42,43, 45,46) to solve for $\hat{u}_1$, $\hat{v}_1$, g and $\hat{P}/P$ at each shock point.

3. Use equation (3.4.48) to find $\hat{\phi}_1$ from the pressure jump at each shock point.

The latter method results in a larger system of equations at each point, but no assumptions concerning the continuity of the velocity potential are required.

3.8.1 Details of the Jump-Condition Computations.

Step 2 above requires some additional comment. The shock equations (3.4.27,28,37) are applied in difference form from one shock point to the next. They are the last six equations in the matrix equation given in appendix section A.5. The β relation supplies the first two equations in that matrix equation. Note from figure 3.7.1 D that using the β relation at shock point (1,I) requires two tacit assumptions. First, the flow variables at the point where the β characteristic through (1,I) leaves the blade are essentially those at the point (1,1) immediately behind the shock. Second, the flow variables on the β characteristic through (1,I+1) and just behind (1,I) are about the same as those at (1,I) behind the shock.

In the computer program the flow variables at shock point (1,I), ahead of the shock, have the form

$$u_1 = \text{U12}(1,I) - i\ \text{U12I}(1,I) \qquad (3.8.1)$$

while, at the same point immediately behind the shock, they are designated

$$u_1 = \text{URJ(I)} + i\ \text{UIJ(I)} \qquad (3.8.2)$$

until stored in the form of (3.8.1).

3.9 Computing the Unsteady Flow Variables at the Curved-Mesh Grid Points.

3.9.1 The Blade-Two Lower-Surface Grid Points. The unsteady boundary condition for the second blade provides the lower-surface v_1 velocities (figure 3.9.1 A). The equations are given in section A.6 of the appendix. The u_1 velocities are found via the $\propto$ compatibility relation (section A.7) and the velocity potential follows from equation (3.3.17) (appendix section A.8).

3.9.2 The Curved-Mesh Field Points. Both compatibility relations are used at a field point, as seen from figure 3.9.1 B. The resultant matrix equation appears in appendix section A.9. The velocity potential is found from equations (3.3.17,18) (appendix section A.10).

With the curved mesh completely computed the unsteady pressures at blade-two, lower-surface grid points are given by

$$C_{p_1}^L = -2\left[\text{U12R(I,I)} - k\ \text{F2I(I,I)}\right] - 2i\left[\text{U12I(I,I)} + k\ \text{F2R(I,I)}\right] \qquad (3.9.1)$$

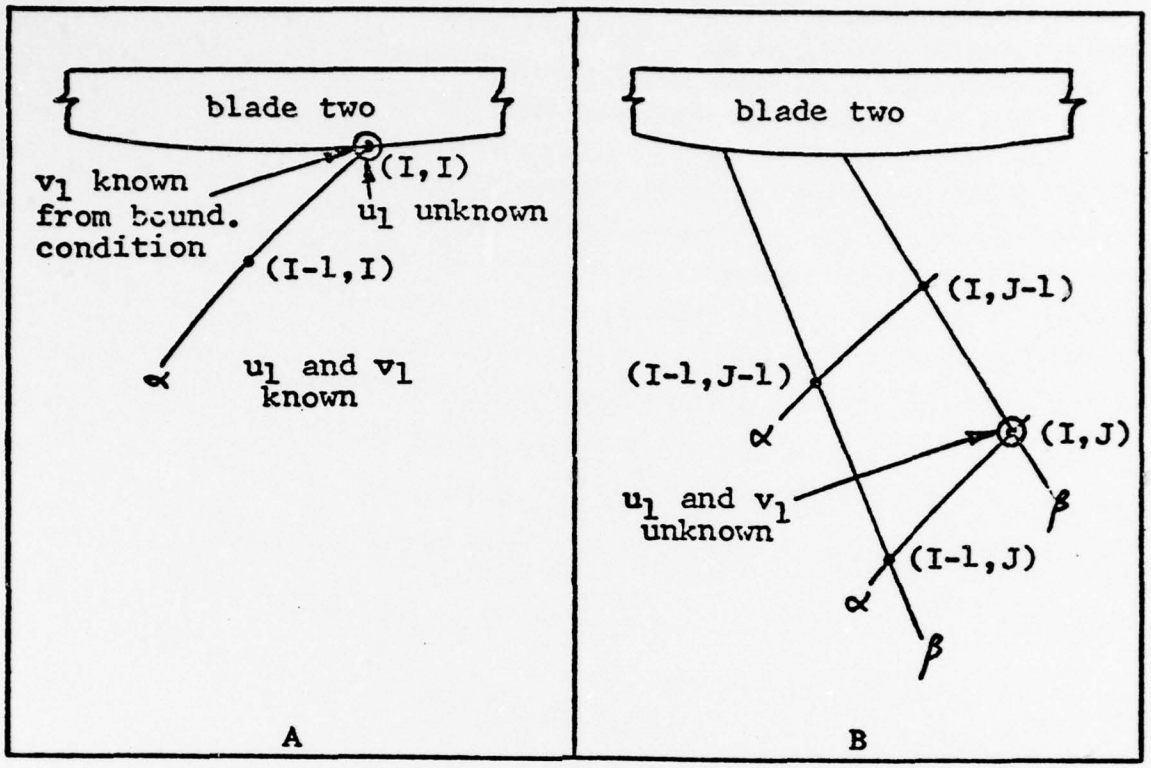

Figure 3.9.1 Computing the curved-mesh grid points.

3.10 Results and Conclusions.

3.10.1 The Isolated-Blade Case. If the unsteady boundary condition along the first blade is set to zero, the second blade sees freestream conditions and its unsteady pressures can be compared with Teipel's isolated-blade results [23]. This is accomplished in figure 3.10.1, where it is noted that a small discrepancy between the two solutions exists. This discrepancy is attributable in part to the different techniques used by Teipel and the author in solving the shock equations (see section 3.8). But it is also noted that Chadwick [5] too encountered a discrepancy when he applied Teipel's method to the single, biconvex airfoil.

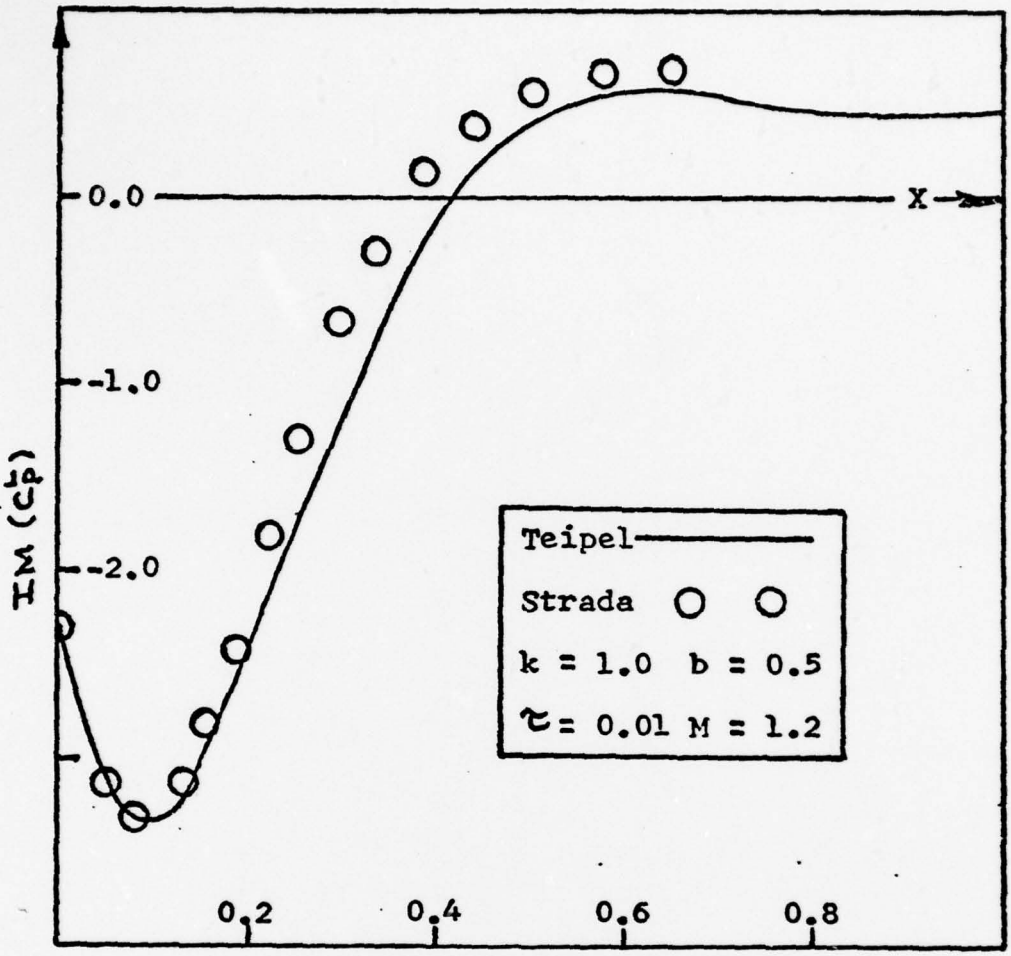

Figure 3.10.1 Isolated-Blade Results.

Teipel points out that, for the single blade, as k gets large the linear and nonlinear solutions approach each other. This phenomenon is also evident for the second blade in cascade T, as seen in figure 3.10.2 which compares Platzer's linear solution [17] with the nonlinear results of this investigation for a k of 1.5 .

3.10.2 The Steady Pressure Results. Figure 3.10.3 shows the steady pressures for the lower surface of blade two. It is seen that agreement between the experimental results

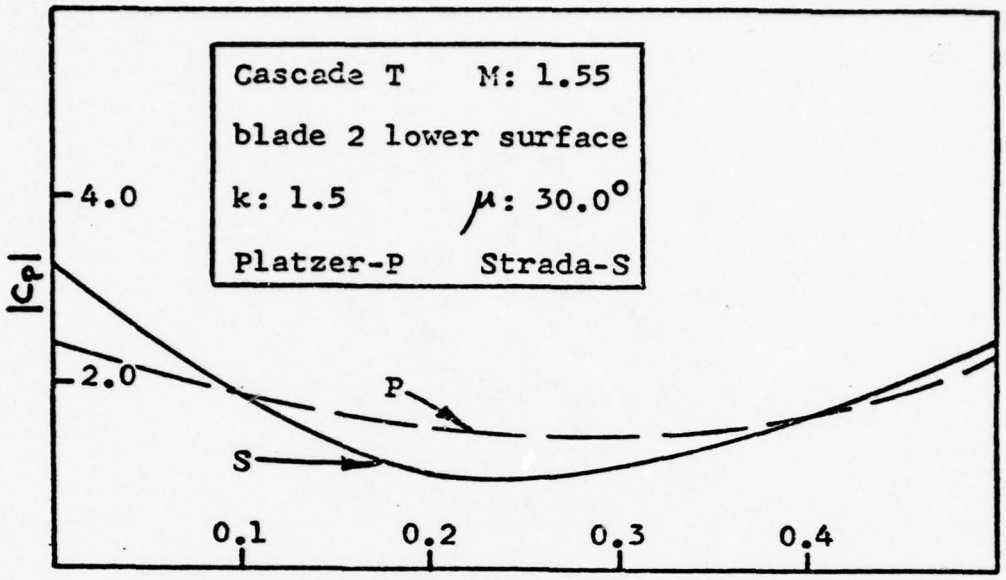

Figure 3.10.2 High-k comparison of the linear and non-linear solutions.

of Fleeter [25] and the numerical results of the computer model is good at midchord and fair at the leading edge. The program results compare favorably with theoretical predictions from second-order Prandtl-Busemann theory and a third-order theory due to Ferri [30] which takes entropy losses into account. This latter comparison again demonstrates that the computer solution is not limited by its use of the isentropic Rankine-Hugoniot pressure relation (3.4.8).

3.10.3 The Unsteady Pressure Results. Figures 3.10.4 through 3.10.12 show the computer results of the present study, the experimental data from Fleeter's investigation, and the linear results of Platzer's method-of-characteristics program for nine interblade phase angles. The pressure

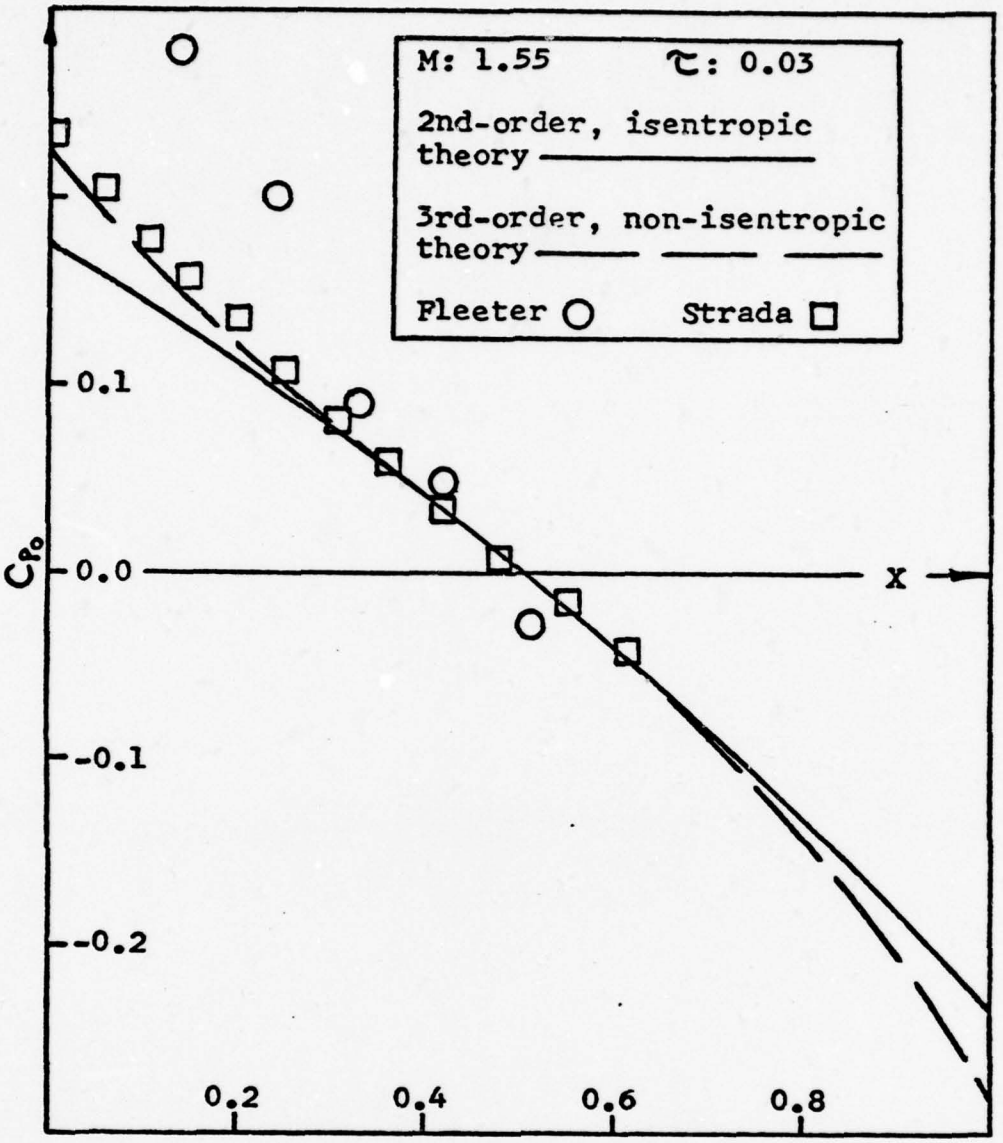

Figure 3.10.3 Blade-two lower-surface steady pressures.

data are presented as an amplitude and phase angle relative to the motion of the second blade. The phase angle is measured from the point where the second blade attains maximum up pitch to the point of peak blade pressure. Along the upper surface of blade two the linear and nonlinear numerical results agree exactly – because the upper surface

is flat – providing an additional check of the nonlinear program. Along the lower surface the nonlinear effects show up as differences between the two predicted pressure distributions – differences which vary with interblade phase angle. The predicted nonlinear pressure amplitude is, in all cases examined, at least as large as the linear predictions, which is as expected. In figure 3.10.5 ($\mu = -4.4°$) the linear and nonlinear amplitude predictions are nearly coincident, while in figure 3.10.9 ($\mu = 130.6°$) they differ considerably. Figure 3.10.13 is a plot of the difference between the nonlinear and linear amplitude predictions versus the turning angles experienced by the flow at the leading edge of blade two. It shows that the nonlinear computer predictions are consistent since the variation from the linear solution increases with the flow turning angle. That turning angle is given by

$$T.A. = 57.3°(1 - \cos\mu) + 6.8° \qquad (3.10.1)$$

when blade two is in the maximum up-pitch position. Note that the large turning angles in figure 3.10.13 result from the choice of a one radian maximum pitch amplitude for nondimensionalization purposes.

Comparison of the nonlinear computer predictions with Fleeter's experimental data, however, reveals that the theory and the experimental results do not consistently agree.

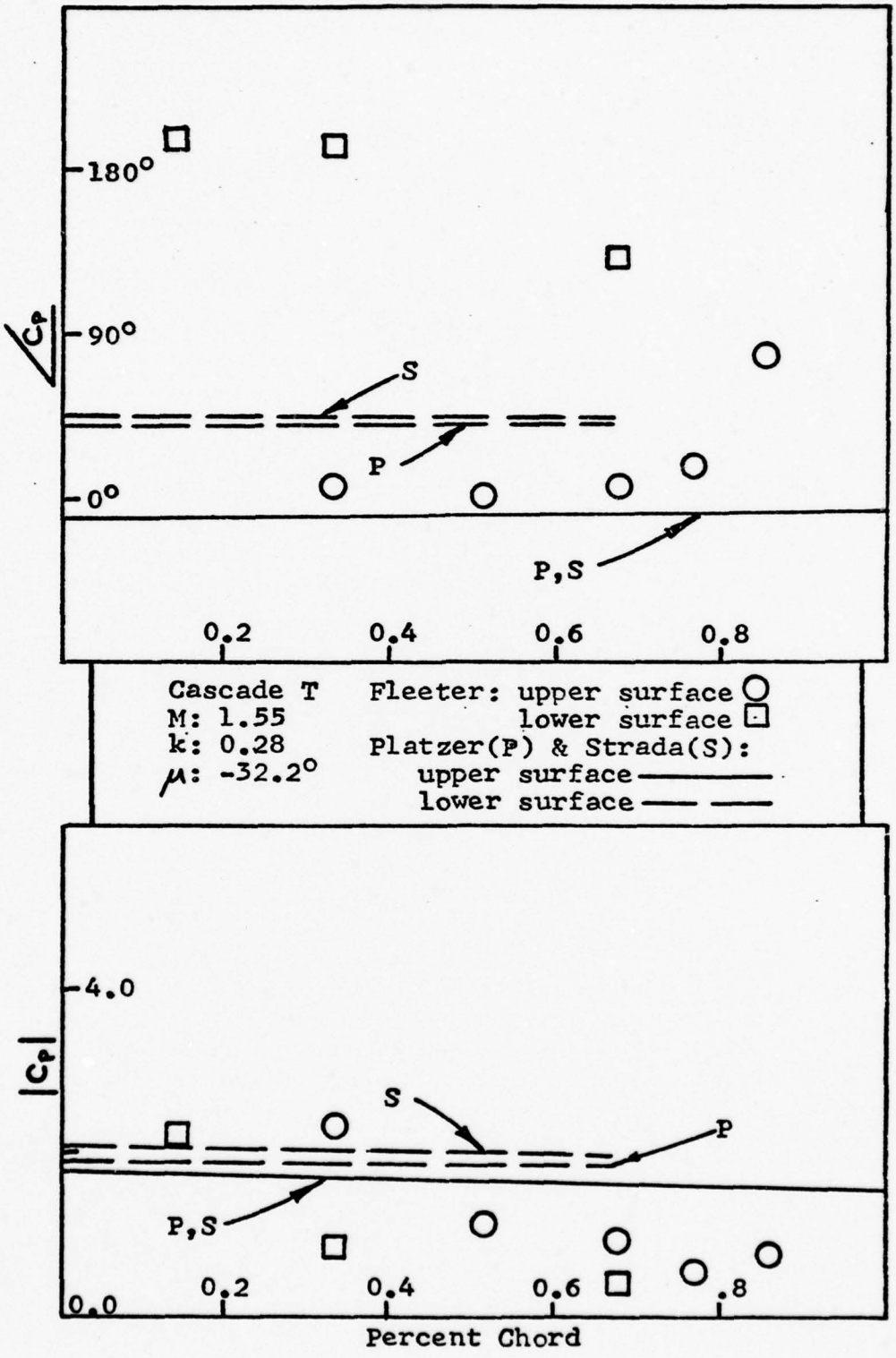

Figure 3.10.4 Blade-two unsteady pressures.

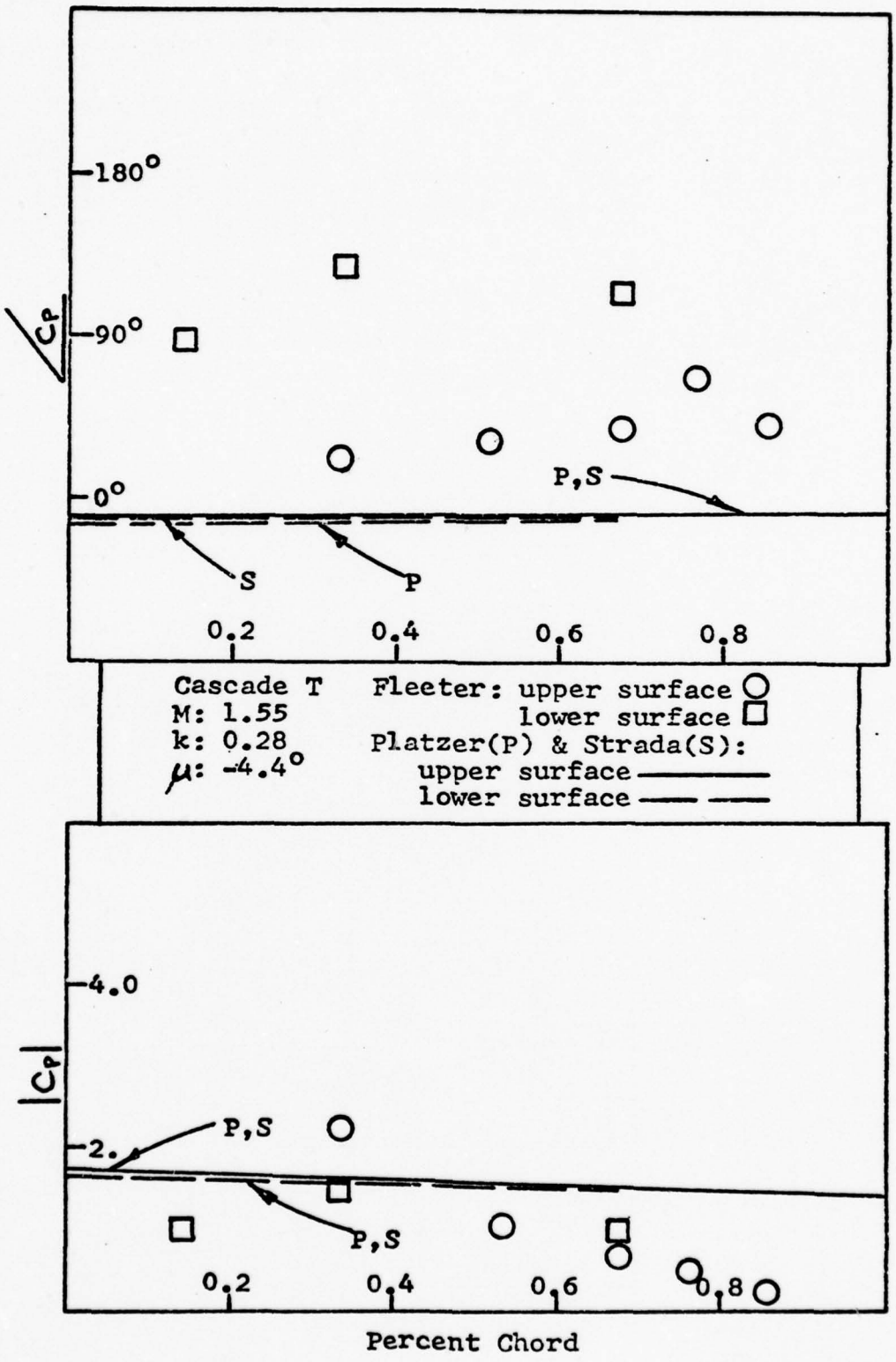

Figure 3.10.5 Blade-two unsteady pressures.

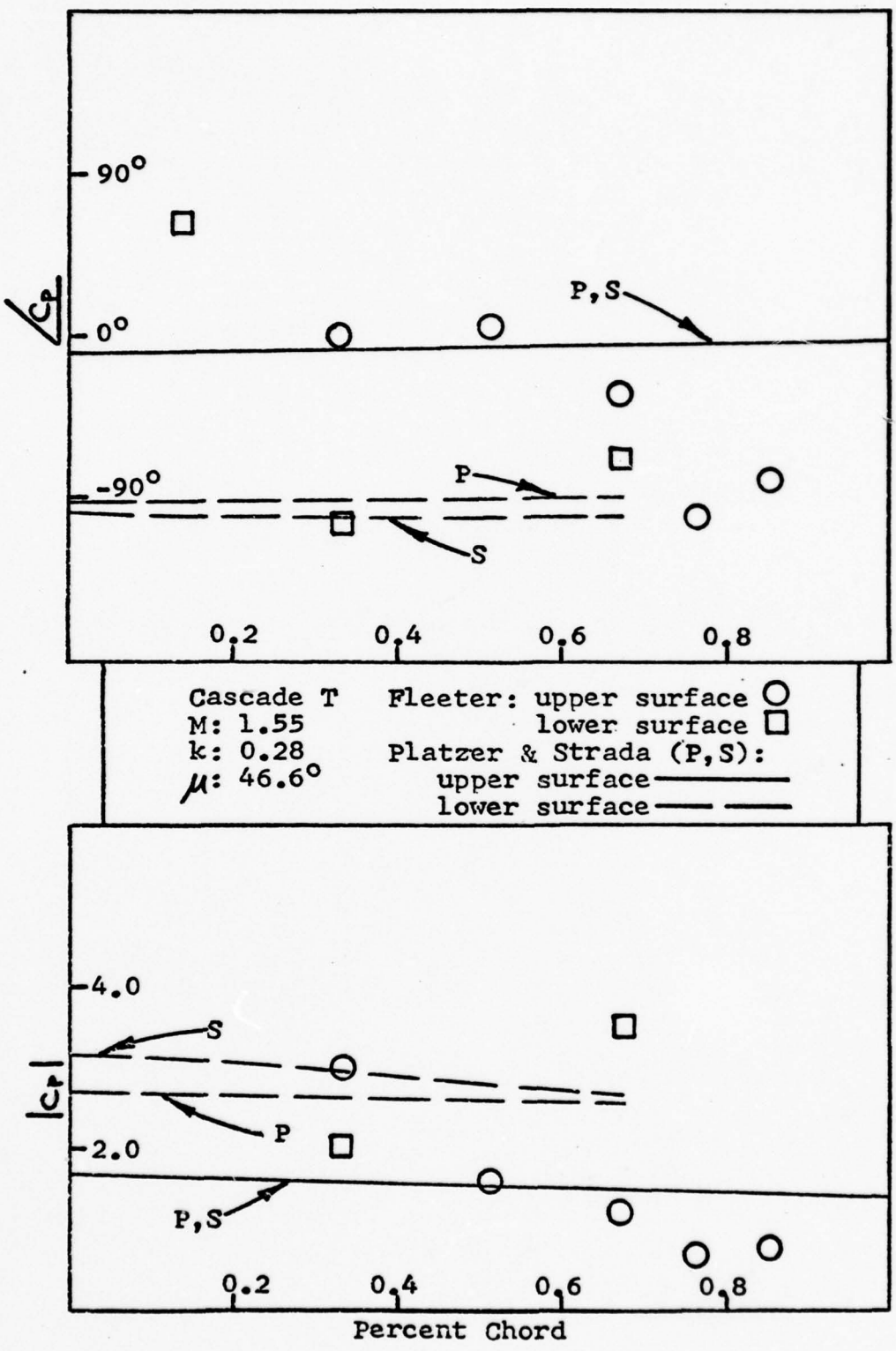

Figure 3.10.6 Blade-two unsteady pressures.

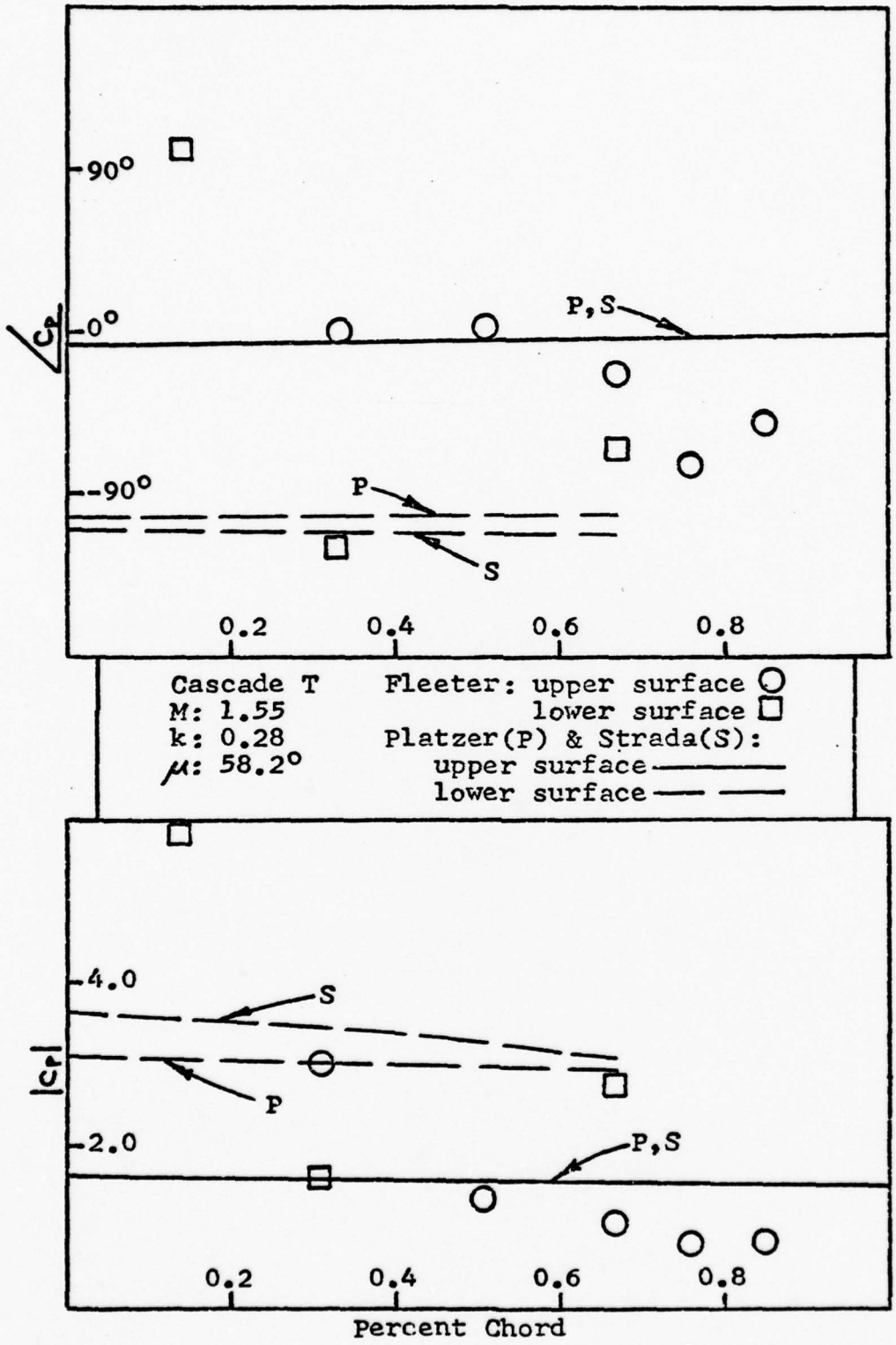

Figure 3.10.7 Blade-two unsteady pressures.

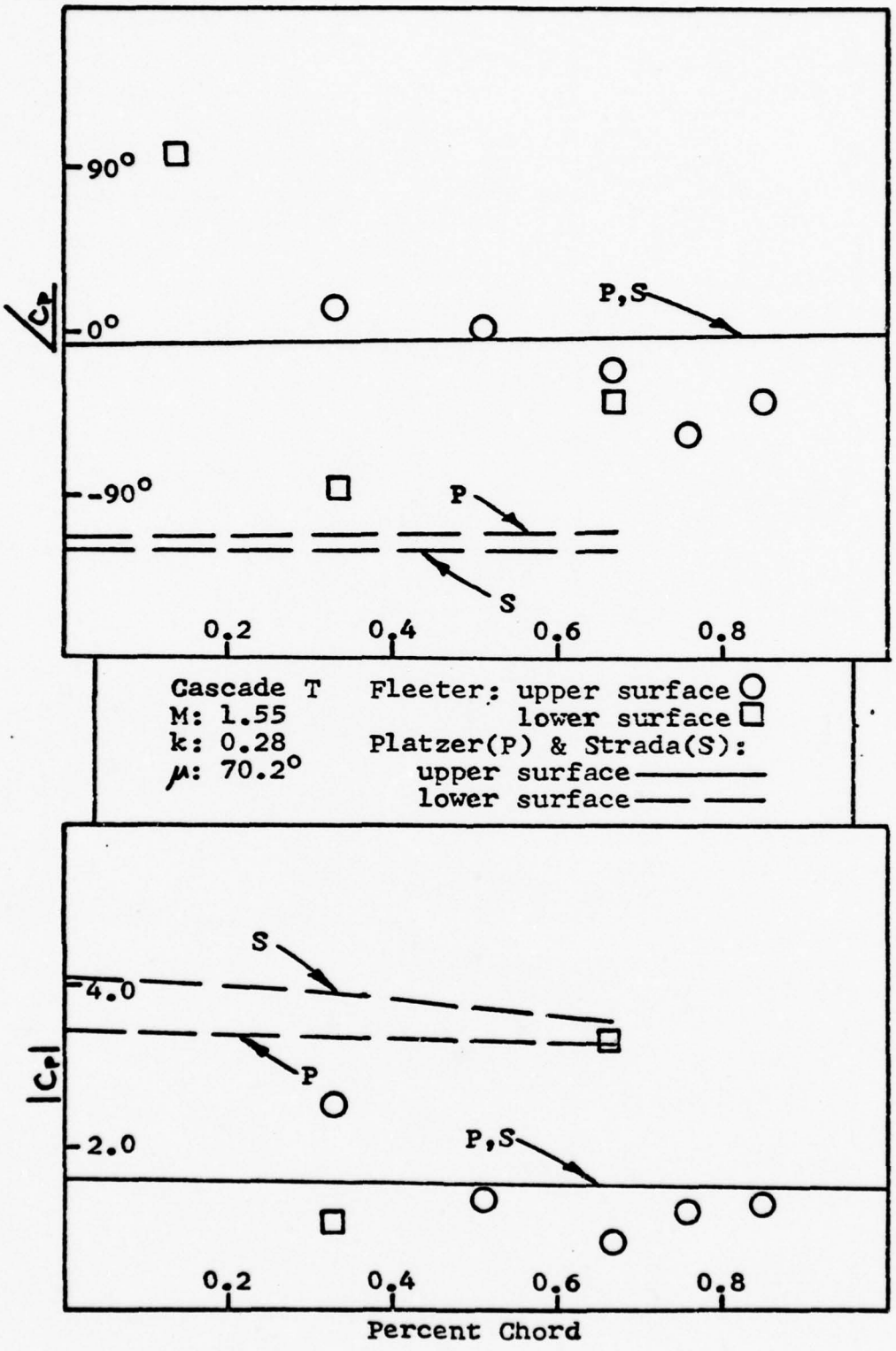

Figure 3.10.8 Blade-two unsteady pressures.

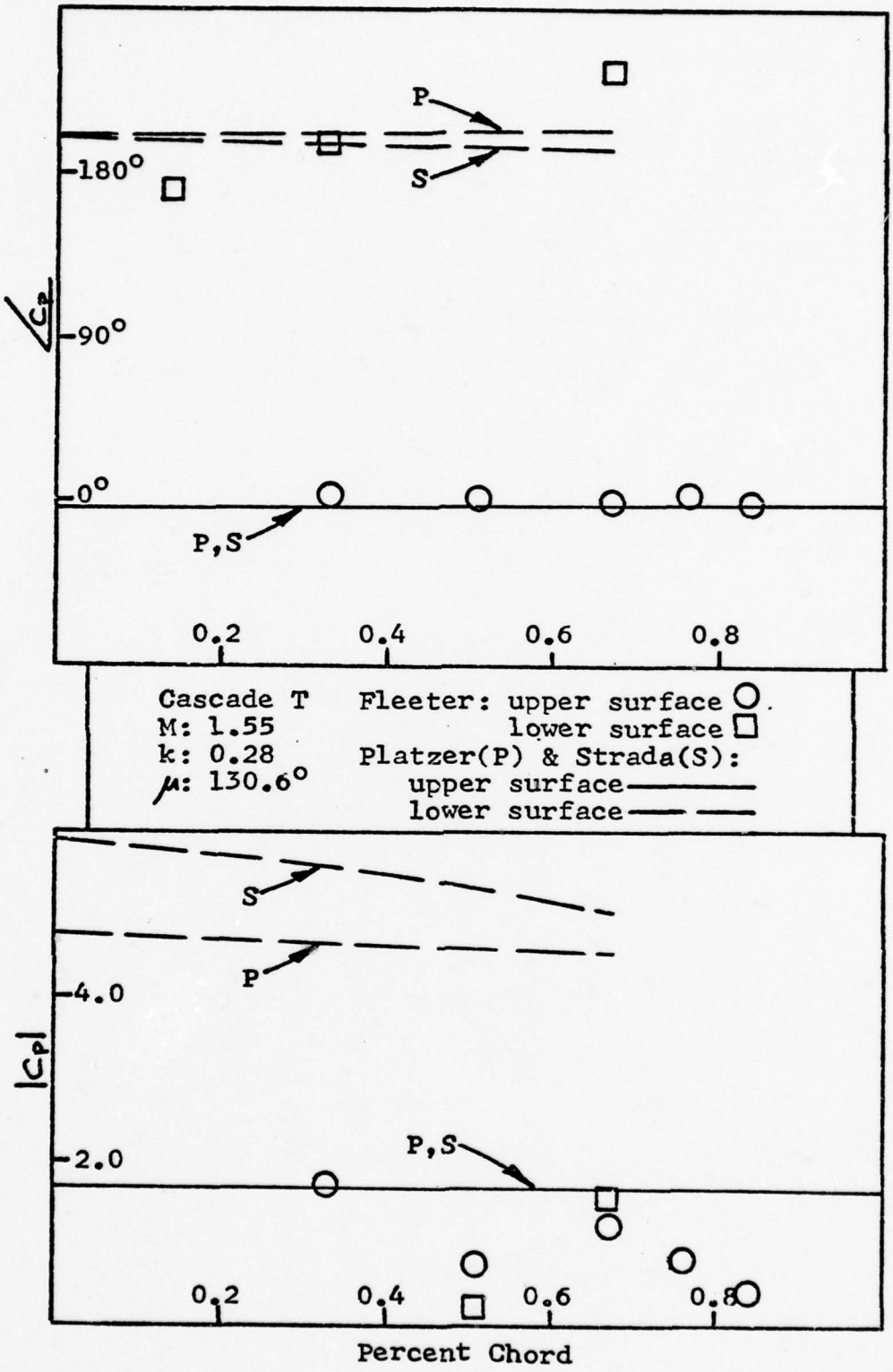

Figure 3.10.9 Blade-two unsteady pressures.

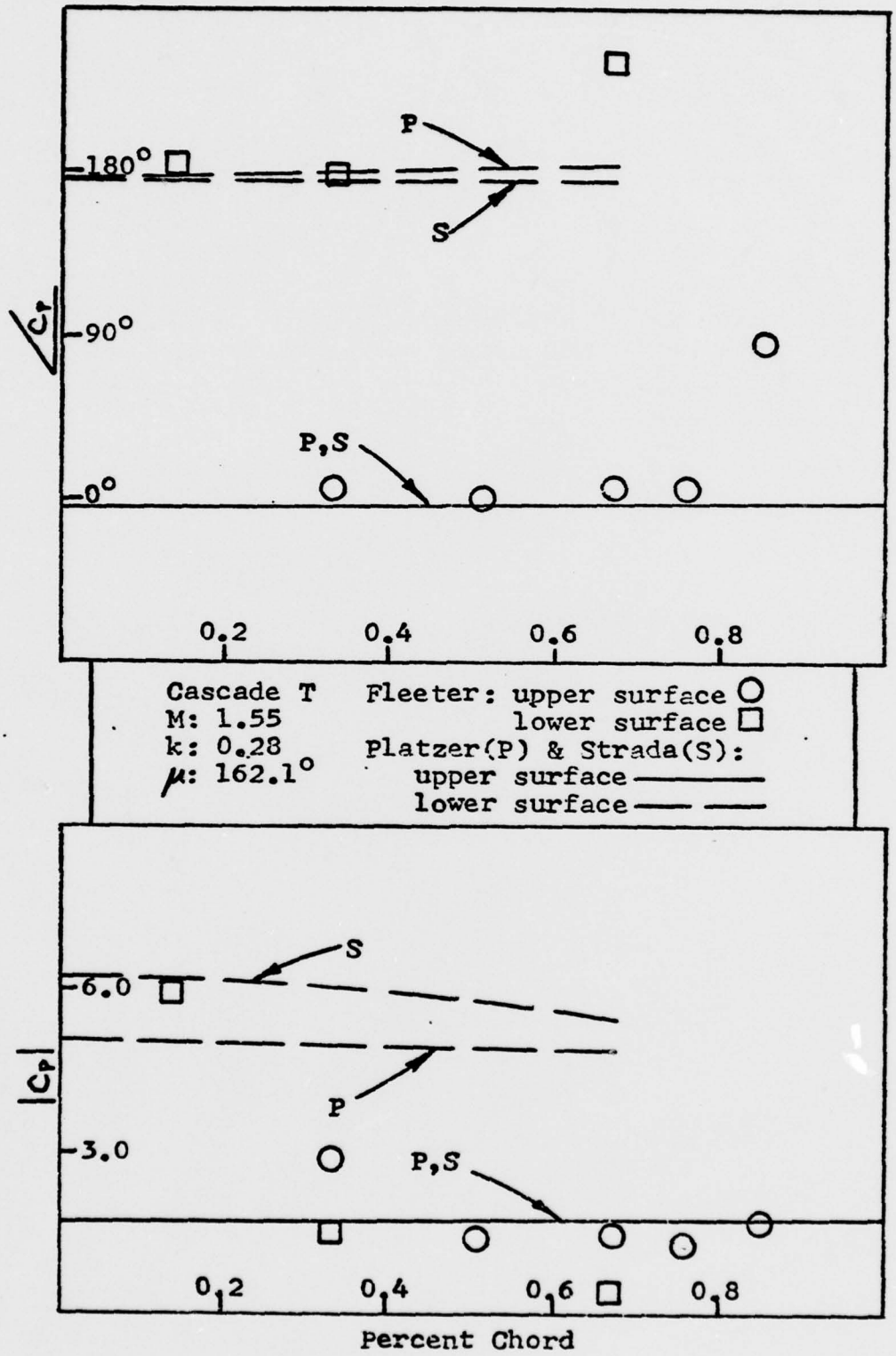

Figure 3.10.10 Blade-two unsteady pressures.

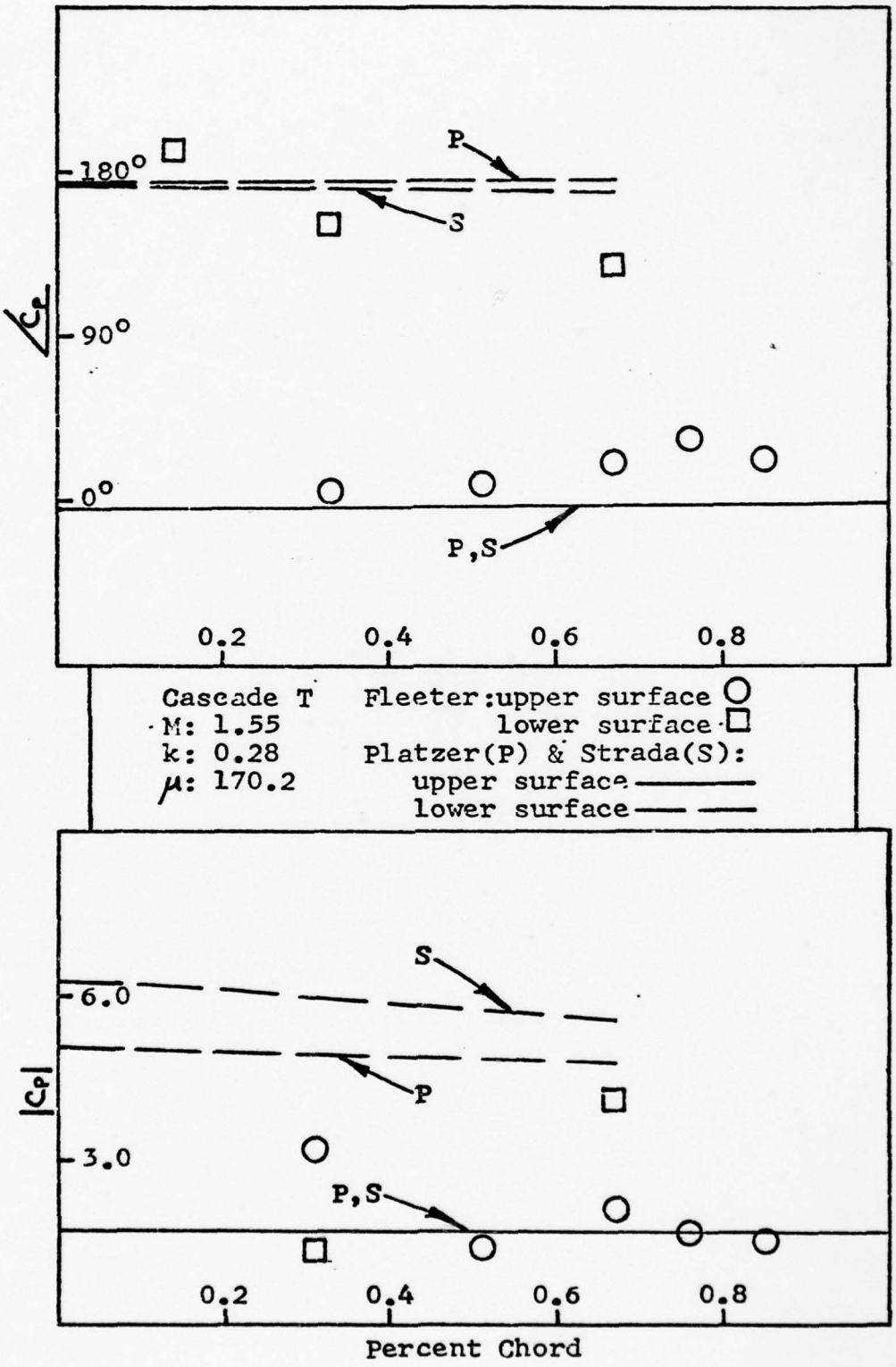

Figure 3.10.11 Blade-two unsteady pressures.

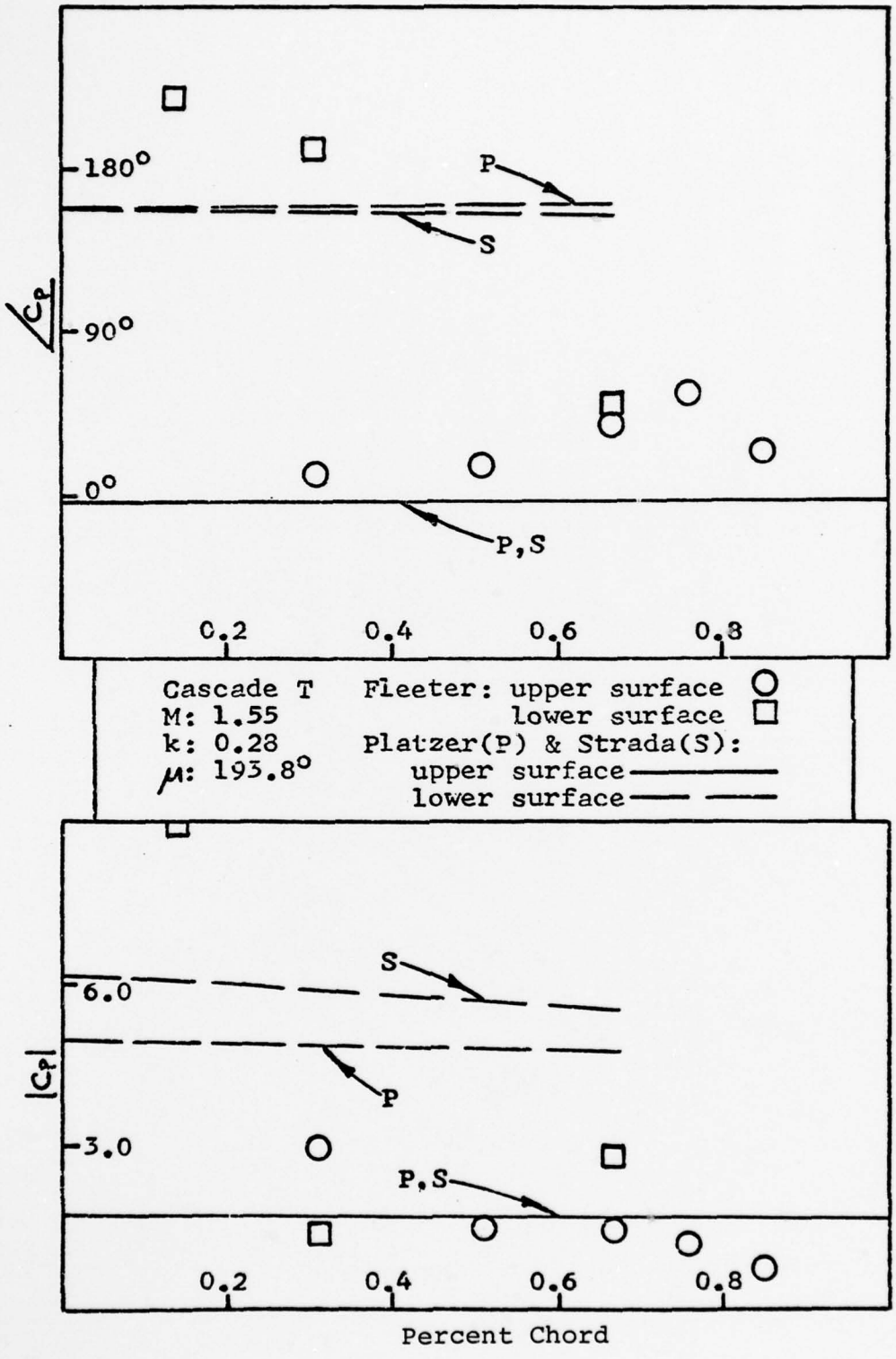

Figure 3.10.12 Blade-two unsteady pressures.

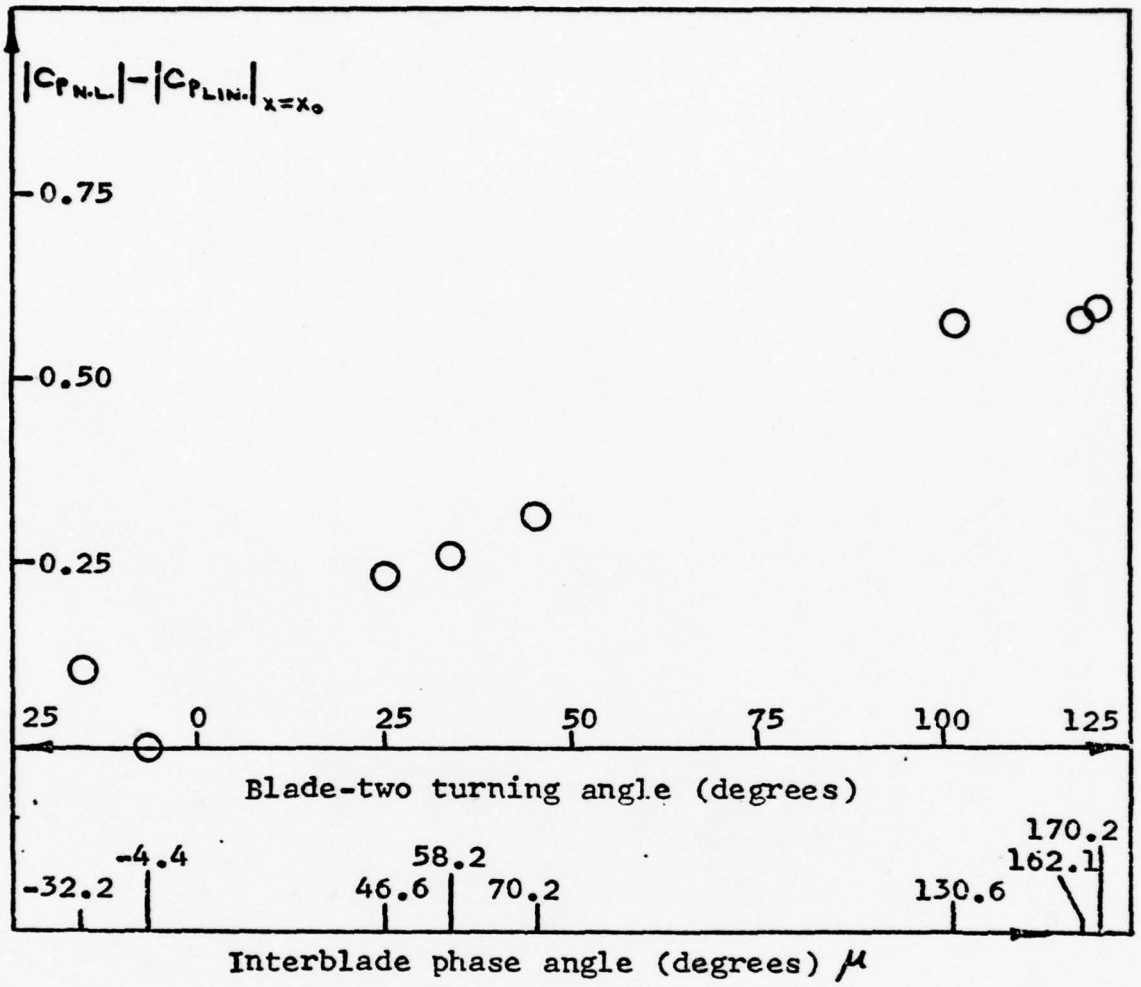

Figure 3.10.13 Nonlinear variations from linear theory.

In figure 3.10.11, for example, there is adequate upper-surface agreement with the theory, but the lower-surface pressure-amplitude comparison is poor. In fact, in no case is there agreement between data and theory for both phase and amplitude along the lower surface. The lower-surface experimental data appear to be somewhat inconsistent. They sometimes vary widely from one point to the next for the same interblade phase angle (figure 3.10.6) and they also

vary a great deal for rather small changes in interblade phase angle (figures 3.10.10,11,12). In addition, in each of the figures there is at least one amplitude data point for the nonlinear (lower) surface that is below the corresponding linear-surface data point. This phenomenon is contrary to expectation because the thickness surface must generate a larger magnitude disturbance than the flat surface. Certainly, additional experimental data are required to adequately evaluate the theoretical methods.

3.10.4 Conclusions. In summary, it is concluded that the extension of Teipel's single-blade methods to the nonlinear cascade results in:

1. Steady pressure predictions which are in accord with other nonlinear theories and which are supported, to some extent, by experimental results.

2. Unsteady pressure predictions which exhibit expected trends relative to linear theory, but which are not consistently in agreement with experimental data presently available. The significant influence of thickness on the unsteady pressures is apparent in both the theory and data.

3. A numerical approach to the unsteady cascade which appears to have the potential to treat the effects of blade thickness, blade camber, and steady angle-of-attack loading to provide a more realistic model of the fan and compressor blades in a turbomachine.

APPENDIX A

A.1 Equations for the Unknown u_1 Velocity at Blade-One Surface Points.

1. References: section 3.7.1; figure 3.7.1 A.

2. Auxiliary constants:

$$A1 = 2kM^2(0.025)/\lambda_A \qquad A2 = k^2M^2(0.025)/\lambda_A$$

$$A3 = 1 + 0.0125\ A2 \qquad A4 = A3/\lambda_A^{1/2}$$

$$A5 = 1 - 0.0125\ A2 \qquad A6 = A5/\lambda_A^{1/2}$$

3. Matrix equation:

$$\begin{bmatrix} A5 & -A1/2 \\ A1/2 & A5 \end{bmatrix} \begin{bmatrix} U1lR(I,I) \\ U1lI(I,I) \end{bmatrix} = \begin{bmatrix} A3\ U1lR(I-1,I) + \\ A3\ U1lI(I-1,I) - \end{bmatrix}$$

$$\overline{+ A1\ U1lI(I-1,I)/2 - A4\ V1lR(I,I) + A6\ V1lR(I-1,I)+}$$

$$\underline{- A1\ U1lR(I-1,I)/2 - A4\ V1lI(I,I) + A6\ V1lI(I-1,I)+}$$

$$\begin{bmatrix} +A2\ F1R(I-1,I) \\ +A2\ F1I(I-1,I) \end{bmatrix}$$

A.2 Equations for ϕ_1 at Blade-One Surface Points.

1. Reference: section 3.7.1; figure 3.7.1 A.

2. Equations:

$$F1R(I,I) = F1R(I-1,I) + \{U1lR(I,I) + U1lR(I-1,I) - [V1lR(I,I) + V1lR(I-1,I)]/\lambda_A^{1/2}\}(0.0125)$$

$$F1I(I,I) = F1I(I-1,I) + \{U1lI(I,I) + U1lI(I-1,I) - [V1lI(I,I) + V1lI(I-1,I)]/\lambda_A^{1/2}\}(0.0125)$$

A.3 Equations for the Velocities u_1 and v_1 at Straight-Mesh Grid Points.

1. References: section 3.7.2; figure 3.7.1 B.

2. Auxiliary constants:

$$A1 = 2kM^2(0.025)/\hat{\lambda} \qquad A2 = k^2M^2(0.025)/\hat{\lambda}$$

$$A3 = 1 - 0.0125\ A2 \qquad A4 = 1 + 0.0125\ A2$$

$$A5 = A3/\hat{\lambda}^{1/2} \qquad A6 = A4/\hat{\lambda}^{1/2}$$

3. Matrix equation:

$$\begin{bmatrix} A3 & -A1/2 & -A6 & 0 \\ A1/2 & A3 & 0 & -A6 \\ A3 & -A1/2 & A6 & 0 \\ A1/2 & A3 & 0 & A6 \end{bmatrix} \begin{bmatrix} U11R(I,J) \\ U11I(I,J) \\ V11R(I,J) \\ V11I(I,J) \end{bmatrix} = \begin{bmatrix} A4\ U11R(I,J-1) + \\ A4\ U11I(I,J-1) - \\ A4\ U11R(I-1,J) + \\ A4\ U11I(I-1,J) - \end{bmatrix}$$

$$\begin{bmatrix} + \frac{A1}{2} U11I(I,J-1) - A5\ V11R(I,J-1) + A2\ F1R(I,J-1) \\ - \frac{A1}{2} U11R(I,J-1) - A5\ V11I(I,J-1) + A2\ F1I(I,J-1) \\ + \frac{A1}{2} U11I(I-1,J) + A5\ V11R(I-1,J) + A2\ F1R(I-1,J) \\ - \frac{A1}{2} U11R(I-1,J) + A5\ V11I(I-1,J) + A2\ F1I(I-1,J) \end{bmatrix}$$

A.4 Equations for ϕ_1 at Straight-Mesh Grid Points.

$$F1R(I,J) = \tfrac{1}{2}\left[F1R(I,J-1) + F1R(I-1,J)\right] + 0.0125\ U11R(I,J) +$$
$$+ 0.00625\left[U11R(I,J-1) + U11R(I-1,J)\right] +$$
$$+ 0.00625\left[V11R(I,J-1) - V11R(I-1,J)\right]/\hat{\lambda}^{1/2}$$

$$F1I(I,J) = \tfrac{1}{2}\left[F1I(I,J-1) + F1I(I-1,J)\right] + 0.0125\ U11I(I,J) +$$
$$+ 0.00625\left[U11I(I,J-1) + U11I(I-1,J)\right] +$$
$$+ 0.00625\left[V11I(I,J-1) - V11I(I-1,J)\right]/\hat{\lambda}^{1/2}$$

1. References: section 3.7.2; figure 3.7.1 B.

A.5 Equations for the Jump Conditions across the Blade-Two Leading-Edge Shock.

1. References: section 3.8.1; figure 3.7.1 D.

2. Auxiliary constants:

$$A1 = 2/\left[\lambda^{1/2}(1,I) + \lambda^{1/2}(1,I-1)\right]$$

$$A2 = 4kM^2\left[X2(1,I) - X2(1,I-1)\right] / \left[\lambda(1,I) + \lambda(1,I-1)\right]$$

$$A3 = A2\ k/2$$

$$DY = \left[Y2(1,I) - Y2(1,I-1)\right]/2$$

3. Matrix equations:

$$\begin{bmatrix} 1 & -A2/2 & A1 & 0 & -A3/2 & 0 & 0 & 0 \\ A2/2 & 1 & 0 & A1 & 0 & -A3/2 & 0 & 0 \\ 1 & 0 & 0 & 0 & 0 & 0 & -m_1/DY & m_2 \\ 0 & 1 & 0 & 0 & 0 & 0 & -m_2 & -m_1/DY \\ 0 & 0 & 1 & 0 & 0 & 0 & -n_1/DY & n_2 \\ 0 & 0 & 0 & 1 & 0 & 0 & -n_2 & -n_1/DY \\ -\gamma M^2 & 0 & 0 & 0 & 0 & \gamma M^2 k & -p_1/DY & p_2 \\ 0 & -\gamma M^2 & 0 & 0 & -\gamma M^2 k & 0 & -p_2 & -p_1/DY \end{bmatrix} \begin{bmatrix} URJ(I) \\ UIJ(I) \\ VRJ(I) \\ VIJ(I) \\ FRJ(I) \\ FIJ(I) \\ GR(I) \\ GI(I) \end{bmatrix} =$$

$$= \begin{bmatrix} URJ(I-1) + A2\ UIJ(I-1)/2 + A1\ VRJ(I-1) + A3\ FRJ(I-1)/2 \\ UIJ(I-1) - A2\ URJ(I-1)/2 + A1\ VIJ(I-1) + A3\ FIJ(I-1)/2 \\ m_3\left[U12R(1,I) + U12R(1,I-1)\right] + m_4\left[V12R(1,I) + V12R(1,I-1)\right] - \\ m_3\left[U12I(1,I) + U12I(1,I-1)\right] + m_4\left[V12I(1,I) + V12I(1,I-1)\right] - \\ m_4\left[U12R(1,I) + U12R(1,I-1)\right] + n_4\left[V12R(1,I) + V12R(1,I-1)\right] - \\ m_4\left[U12I(1,I) + U12I(1,I-1)\right] + n_4\left[V12I(1,I) + V12I(1,I-1)\right] - \\ (p_3 - M^2)\left[U12R(1,I) + U12R(1,I-1)\right] + p_4\left[V12R(1,I) + \right. \\ (p_3 - M^2)\left[U12I(1,I) + U12I(1,I-1)\right] + p_4\left[V12I(1,I) + \right. \end{bmatrix}$$

A.5 (Continued):

3. Matrix equation (right hand side continued):

$$
\begin{bmatrix}
* \\
* \\
- URJ(I-1) - m_1\, GR(I-1)/DY - m_2\, GI(I-1) \\
- UIJ(I-1) - m_1\, GI(I-1)/DY + m_2\, GR(I-1) \\
- VRJ(I-1) - n_1\, GR(I-1)/DY - n_2\, GI(I-1) \\
- VIJ(I-1) - n_1\, GI(I-1)/DY + n_2\, GR(I-1) \\
+ V12R(I-1)\big] + k\gamma M^2\big[F2I(I) + F2I(I-1)\big] + \gamma M^2 URJ(I-1) - \\
+ V12I(I-1)\big] - k\gamma M^2\big[F2R(I) + F2R(I-1)\big] + \gamma M^2 UIJ(I-1) + \\
\hline
* \\
* \\
* \\
* \\
* \\
* \\
- \gamma M^2 k\, FIJ(I-1) - p_1\, GR(I-1)/DY - p_2\, GI(I-1) \\
+ \gamma M^2 k\, FRJ(I-1) - p_1\, GI(I-1)/DY + p_2\, GR(I-1)
\end{bmatrix}
$$

A.6 Boundary-Condition Equations for the v_1 Velocity at the Blade-Two Surface Points.

1. References: section 3.9.1; figure 3.9.1 A.

2. Auxiliary constants: X = X2(I,I) - X2(1,1)

3. Equations:

V12R(I,I) = - COS(μ) - k(X-b)SIN(μ)

V12I(I,I) = - SIN(μ) - k(X-b)COS(μ)

A.7 Equations for the u_1 Velocity at Blade-Two Surface Points.

1. References: section 3.9.1; figure 3.9.1 A.

2. Auxiliary constants (also used in A.9 equations):

$$DXA = X2(I,J) - X2(I-1,J) \qquad XLA = \tfrac{1}{2}\left[\lambda(I,J) + \lambda(I-1,J)\right]$$

$$DXB = X2(I,J) - X2(I,J-1) \qquad XLB = \tfrac{1}{2}\left[\lambda(I,J) + \lambda(I,J-1)\right]$$

$$VAR = \tfrac{1}{2}\left[V12R(I,J) + V12R(I-1,J)\right] \qquad DLB = \lambda(I,J) - \lambda(I,J-1)$$

$$VAI = \tfrac{1}{2}\left[V12I(I,J) + V12I(I,J-1)\right] \qquad A1 = 2\,k\,M^2$$

$$DVAR = V12R(I,J) - V12R(I-1,J) \qquad A2 = k\,A1/2$$

$$DVAI = V12I(I,J) - V12I(I-1,J)$$

$$SLA = \tfrac{1}{2}\left[\lambda(I,J)^{1/2} + \lambda(I-1,J)^{1/2}\right] \qquad SLB = \tfrac{1}{2}\left[\lambda(I,J)^{1/2} + \lambda(I,J-1)^{1/2}\right]$$

$$DLXB = \left[\lambda(I,J+1) - \lambda(I,J)\right] \Big/ \left[X2(I,J+1) - X2(I,J)\right]$$

3. Matrix equation:

$$\begin{bmatrix} 1 + \frac{DLXB\ DXA}{4\ XLA} - \frac{A2\ DXA^2}{2\ XLA} & -\frac{A1\ DXA}{2\ XLA} \\ \frac{A1\ DXA}{2\ XLA} & 1 + \frac{DLXB\ DXA}{4\ XLA} - \frac{A2\ DXA^2}{2\ XLA} \end{bmatrix} \begin{bmatrix} U12R(I,J) \\ U12I(I,J) \end{bmatrix} =$$

$$\begin{bmatrix} U12R(I-1,J)\left[1 - \frac{DLXB\ DXA}{4\ XLA} + \frac{A2\ DXA^2}{2\ XLA}\right] + U12I(I-1,J)\,\frac{A1\ DXA}{2\ XLA} + \\ U12I(I-1,J)\left[1 - \frac{DLXB\ DXA}{4\ XLA} + \frac{A2\ DXA^2}{2\ XLA}\right] - U12R(I-1,J)\,\frac{A1\ DXA}{2\ XLA} + \end{bmatrix}$$

$$\begin{bmatrix} +\frac{DVAR}{SLA} + \frac{A2\ VAR\ DXA^2}{XLA\ SLA} + F2R(I-1,J)\,\frac{A2\ DXA}{XLA} \\ +\frac{DVAI}{SLA} + \frac{A2\ VAI\ DXA^2}{XLA\ SLA} + F2I(I-1,J)\,\frac{A2\ DXA}{XLA} \end{bmatrix}$$

4. Note: at surface points I = J.

A.8 Equations for ϕ_1 at Blade-Two Surface Points.

1. References: section 3.9.1; figure 3.9.1 A.

2. Auxiliary constants: as defined in A.7.

3. Equations:

$$F2R(I,J) = F2R(I-1,J) + \left\{\tfrac{1}{2}\left[U12R(I,J) + U12R(I-1,J)\right] + VAR/SLA\right\} DXA$$

$$F2I(I,J) = F2I(I-1,J) + \left\{\tfrac{1}{2}\left[U12I(I,J) + U12I(I-1,J)\right] + VAI/SLA\right\} DXA$$

4. Note: at surface points I = J.

A.9 Equations for the Velocities u_1 and v_1 at Curved-Mesh Grid Points.

1. References: section 3.9.2; figure 3.9.1 B.

2. Auxiliary constants: as defined in A.7.

3. Matrix equation:

$$\begin{bmatrix} 1 + \frac{DLXB\ DXA}{4\ XLA} - \frac{A2\ DXA^2}{2\ XLA} & -\frac{A1\ DXA}{2\ XLA} & -\frac{1}{SLA} - \frac{A2\ DXA^2}{2\ XLA\ SLA} & 0 \\ \frac{A1\ DXA}{2\ XLA} & 1 + \frac{DLXB\ DXA}{4\ XLA} - \frac{A2\ DXA^2}{2\ XLA} & 0 & -\frac{1}{SLA} - \frac{A2\ DXA^2}{2\ XLA\ SLA} \\ 1 + \frac{DLB}{4\ XLB} - \frac{A2\ DXB^2}{2\ XLB} & -\frac{A1\ DXB}{2\ XLB} & \frac{1}{SLB} + \frac{A2\ DXB^2}{2\ XLB\ SLB} & 0 \\ \frac{A1\ DXB}{2\ XLB} & 1 + \frac{DLB}{4\ XLB} - \frac{A2\ DXB^2}{2\ XLB} & 0 & \frac{1}{SLB} + \frac{A2\ DXB^2}{2\ XLB\ SLB} \end{bmatrix}$$

(Note: continued on next page.)

A.9 (Continued):

3. Matrix equation (unknown vector and right-hand-side matrix continued):

$$
\begin{bmatrix} U12R(I,J) \\ U12I(I,J) \\ V12R(I,J) \\ V12I(I,J) \end{bmatrix} = \begin{bmatrix} U12R(I-1,J)\left[1 - \frac{DLXB\ DXA}{4\ XLA} + \frac{A2\ DXA^2}{2\ XLA}\right] + \\ U12I(I-1,J)\left[1 - \frac{DLXB\ DXA}{4\ XLA} + \frac{A2\ DXA^2}{2\ XLA}\right] - \\ U12R(I,J-1)\left[1 - \frac{DLB}{4\ XLB} + \frac{A2\ DXB^2}{2\ XLB}\right] + \\ U12I(I,J-1)\left[1 - \frac{DLB}{4\ XLB} + \frac{A2\ DXB^2}{2\ XLB}\right] - \end{bmatrix}
$$

$$
+ U12I(I-1,J)\frac{A1\ DXA}{2\ XLA} + V12R(I-1,J)\left[-\frac{1}{SLA} + \frac{A2\ DXA^2}{2\ XLA\ SLA}\right] +
$$

$$
- U12R(I-1,J)\frac{A1\ DXA}{2\ XLA} + V12I(I-1,J)\left[-\frac{1}{SLA} + \frac{A2\ DXA^2}{2\ XLA\ SLA}\right] +
$$

$$
+ U12I(I,J-1)\frac{A1\ DXB}{2\ XLB} + V12R(I,J-1)\left[+\frac{1}{SLB} - \frac{A2\ DXB^2}{2\ XLB\ SLB}\right] +
$$

$$
- U12R(I,J-1)\frac{A1\ DXB}{2\ XLB} + V12I(I,J-1)\left[+\frac{1}{SLB} - \frac{A2\ DXB^2}{2\ XLB\ SLB}\right] +
$$

$$
\begin{bmatrix} + F2R(I-1,J)\frac{A2\ DXA}{XLA} \\ + F2I(I-1,J)\frac{A2\ DXA}{XLA} \\ + F2R(I,J-1)\frac{A2\ DXB}{XLB} \\ + F2I(I,J-1)\frac{A2\ DXB}{XLB} \end{bmatrix}
$$

A.10 Equations for ϕ_1 at Curved-Mesh Grid Points.

1. References: section 3.9.2; figure 3.9.1 B.

2. Auxiliary constants: as defined in A.7.

3. Equations:

$$F2R(I,J) = \tfrac{1}{2}\left[F2R(I-1,J) + F2R(I,J-1)\right]$$
$$+ \tfrac{1}{4}\left\{U12R(I,J) + U12R(I-1,J) + \frac{V12R(I,J) + V12R(I-1,J)}{SLA}\right\} DXA$$
$$+ \tfrac{1}{4}\left\{U12R(I,J) + U12R(I,J-1) - \frac{V12R(I,J) - V12R(I,J-1)}{SLB}\right\} DXB$$

$$F2I(I,J) = \tfrac{1}{2}\left[F2I(I-1,J) + F2I(I,J-1)\right]$$
$$+ \tfrac{1}{4}\left\{U12I(I,J) + U12I(I-1,J) + \frac{V12I(I,J) + V12I(I-1,J)}{SLA}\right\} DXA$$
$$+ \tfrac{1}{4}\left\{U12I(I,J) + U12I(I,J-1) - \frac{V12I(I,J) + V12I(I,J-1)}{SLB}\right\} DXB$$

```
CCCCCCCCCCCCCCCCCCCCCCCCCCCCCCCCCCCCCCCCCCCCCCCCCCCCCCCCCCCCCCCCCCCCCCCCCCC
C                                                                           C
C  PROGRAM INPUT VARIABLES.                                                 C
C                                                                           C
C     FIRST DATA CARD:                                                      C
C       XM-----FREESTREAM MACH NUMBER.....................SPACES  1 TO 10   C
C       T------BLADE THICKNESS RATIO AT MIDCHORD..........SPACES 11 TO 20   C
C       XXK----REDUCED FREQUENCY OF OSCILLATION...........SPACES 21 TO 30   C
C       XROT---PITCH AXIS LOCATION IN PERCENT CHORD.......SPACES 31 TO 40   C
C       FAZE---INTERBLADE PHASE ANGLE IN DEGREES..........SPACES 41 TO 50   C
C                                                                           C
C     SECOND DATA CARD:                                                     C
C                                                                           C
C       K------FIXES VERTICAL BLADE SPACING(YB) ACCORDING TO:               C
C         YB=.025*K/SQRT(XM*XM-1).....RIGHT JUSTIFIED IN SPACES  1 TO 10    C
C       N------FIXES HORIZONTAL BLADE SPACING(XB) ACCORDING TO:             C
C         XB=YB*SQRT(XM*XM-1)+.05*N....RIGHT JUSTIFIED IN SPACES 11 TO 20   C
C                                                                           C
CCCCCCCCCCCCCCCCCCCCCCCCCCCCCCCCCCCCCCCCCCCCCCCCCCCCCCCCCCCCCCCCCCCCCCCCCCC


      REAL*8 X2,Y2,XL2,XMU2
      COMMON X1(40,80),Y1(40,80),X2(40,40),Y2(40,40),XL2(40,40),XMU2(40,
     140),CPO(20),XM,T,XXK,XROT,N,K
      EXTERNAL FNL,FM1,FM2,FM3,FM4,FN1,FN2,FN4,FP1,FP2,FP3,FP4
      DIMENSION U11R(40,80),V11R(40,80),U11I(40,80),V11I(40,80),F1R(40,8
     10),F1I(40,80),U12R(40,40),U12I(40,40),V12R(40,40),V12I(40,40),GR(2
     20),GI(20),F2R(40,40),F2I(40,40),GAM(20),XA1(21),CC2(4),CC4(16),RHS
     32(2),RHS4(4),URJ(20),UIJ(20),VRJ(20),VIJ(20),CC6(36),RHS6(6),FRJ(2
     40),FIJ(20),CC8(64),RHS8(8)
      DIMENSION P1R(21),P1I(21),P2R(21),P2I(21)
2000  FORMAT(5F10.5)
3000  FORMAT(2I10)
4000  FORMAT('0',5X,'MACH NUMBER =',2X,F9.5,10X,'REDUCED FREQUENCY = ',2
     1X,F9.5)
5000  FORMAT('0',5X,'BLADE THICKNESS RATIO =',2X,F9.5,10X,'BLADE PIVOT P
     1OINT =',2X,F9.5)
6000  FORMAT('0',5X,'HORIZONTAL BLADE SPACING =',2X,F9.5,10X,'VERTICAL B
     1LADE SPACING =',2X,F9.5)
7000  FORMAT('0',5X,'NUMBER OF POINTS ON BLADE TWO IS ',2X,I4)
8000  FORMAT('0',5X,'INTERBLADE PHASE ANGLE =',2X,F9.5)
9000  FORMAT('0',T5,'UPPER SURFACE UNSTEADY PRESSURE COEFFICIENT: REAL A
     1ND IMAGINARY')
10500 FORMAT(T5,'PARTS, AND AMPLITUDE AND PHASE (IN DEGREES) RELATIVE TO
     1 BLADE TWO')
11000 FORMAT('0',T9,'X/C',T22,'CPR',T34,'CPI',T44,'AMPLITUDE',T59,
     1'PHASE')
12000 FORMAT(T5,F9.5,T18,F9.5,T31,F9.5,T44,F9.5,T57,F9.5)
```

```
1300C FORMAT('0',T5,'LOWER SURFACE UNSTEADY PRESSURE COEFFICIENT: REAL A
     1ND IMAGINARY')
1400C FORMAT('0',T5,'LOWER SURFACE STEADY PRESSURE COEFFICIENT.')
1500C FORMAT('0',T9,'X/C',T19,'CP-STEADY')
1600C FORMAT(T5,F9.5,T18,F9.5)
      READ(5,2CCC)XM,T,XXK,XROT,FAZE
      READ(5,3CCC)K,N
C
C COMPUTING SOME REQUIRED CONSTANTS
C
      B2=XM*XM-1.C
      B=SQRT(B2)
      YB=FLOAT(K)*.025/B
      XB=YB*B+FLOAT(N)*.C5
      WRITE(6,4000)XM,XXK
      WRITE(6,5CCC)T,XROT
      WRITE(6,6CCC)XB,YB
      WRITE(6,8CCC)FAZE
      XLINF=B2
      NK=N+K-20
      M1=N+21
      M2=NK+41
      M3=N+1
      M4=NK+21
C
C COMPUTING THE STRAIGHT-LINE MESHPOINTS COVERING ZONES A AND C
C
      DO 10 I=1,M1
      DO 10 J=I,M2
      XI=FLOAT(I)
      XJ=FLOAT(J)
      X1(I,J)=(XI+XJ-2.0)*.025
      Y1(I,J)=(XJ-XI)*.025/B
10    CONTINUE
C
C COMPUTING SOME INITIAL VALUES FOR THE CURVED MESH PROBLEM
C
      X2(1,1)=X1(M3,M4)
      Y2(1,1)=Y1(M3,M4)
      XMU2(1,1)=FMU(X2(1,1))
      XX1=DABS(XLINF**1.5+XMU2(1,1))
      XL2(1,1)=XX1**.66667
      KSHOK=2
      XA=X2(1,1)
      YA=Y2(1,1)
      XA1(1)=XA
C
C COMPUTING THE CURVED MESH POINTS (1,2), AND (2,2).
```

```
C
      XA=X2(1,1)+.005
      XA1(2)=XA
      XMU2(1,KSHCK)=FMU(XA)
      XX2=CABS(XLINF**1.5+XMU2(1,KSHCK))
      XL2(1,KSHCK)=XX2**.66667
      D1=-1.C/DSQRT(XL2(1,KSHCK))
      M5=KSHCK-1
      D2=-4.C/(2.0*SQRT(XLINF)+DSQRT(XL2(1,KSHCK))+DSQRT(XL2(1,M5)))
      GAM(1)=ATAN(ABS(D2))
      GAM(2)=GAM(1)
      CALL SOLVE(XA,YA,D1,X2(1,M5),Y2(1,M5),D2,X2(1,KSHOK),Y2(1,KSHCK
     1))
      CALL ITER(2)
C
C COMPUTING SUBSEQUENT SHOCK-FRONT POINTS
C
      DXA=(X2(2,2)-XA)/15.
100   KSHOK=KSHCK+1
      XA=XA+DXA
      XA1(KSHCK)=XA
      CALL SHCKPT(KSHOK,XA,D3)
      GAM(KSHOK)=ATAN(ABS(D3))
C
C COMPUTING THE INTERIOR CURVED MESH POINTS.
C
300   M6=KSHCK-2
      DO 20 I=1,M6
      D1=1.0/DSQRT(XL2(I,KSHOK))
      J=I+1
      D2=-1.C/DSQRT(XL2(J,J))
      CALL SOLVE(X2(I,KSHOK),Y2(I,KSHOK),D1,X2(J,J),Y2(J,J),D2,X2(J,KSHC
     1K),Y2(J,KSHCK))
      XL2(J,KSHCK)=XL2(J,J)
      XMU2(J,KSHCK)=XMU2(J,J)
20    CONTINUE
      CALL ITER(KSHOK)
C
C STOPPING CRITERIA
C
      IF(KSHCK.GE.11) GO TO 600
      IF(XA-X2(2,2)) 120,600,600
C
C CHECKING TO SEE IF THE END OF THE SECOND BLADE HAS BEEN REACHED.
C
120   XCHECK=X2(1,1)+1.0
      IF (X2(KSHCK,KSHOK)-XCHECK)100,600,600
600   WRITE(6,7CCC)KSHOK
```

```
C
C COMPUTING THE STEADY PRESSURE-DIFFERENCE DISTRIBUTION FOR THE SECOND BLADE
C
      WRITE(6,14000)
      WRITE(6,15000)
      DO 30 I=1,KSHOK
      DPO(I)=2.0*(B2-XL2(I,I))/(2.4*XM*XM)
      XXX=X2(I,1)-X2(1,1)
      WRITE(6,16000)XXX,DPO(I)
30    CONTINUE
C
C COMPUTING THE UNSTEADY VELOCITIES ALONG THE STRAIGHT-LINE MESH.
C
C
C     APPLYING THE BOUNDARY CONDITION ALONG THE UPPER SURFACE OF BLADE ONE.
C
      DO 40 I=1,21
      V11R(I,I)=-1.
      V11I(I,I)=-XXK*(X1(I,I)-XROT)
40    CONTINUE
C
C     APPLYING THE BOUNDARY CONDITION ALONG THE UPPER SURFACE OF BLADE TWO.
C
      FFAZE=FAZE/57.3
      DO 50 I=1,21
      I1=M+I
      J1=M4-1+I
      V11R(I1,J1)=-COS(FFAZE)+XXK*(X1(I1,J1)-X2(1,1)-XROT)*SIN(FFAZE)
      V11I(I1,J1)=-SIN(FFAZE)-XXK*(X1(I1,J1)-X2(1,1)-XROT)*COS(FFAZE)
50    CONTINUE
C
C     ALONG THE LEADING MACH WAVE OF BLADE ONE THE PERTURBATIONS ARE ZERO.
C
      DO 60 J=1,M2
      U11R(1,J)=0.
      U11I(1,J)=0.
      V11R(1,J)=0.
      V11I(1,J)=0.
      F1R(1,J)=0.
      F1I(1,J)=0.
60    CONTINUE
C
C     COMPUTING U,V, AND PHI AT THE STRAIGHT-MESH FIELD POINTS.
C
      A1=.05*XXK*XM*XM/B2
      A2=XXK*A1/2.
      COS=1.+.0125*A2
      DO 70 I=2,21
```

```
      I1=I-1
      DO 80 J=I,M2
      J1=J-1
      IF(J-I)700,700,800
800   IF(I-M3)1100,900,900
900   IF(J-I-K)   1100,700,1100
700   CO2(1)=1.-.0125*A2
      CO2(2)=A1/2.
      CO2(3)=-CO2(2)
      CO2(4)=CO2(1)
      RHS2(1)=U11R(I1,J)*CO5+A1*U11I(I1,J)/2.-V11R(I,J)*CO5/B+V11R(I1,J)
     1*CO2(1)/B+A2*F1R(I1,J)
      RHS2(2)=U11I(I1,J)*CO5-A1*U11R(I1,J)/2.-V11I(I,J)*CO5/B+V11I(I1,J)
     1*CO2(1)/B+A2*F1I(I1,J)
      CALL SIMQ(CO2,RHS2,2,KS)
      IF(KS.EQ.1) GO TO 10000
      U11R(I,J)=RHS2(1)
      U11I(I,J)=RHS2(2)
      F1R(I,J)=F1R(I1,J)+.0125*(U11R(I,J)+U11R(I1,J)-(V11R(I,J)+V11R(I1,
     1J))/B)
      F1I(I,J)=F1I(I1,J)+.0125*(U11I(I,J)+U11I(I1,J)-(V11I(I,J)+V11I(I1,
     1J))/B)
      GO TO 80
1100  CO4(1)=1.-.0125*A2
      CO4(2)=A1/2.
      CO4(3)=CO4(1)
      CO4(4)=CO4(2)
      CO4(5)=-CO4(2)
      CO4(6)=CO4(1)
      CO4(7)=-CO4(2)
      CO4(8)=CO4(1)
      CO4(9)=-CO5/B
      CO4(10)=0.
      CO4(11)=-CO4(9)
      CO4(12)=0.
      CO4(13)=0.
      CO4(14)=CO4(9)
      CO4(15)=0.
      CO4(16)=CO4(11)
      RHS4(1)=U11R(I,J1)*CO5+A1*U11I(I,J1)/2.-V11R(I,J1)*CO2(1)/B+A2*F1R
     1(I,J1)
      RHS4(2)=-A1*U11R(I,J1)/2.+U11I(I,J1)*CO5-V11I(I,J1)*CO2(1)/B+A2*F1
     1I(I,J1)
      RHS4(3)=U11R(I1,J)*CO5+A1*U11I(I1,J)/2.+V11R(I1,J)*CO2(1)/B+A2*F1R
     1(I1,J)
      RHS4(4)=-A1*U11R(I1,J)/2.+U11I(I1,J)*CO5+V11I(I1,J)*CO2(1)/B+A2*F1
     1I(I1,J)
      CALL SIMQ(CO4,RHS4,4,KS)
```

```
      IF(KS.EQ.1) GO TO 10000
      U11R(I,J)=RHS4(1)
      U11I(I,J)=RHS4(2)
      V11R(I,J)=RHS4(3)
      V11I(I,J)=RHS4(4)
      F1R(I,J)=(F1R(I,J1)+F1R(I1,J))/2.+.0125*(U11R(I,J)+(U11R(I,J1)+U11
     1R(I1,J))/2.+(V11R(I,J1)-V11R(I1,J))/(2.*B))
      F1I(I,J)=(F1I(I,J1)+F1I(I1,J))/2.+.0125*(U11I(I,J)+(U11I(I,J1)+U11
     1I(I1,J))/2.+(V11I(I,J1)-V11I(I1,J))/(2.*B))
80    CONTINUE
70    CONTINUE
C
C  DETERMINING THE VALUES OF U,V, AND PHI ALONG THE CURVED BOW SHOCK.
C
      DO 90 L=2,KSHCK
      DO 110 I=M3,21
      CHECK1=Y2(1,L)-(X2(1,L)-X1(I,I))/B
      IF(CHECK1)110,110,130
110   CONTINUE
130   DO 140 J=K,M2
      CHECK2=Y2(1,L)-Y1(1,J)+(X2(1,L)-X1(1,J))/B
      IF(CHECK2)150,140,140
140   CONTINUE
150   I1=I-1
      J1=J-1
      R1=DSQRT((X2(1,L)-X1(I1,J1))**2 +(Y2(1,L)-Y1(I1,J1))**2)
      R2=DSQRT((X2(1,L)-X1(I1,J ))**2 +(Y2(1,L)-Y1(I1,J ))**2)
      R3=DSQRT((X2(1,L)-X1(I ,J ))**2 +(Y2(1,L)-Y1(I ,J ))**2)
      R4=DSQRT((X2(1,L)-X1(I ,J1))**2 +(Y2(1,L)-Y1(I ,J1))**2)
      RR1=R2*R3*R4
      RR2=R1*R3*R4
      RR3=R1*R2*R4
      RR4=R1*R2*R3
      RD=RR1+RR2+RR3+RR4
      U12R(1,L)=(RR1*U11R(I1,J1)+RR2*U11R(I1,J)+RR3*U11R(I,J)+RR4*U11R(I
     1,J1))/RD
      U12I(1,L)=(RR1*U11I(I1,J1)+RR2*U11I(I1,J)+RR3*U11I(I,J)+RR4*U11I(I
     1,J1))/RD
      V12R(1,L)=(RR1*V11R(I1,J1)+RR2*V11R(I1,J)+RR3*V11R(I,J)+RR4*V11R(I
     1,J1))/RD
      V12I(1,L)=(RR1*V11I(I1,J1)+RR2*V11I(I1,J)+RR3*V11I(I,J)+RR4*V11I(I
     1,J1))/RD
      F2R(1,L)=(RR1*F1R(I1,J1)+RR2*F1R(I1,J)+RR3*F1R(I,J)+RR4*F1R(I,J1))
     1/RD
      F2I(1,L)=(RR1*F1I(I1,J1)+RR2*F1I(I1,J)+RR3*F1I(I,J)+RR4*F1I(I,J1))
     1/RD
90    CONTINUE
C
```

```
C COMPUTING THE JUMP CONDITIONS ACROSS THE SHOCK.
C
CC
CC      COMPUTING REFERENCE POINTS JUST BEHIND EACH SHOCK-FRONT POINT.
C
        DO 160 I=2,KSHOK
        D1=-1./DSQRT(XL2(1,I))
        D2=-D1
        CALL SOLVE(XA1(I),Y2(1,1),D1,X2(1,I),Y2(1,I),D2,X,Y)
        XA1(I)=X
160     CONTINUE
C
CC      COMPUTING THE FLOW VARIABLES AT A POINT JUST UPSTREAM OF THE LEADING
CC      EDGE OF THE SECOND BLADE.
C
        A1=.C5*XXK*XM*XM/B2
        A2=XXK*A1/2.
        CO5=1.+.0125*A2
        I=M3
        J=M4
        I1=I-1
        J1=J-1
        CO4(1)=1.-.0125*A2
        CC4(2)=A1/2.
        CO4(3)=CO4(1)
        CC4(4)=CC4(2)
        CO4(5)=-CC4(2)
        CO4(6)=CO4(1)
        CC4(7)=-CC4(2)
        CO4(8)=CC4(1)
        CO4(9)=-CC5/B
        CO4(10)=C.
        CO4(11)=-CO4(9)
        CO4(12)=0.
        CO4(13)=C.
        CO4(14)=CO4(9)
        CO4(15)=0.
        CO4(16)=CC4(11)
        RHS4(1)=U11R(I,J1)*CO5+A1*L11I(I,J1)/2.-V11R(I,J1)*CC2(1)/B+A2*F1R
       1(I,J1)
        RHS4(2)=-A1*U11R(I,J1)/2.+L11I(I,J1)*CC5-V11I(I,J1)*CC2(1)/B+A2*F1
       1I(I,J1)
        RHS4(3)=U11R(I1,J)*CC5+A1*U11I(I1,J)/2.+V11R(I1,J)*CO2(1)/B+A2*F1R
       1(I1,J)
        RHS4(4)=-A1*U11R(I1,J)/2.+U11I(I1,J)*CO5+V11I(I1,J)*CO2(1)/B+A2*F1
       1I(I1,J)
        CALL SIMC(CO4,RHS4,4,KS)
        IF(KS.EC.1) GO TC 10000
```

```
      U12R(1,1)=RHS4(1)
      U12I(1,1)=RHS4(2)
      V12R(1,1)=RHS4(3)
      V12I(1,1)=RHS4(4)
      F2R(1,1)=(F1R(I,J1)+F1R(I1,J))/2.+.0125*(U11R(I,J)+(U11R(I,J1)+U11
     1R(I1,J))/2.+(V11R(I,J1)-V11R(I1,J))/(2.*B))
      F2I(1,1)=(F1I(I,J1)+F1I(I1,J))/2.+.0125*(U11I(I,J)+(U11I(I,J1)+U11
     1I(I1,J))/2.+(V11I(I,J1)-V11I(I1,J))/(2.*B))
C
CC    COMPUTING THE INITIAL CONDITIONS NECESSARY TO SOLVE THE SHOCK-FRONT
CC    DIFFERENTIAL EQUATION ALONG THE CURVED SHOCK.
C
      GR(1)=C.
      GI(1)=C.
      P1R(1)=-1.4*XM*XM*(U12R(1,1)-XXK*F2I(1,1))
      P1I(1)=-1.4*XM*XM*(U12I(1,1)+XXK*F2R(1,1))
      U1=-FM1(GAM(1))*(COS(FFAZE)+XXK*XROT*SIN(FFAZE))/FN1(GAM(1))
      L2=(FM3(GAM(1))*FN1(GAM(1))-FM1(GAM(1))*FM4(GAM(1)))/FN1(GAM(1))
      L3=(FM4(GAM(1))*FN1(GAM(1))-FM1(GAM(1))*FN4(GAM(1)))/FN1(GAM(1))
      U4=-FM1(GAM(1))*(SIN(FFAZE)-XXK*XROT*COS(FFAZE))/FN1(GAM(1))
      URJ(1)=   U1+U2*U12R(1,1)+U3*V12R(1,1)
      UIJ(1)=   U4+U2*U12I(1,1)+L3*V12I(1,1)
      VRJ(1)=V11R(M3,M4)
      VIJ(1)=V11I(M3,M4)
      U1=-FP1(GAM(1))*(COS(FFAZE)+XXK*XROT*SIN(FFAZE))/FN1(GAM(1))
      L2=(FP3(GAM(1))*FN1(GAM(1))-FP1(GAM(1))*FM4(GAM(1)))/FN1(GAM(1))
      L3=(FP4(GAM(1))*FN1(GAM(1))-FP1(GAM(1))*FN4(GAM(1)))/FN1(GAM(1))
      U4=-FP1(GAM(1))*(SIN(FFAZE)-XXK*XROT*COS(FFAZE))/FN1(GAM(1))
      P2R(1)=P1R(1)+U1+U2*L12R(1,1)+U3*V12R(1,1)
      P2I(1)=P1I(1)+U4+L2*L12I(1,1)+L3*V12I(1,1)
      FRJ(1)=-(UIJ(1)+P2I(1)/(1.4*XM*XM))/XXK
      FIJ(1)=  (URJ(1)+P2R(1)/(1.4*XM*XM))/XXK
C
CC    SOLVING THE SIMULTANEOUS JUMP-CONDITION EQUATIONS.
C
      DO 170 I=2,KSHOK
      DO 165 J=1,64
      COB(J)=C.C
165   CONTINUE
      I1=I-1
      DX=X2(1,I)-XA1(I1)
      DY=(Y2(1,I)-Y2(1,I1))/2.
      DL=DSQRT(XL2(1,I))+DSQRT(XL2(1,I1))
      A1=2./DL
      A2=4.*XXK*XM*XM*DX/(XL2(1,I)+XL2(1,I1))
      A3=XXK*A2/2.
      G=(GAM(I)+GAM(I1))/2.
167   COB(1)=1.
```

```
      CC8(2)=A2/2.
      CC8(3)=1.
      CC8(7)=-1.4*XM*XM
      CC8(9)=-CC8(2)
      CC8(10)=1.
      CC8(12)=1.
      CC8(16)=CC8(7)
      CC8(17)=A1
      CC8(21)=1.
      CC8(26)=A1
      CC8(30)=1.
      CC8(33)=-A3/2.
      CC8(40)=CC8(7)*XXK
      CC8(42)=CC8(33)
      CC8(47)=-CC8(40)
      CC8(51)=-FM1(G)/DY
      CC8(52)=-FM2(G)
      CC8(53)=-FN1(G)/DY
      CC8(54)=-FN2(G)
      CC8(55)=-FP1(G)/DY
      CC8(56)=-FP2(G)
      CC8(59)= FM2(G)
      CC8(60)=CC8(51)
      CC8(61)= FN2(G)
      CC8(62)=CC8(53)
      CC8(63)= FP2(G)
      CC8(64)=CC8(55)
      RUR=U12R(1,I)+U12R(1,I1)
      RUI=U12I(1,I)+U12I(1,I1)
      RVR=V12R(1,I)+V12R(1,I1)
      RVI=V12I(1,I)+V12I(1,I1)
      RFR=F2R(1,I)+F2R(1,I1)
      RFI=F2I(1,I)+F2I(1,I1)
      RHS8(1)=URJ(I1)+A2*UIJ(I1)/2.+A1*VRJ(I1)+A3*FRJ(I1)/2.
      RHS8(2)=UIJ(I1)-A2*URJ(I1)/2.+A1*VIJ(I1)+A3*FIJ(I1)/2.
      RHS8(3)=FM3(G)*RUR+FM4(G)*RVR-URJ(I1)-FM1(G)*GR(I1)/DY-FM2(G)*GI(I
     11)
      RHS8(4)=FM3(G)*RUI+FM4(G)*RVI-UIJ(I1)-FM1(G)*GI(I1)/DY+FM2(G)*GR(I
     11)
      RHS8(5)=FM4(G)*RUR+FN4(G)*RVR-VRJ(I1)-FN1(G)*GR(I1)/DY-FN2(G)*GI(I
     11)
      RHS8(6)=FM4(G)*RUI+FN4(G)*RVI-VIJ(I1)-FN1(G)*GI(I1)/DY+FN2(G)*GR(I
     11)
      RHS8(7)=(FP3(G)+CC8(7))*RUR+FP4(G)*RVR+CC8(47)*RFI-CC8(7)*URJ(I1)
     1-CC8(47)*FIJ(I1)-FP1(G)*GR(I1)/DY-FP2(G)*GI(I1)
      RHS8(8)=(FP3(G)+CC8(7))*RUI+FP4(G)*RVI-CC8(47)*RFR-CC8(7)*UIJ(I1)
     1+CC8(47)*FRJ(I1)-FP1(G)*GI(I1)/DY+FP2(G)*GR(I1)
168   CALL SIMQ(CC8,RHS8,8,KS)
```

```
      IF (KS.EC.1) GO TC 10000
      URJ(I)=RHSE(1)
      UIJ(I)=RHS8(2)
      VRJ(I)=RHSE(3)
      VIJ(I)=RHSE(4)
      FRJ(I)=RHS8(5)
      FIJ(I)=RHSE(6)
      GR(I)=RHSE(7)
      GI(I)=RHSE(8)
170   CONTINUE
C
C     STORING COMPUTED JUMP VALUES.
C
      DO 180 I=2,KSHOK
      U12R(1,I)=URJ(I)
      U12I(1,I)=UIJ(I)
      V12R(1,I)=VRJ(I)
      V12I(1,I)=VIJ(I)
      F2R(1,I)=FRJ(I)
      F2I(1,I)=FIJ(I)
180   CONTINUE
C
C  COMPUTING THE UNSTEADY VELOCITIES ALONG THE CURVED MESH.
C
C
C     APPLYING THE LINEAR BOUNDARY CONDITION ALONG THE LOWER SURFACE OF
C     THE SECOND BLADE
C
      DO 210 I=1,KSHOK
      I1=N+I
      J1=M4-1+I
      V12R(I,I)=V11R(I1,J1)
      V12I(I,I)=V11I(I1,J1)
210   CONTINUE
C
C     COMPUTING U,V, AND PHI AT THE CURVED-MESH FIELD POINTS.
C
      A1=2.*XXK*XM*XM
      A2=XXK*A1/2.
      KSHOK1=KSHOK-1
      DO 220 J=2,KSHOK1
      J1=J-1
      J2=J+1
      DO 220 I=2,J
      I1=I-1
      DXA=X2(I,J)-X2(I1,J)
      XLA=.5*(XL2(I,J)+XL2(I1,J))
      DLXB=(XL2(I,J2)-XL2(I,J))/(X2(I,J2)-X2(I,J))
```

```
      SLA=.5*(DSQRT(XL2(I,J))+DSQRT(XL2(I1,J)))
      IF(I.NE.J) GO TO 1200
      VAR=.5*(V12R(I,J)+V12R(I1,J))
      DVAR=V12R(I,J)-V12R(I1,J)
      VAI=.5*(V12I(I,J)+V12I(I1,J))
      DVAI=V12I(I,J)-V12I(I1,J)
      CO2(1)=1.+DLXB*DXA/(4.*XLA)-A2*DXA*DXA/(2.*XLA)
      CO25  =1.-DLXB*DXA/(4.*XLA)+A2*DXA*DXA/(2.*XLA)
      CO2(2)=A1*DXA/(2.*XLA)
      CO27  =A2*DXA/XLA
      CO26=DVAR/SLA+VAR*CO27*DXA/SLA
      CO28=DVAI/SLA+VAI*CO27*DXA/SLA
      CO2(3)=-CO2(2)
      CO2(4)= CO2(1)
      RHS2(1)=U12R(I1,J)*CO25+U12I(I1,J)*CO2(2)+    CO26    +F2R(I1,J)*
     1CO27
      RHS2(2)=U12I(I1,J)*CO25-U12R(I1,J)*CO2(2)+    CO28    +F2I(I1,J)*
     1CO27
      CALL SIMQ(CO2,RHS2,2,KS)
      IF(KS.EQ.1) GO TO 10000
      U12R(I,J)=RHS2(1)
      U12I(I,J)=RHS2(2)
      F2R(I,J)=F2R(I1,J)+(.5*(U12R(I,J)+U12R(I1,J))+VAR/SLA)*DXA
      F2I(I,J)=F2I(I1,J)+(.5*(U12I(I,J)+U12I(I1,J))+VAI/SLA)*DXA
      GO TO 220
1200  DXB=X2(I,J)-X2(I,J1)
      XLB=.5*(XL2(I,J)+XL2(I,J1))
      DLB=XL2(I,J)-XL2(I,J1)
      SLB=.5*(DSQRT(XL2(I,J))+DSQRT(XL2(I,J1)))
      CO4(1)=1.+DLXB*DXA/(4.*XLA)-A2*DXA*DXA/(2.*XLA)
      CO41  =1.-DLXB*DXA/(4.*XLA)+A2*DXA*DXA/(2.*XLA)
      CO4(2)=A1*DXA/(2.*XLA)
      CO43  =A2*DXA/XLA
      CO42  =(-1.+CO43*DXA/2.)/SLA
      CO4(3)=1.+DLB/(4.*XLB)-A2*DXB*DXB/(2.*XLB)
      CO44  =1.-DLB/(4.*XLB)+A2*DXB*DXB/(2.*XLB)
      CO4(4)=A1*DXB/(2.*XLB)
      CO46  =A2*DXB/XLB
      CO45  =(1.-CO46*DXB/2.)/SLB
      CO4(5)=-CO4(2)
      CO4(6)= CO4(1)
      CO4(7)=-CO4(4)
      CO4(8)= CO4(3)
      CO4(9)=-(1.+A2*DXA*DXA/(2.*XLA))/SLA
      CO4(10)=0.
      CO4(11)=(1.+A2*DXB*DXB/(2.*XLB))/SLB
      CO4(12)=0.
      CO4(13)=0.
```

```
      CO4(14)=CC4(9)
      CO4(15)=C.
      CO4(16)=CC4(11)
      RHS4(1)=U12R(I1,J)*CC41+U12I(I1,J)*CC4(2)+V12R(I1,J)*CO42+F2R(I1,J
     1)*CC43
      RHS4(2)=U12I(I1,J)*CC41-U12R(I1,J)*CC4(2)+V12I(I1,J)*CO42+F2I(I1,J
     1)*CO43
      RHS4(3)=U12R(I,J1)*CC44+U12I(I,J1)*CO4(4)+V12R(I,J1)*CO45+F2R(I,J1
     1)*CO46
      RHS4(4)=U12I(I,J1)*CO44-U12R(I,J1)*CC4(4)+V12I(I,J1)*CC45+F2I(I,J1
     1)*CO46
      CALL SIMQ(CO4,RHS4,4,KS)
      IF(KS.EC.1) GO TO 10000
      U12R(I,J)=RHS4(1)
      U12I(I,J)=RHS4(2)
      V12R(I,J)=RHS4(3)
      V12I(I,J)=RHS4(4)
      F2R(I,J)=.5*(F2R(I1,J)+F2R(I,J1))+.25*(U12R(I,J)+U12R(I1,J)+
     1(V12R(I,J)+V12R(I1,J))/SLA)*CXA  +.25*(U12R(I,J)+U12R(I,J1)-
     2(V12R(I,J)+V12R(I,J1))/SLB)*DXB
      F2I(I,J)=.5*(F2I(I1,J)+F2I(I,J1))+.25*(U12I(I,J)+U12I(I1,J)+
     1(V12I(I,J)+V12I(I1,J))/SLA)*CXA  +.25*(U12I(I,J)+U12I(I,J1)-
     2(V12I(I,J)+V12I(I,J1))/SLB)*DXB
220   CONTINUE
C
C  COMPUTING THE UNSTEADY PRESSURE DISTRIBUTIONS ALONG THE SECOND BLADE.
C
C
C     COMPUTING THE UNSTEADY PRESSURE ALONG THE UPPER SURFACE OF BLADE TWO.
C
      NN=21-N
      DO 230 I=1,NN
      I1=N+I
      J1=M4-1+I
      P1R(I)=-2.*(U11R(I1,J1)-XXK*F1I(I1,J1))
      P1I(I)=-2.*(U11I(I1,J1)+XXK*F1R(I1,J1))
      XA1(I)=X1(I1,J1)-X2(1,1)
230   CONTINUE
C
C     COMPUTING THE UNSTEADY PRESSURE ALONG THE LOWER SURFACE OF BLADE TWO.
C
      P2R(1)=2.*F2R(1)/(1.4*XM*XM)
      P2I(1)=2.*F2I(1)/(1.4*XM*XM)
      DO 240 I=2,KSHOK1
      P2R(I)=-2.*(U12R(I,I)-XXK*F2I(I,I))
      P2I(I)=-2.*(U12I(I,I)+XXK*F2R(I,I))
240   CONTINUE
C
```

```
C       COMPUTING THE AMPLITUDE AND PHASE OF THE UNSTEADY PRESSURE ON THE UPPER
C       SURFACE OF THE SECOND BLADE, RELATIVE TO BLADE TWO.
C
        WRITE(6,9000)
        WRITE(6,10500)
        WRITE(6,11000)
        DO 250 I=1,NN
        PR=P1R(I)
        PI=P1I(I)
        P1R(I)= PR*COS(FFAZE)+PI*SIN(FFAZE)
        P1I(I)=-PR*SIN(FFAZE)+PI*COS(FFAZE)
        AMP=SQRT(P1R(I)**2+P1I(I)**2)
        IF (P1R(I).GE.0.) GO TO 260
        XLAG=ATAN(P1I(I)/P1R(I))*57.3+180.
        GO TO 280
260     IF (P1I(I).GE.0.) GO TO 290
        XLAG=ATAN(P1I(I)/P1R(I))*57.3+360.
        GO TO 280
290     XLAG=ATAN(P1I(I)/P1R(I))*57.3
280     XLAG=XLAG+180.
        IF(XLAG.LE.360.) GO TO 360
        XLAG=XLAG-360.
360     WRITE(6,12000)XA1(I),P1R(I),P1I(I),AMP,XLAG
250     CONTINUE
C
C       COMPUTING THE AMPLITUDE AND PHASE OF THE UNSTEADY PRESSURE ON THE LOWER
C       SURFACE OF THE SECOND BLADE, RELATIVE TO BLADE TWO.
C
        WRITE(6,13000)
        WRITE(6,10500)
        WRITE(6,11000)
        DO 340 I=1,KSHOK1
        PR=P2R(I)
        PI=P2I(I)
        P2R(I)= PR*COS(FFAZE)+PI*SIN(FFAZE)
        P2I(I)=-PR*SIN(FFAZE)+PI*COS(FFAZE)
        AMP=SQRT(P2R(I)**2+P2I(I)**2)
        IF (P2R(I).GE.0.) GO TO 310
        XLAG=ATAN(P2I(I)/P2R(I))*57.3+180.
        GO TO 320
310     IF (P2I(I).GE.0.) GO TO 330
        XLAG=ATAN(P2I(I)/P2R(I))*57.3+360.
        GO TO 320
330     XLAG=ATAN(P2I(I)/P2R(I))*57.3
320     XLAG=XLAG+180.
        XXX=X2(I,1)-X2(1,1)
        IF(XLAG.LE.360.) GO TO 350
        XLAG=XLAG-360.
```

```
350   WRITE(6,12000)XXX,P2R(I),P2I(I),AMP,XLAG
340   CONTINUE
      GO TO 12
10001 FORMAT('0','SINGULARITY',2X,'(I,J)=',2(2X,I3))
10000 WRITE(6,10001)I,J
12    STOP
      END


C
C  FUNCTION FMU FINDS THE VALUE OF MU ON THE AIRFOIL SURFACE USING THE FLOW
C  TANGENCY CONDITION
C
      FUNCTION FMU(X)
      REAL*8 X2,Y2,XL2,XMU2
      COMMON X1(40,80),Y1(40,80),X2(40,40),Y2(40,40),XL2(40,40),XMU2(40,
     140),DPC(20),XM,T,XXK,XROT,N,K
      XX=X-X2(1,1)
      FMU=14.4*T*XM*XM*(2.0*XX-1.0)
      RETURN
      END


C
C  THE COEFFICIENT FUNCTIONS ARE USED IN DETERMINING THE JUMP CONDITIONS ACROSS
C  THE CURVED BOW SHOCK.
C

      FUNCTION FM1(X)
      FM1=-.833*SIN(2.*X)*(SIN(X))**2
      RETURN
      END


      FUNCTION FM2(X)
      COMMON X1(40,80),Y1(40,80),X2(40,40),Y2(40,40),XL2(40,40),XMU2(40,
     140),DPC(20),XM,T,XXK,XROT,N,K
      REAL*8 X2,Y2,XL2,XMU2
      Y=1./((XM*SIN(X))**2)
      FM2= .833*XK*(1.+Y)*(SIN(X))**2
      RETURN
      END
```

```
      FUNCTION FM3(X)
      COMMON X1(40,80),Y1(40,80),X2(40,40),Y2(40,40),XL2(40,40),XMU2(40,
     140),DPO(20),XM,T,XXK,XROT,N,K
      REAL*8 X2,Y2,XL2,XMU2
      Y=5./((XM*SIN(X))**2)
      FM3=(COS(X))**2 +.167*(1.-Y)*(SIN(X))**2
      RETURN
      END

      FUNCTION FM4(X)
      COMMON X1(40,80),Y1(40,80),X2(40,40),Y2(40,40),XL2(40,40),XMU2(40,
     140),DPO(20),XM,T,XXK,XROT,N,K
      REAL*8 X2,Y2,XL2,XMU2
      Y=5./((XM*SIN(X))**2)
      FM4=-.5*SIN(2.*X)+.0833*SIN(2.*X)*(1.-Y)
      RETURN
      END

      FUNCTION FN1(X)
      COMMON X1(40,80),Y1(40,80),X2(40,40),Y2(40,40),XL2(40,40),XMU2(40,
     140),DPO(20),XM,T,XXK,XROT,N,K
      REAL*8 X2,Y2,XL2,XMU2
      Y=1./((XM*SIN(X))**2)
      FN1=-.833*(COS(2.*X)+Y)*(SIN(X))**2
      RETURN
      END

      FUNCTION FN2(X)
      COMMON X1(40,80),Y1(40,80),X2(40,40),Y2(40,40),XL2(40,40),XMU2(40,
     140),DPO(20),XM,T,XXK,XROT,N,K
      REAL*8 X2,Y2,XL2,XMU2
      Y=1./((XM*SIN(X))**2)
      FN2= .833*XK*(1.+Y)*COS(X)*SIN(X)
      RETURN
      END

      FUNCTION FN4(X)
      COMMON X1(40,80),Y1(40,80),X2(40,40),Y2(40,40),XL2(40,40),XMU2(40,
     140),DPO(20),XM,T,XXK,XROT,N,K
      REAL*8 X2,Y2,XL2,XMU2
      Y=5./((XM*SIN(X))**2)
      FN4=SIN(X)**2.+.167*(1.-Y)*COS(X)**2
      RETURN
      END
```

```
C
CC  THE P COEFFICIENT FUNCTIONS ARE USED TO COMPUTE THE PRESSURE JUMP ACROSS
CC  THE SHOCK.
C

      FUNCTION FP1(X)
      COMMON X1(40,80),Y1(40,80),X2(40,40),Y2(40,40),XL2(40,40),XMU2(40,
     140),CPC(20),XM,T,XXK,XROT,N,K
      REAL*8 X2,Y2,XL2,XMU2
      XN=XM*SIN(X)
      FP1=1.167*XN*XN*SIN(2.*X)
      RETURN
      END

      FUNCTION FP2(X)
      COMMON X1(40,80),Y1(40,80),X2(40,40),Y2(40,40),XL2(40,40),XMU2(40,
     140),CPC(20),XM,T,XXK,XROT,N,K
      REAL*8 X2,Y2,XL2,XMU2
      XN=XM*SIN(X)
      FP2=-2.333*XN*XN*XXK
      RETURN
      END

      FUNCTION FP3(X)
      COMMON X1(40,80),Y1(40,80),X2(40,40),Y2(40,40),XL2(40,40),XMU2(40,
     140),CPC(20),XM,T,XXK,XROT,N,K
      REAL*8 X2,Y2,XL2,XMU2
      XN=XM*SIN(X)
      FP3=2.333*XN*XN
      RETURN
      END

      FUNCTION FP4(X)
      COMMON X1(40,80),Y1(40,80),X2(40,40),Y2(40,40),XL2(40,40),XMU2(40,
     140),CPC(20),XM,T,XXK,XROT,N,K
      REAL*8 X2,Y2,XL2,XMU2
      XN=XM*SIN(X)
      FP4=2.333*XN*XN/TAN(X)
      RETURN
      END
```

```
C
C  SUBROUTINE SOLVE FINDS THE POINT OF INTERSECTION OF TWO STRAIGHT LINES
C
      SUBROUTINE SOLVE(X1,Y1,XM1,X2,Y2,XM2,X,Y)
      XM12=XM1-XM2
      X=(Y2-XM2*X2-Y1+XM1*X1)/XM12
      Y=(XM1*(Y2-XM2*X2)-XM2*(Y1-XM1*X1))/XM12
      RETURN
      END



C
C  SUBROUTINE ITER SOLVES FOR X,Y, LAMDA, AND MU ON THE SURFACE OF THE CURVED
C  BLADE THROUGH ITERATION.
C
      SUBROUTINE ITER(I)
      REAL*8 X2,Y2,XL2,XMU2
      COMMON X1(40,80),Y1(40,80),X2(40,40),Y2(40,40),XL2(40,40),XMU2(40,
     140),CPC(20),XM,T,XXK,XROT,N,K
      EXTERNAL FMU
      J=I-1
      STEP=X2(J,J)
      Y2(I,I)=Y2(J,J)
10    STEP=STEP+.001
      XMU2(I,I)=FMU(STEP)
      XX=DABS(XL2(J,I)**1.5-XMU2(J,I)+XMU2(I,I))
      XL2(I,I)=XX**.66667
      X2(I,I)=(Y2(I,I)-Y2(J,I))*(DSQRT(XL2(J,I))+DSQRT(XL2(I,I)))/2.0+X2
     1(J,I)
      SSTEP=STEP-X2(J,J)
      IF(SSTEP-.3) 20,30,30
20    DIFF=DABS(X2(I,I)-STEP)
      IF (DIFF-.001) 40,40,10
100   FORMAT('0',5X,'ITERATION DID NOT CONVERGE; I= ',2X,I4)
30    WRITE(6,100)I
40    RETURN
      END



C
```

```
C SUBROUTINE SHOKPT SOLVES FOR THE SHOCK FRONT POINTS THROUGH ITERATION.
C
      SUBROUTINE SHOKPT(I,XA,D1)
      REAL*8 X2,Y2,XL2,XMU2
      COMMON X1(40,80),Y1(40,80),X2(40,40),Y2(40,40),XL2(40,40),XMU2(40,
     140),DPC(20),XM,T,XXK,XRCT,N,K
      EXTERNAL FML
      L=0
      J=I-1
      YA=Y2(J,1)
      XLINF=XM*XM-1.0
      XL2(1,I)=XL2(1,J)
10    XL2(1,I)=XL2(1,I)+.001
      L=L+1
      XMU2(1,I)=XL2(1,I)**1.5-XL2(2,2)**1.5+XMU2(2,2)
      D1=-4.0/(2.0*SQRT(XLINF)+DSQRT(XL2(1,I))+DSQRT(XL2(1,J)))
      D2=-1.0/DSQRT(XL2(1,I))
      CALL SOLVE(X2(1,J),Y2(1,J),D1,XA,YA,D2,X2(1,I),Y2(1,I))
      XMUA=FML(XA)
      DIFF=DABS(XMU2(1,I)-XMUA)
      IF (DIFF-.002) 20,20,30
30    IF(L.EQ.500) GO TO 40
      GO TO 10
1000  FORMAT('0','SHOKPT DID NOT CONVERGE, ISHOK=',2X,I4)
40    WRITE(6,1000)I
20    RETURN
      END
```

150

```
C
C SUBROUTINE SIMQ IS A LINEAR EQUATION SOLUTION ROUTINE.
C
      SUBROUTINE SIMQ(A,B,N,KS)                                          SIMQ  490
      DIMENSION A(1),B(1)                                                SIMQ  500
C                                                                        SIMQ  510
C        FORWARD SOLUTION                                                SIMQ  520
C                                                                        SIMQ  530
      TOL=0.0                                                            SIMQ  540
      KS=0                                                               SIMQ  550
      JJ=-N                                                              SIMQ  560
      DO 65 J=1,N                                                        SIMQ  570
      JY=J+1                                                             SIMQ  580
      JJ=JJ+N+1                                                          SIMQ  590
      BIGA=0                                                             SIMQ  600
      IT=JJ-J                                                            SIMQ  610
      DO 30 I=J,N                                                        SIMQ  620
```

```
C
CC          SEARCH FOR MAXIMUM COEFFICIENT IN COLUMN
C
      IJ=IT+I
      IF(ABS(BIGA)-ABS(A(IJ))) 20,30,30
   20 BIGA=A(IJ)
      IMAX=I
   30 CONTINUE
C
CC          TEST FOR PIVOT LESS THAN TOLERANCE (SINGULAR MATRIX)
C
      IF(ABS(BIGA)-TOL) 35,35,40
   35 KS=1
      RETURN
C
CC          INTERCHANGE ROWS IF NECESSARY
C
   40 I1=J+N*(J-2)
      IT=IMAX-J
      DO 50 K=J,N
      I1=I1+N
      I2=I1+IT
      SAVE=A(I1)
      A(I1)=A(I2)
      A(I2)=SAVE
C
CC          DIVIDE EQUATION BY LEADING COEFFICIENT
C
   50 A(I1)=A(I1)/BIGA
      SAVE=B(IMAX)
      B(IMAX)=B(J)
      B(J)=SAVE/BIGA
C
CC          ELIMINATE NEXT VARIABLE
C
      IF(J-N) 55,70,55
   55 IQS=N*(J-1)
      DO 65 IX=JY,N
      IXJ=IQS+IX
      IT=J-IX
      DO 60 JX=JY,N
      IXJX=N*(JX-1)+IX
      JJX=IXJX+IT
   60 A(IXJX)=A(IXJX)-(A(IXJ)*A(JJX))
   65 B(IX)=B(IX)-(B(J)*A(IXJ))
C
CC          BACK SOLUTION
C
```

```
SIMQ  630
SIMQ  640
SIMQ  650
SIMQ  660
SIMQ  670
SIMQ  680
SIMQ  690
SIMQ  700
SIMQ  710
SIMQ  720
SIMQ  730
SIMQ  740
SIMQ  750
SIMQ  760
SIMQ  770
SIMQ  780
SIMQ  790
SIMQ  800
SIMQ  810
SIMQ  820
SIMQ  830
SIMQ  840
SIMQ  850
SIMQ  860
SIMQ  870
SIMQ  880
SIMQ  890
SIMQ  900
SIMQ  910
SIMQ  920
SIMQ  930
SIMQ  940
SIMQ  950
SIMQ  960
SIMQ  970
SIMQ  980
SIMQ  990
SIMQ1000
SIMQ1010
SIMQ1020
SIMQ1030
SIMQ1040
SIMQ1050
SIMQ1060
SIMQ1070
SIMQ1080
SIMQ1090
SIMQ1100
```

```
 70 NY=N-1                                                      SIMQ1110
    IT=N*N                                                      SIMQ1120
    DO 80 J=1,NY                                                SIMC1130
    IA=IT-J                                                     SIMQ1140
    IB=N-J                                                      SIMC1150
    IC=N                                                        SIMC1160
    DO 80 K=1,J                                                 SIMQ1170
    B(IB)=B(IB)-A(IA)*B(IC)                                     SIMC1180
    IA=IA-N                                                     SIMQ1190
 80 IC=IC-1                                                     SIMQ1200
    RETURN                                                      SIMC1210
    END                                                         SIMQ1220
```

LIST OF REFERENCES

1. Sisto, F., "A Review of the Fluid Mechanics of Aero-elasticity in Turbomachines," Transactions of the ASME, p. 40-44, March 1977.

2. Snyder, L.E. and Commerford, G.L., "Supersonic Unstalled Flutter in Fan Rotors; Analytical and Experimental Results," Journal of Engineering for Power, v. 96, no. 4, p. 379-386, October 1974.

3. Platzer, M.F., "Transonic Blade Flutter — A Survey," The Shock and Vibration Digest, v. 7, no. 7, p. 97, July 1975.

4. Kurosaka, M., "Some Recent Developments in Unsteady Aerodynamics of a Supersonic Cascade," Revue Francaise de Mecanique, Numero Special, p. 57-64, October 1976.

5. Chadwick, W.R., Unsteady Supersonic Cascade Theory Including Nonlinear Thickness Effects, Ph.D. Thesis, Naval Postgraduate School, Monterey, Ca., 1975.

6. Kurosaka, M., "On the Unsteady Supersonic Cascade with a Subsonic Leading Edge — An Exact First-Order Theory — Parts 1 and 2," Journal of Engineering for Power, Series A, v. 96, p. 13-31, January 1974.

7. Miles, J.W., The Potential Theory of Unsteady Flow, p. 49-53, Cambridge University Press, 1959.

8. Miles, J.W., "The Compressible Flow Past an Oscillating Airfoil in a Wind Tunnel", Journal of Aeronautical Sciences, v. 23, p. 671-678, July 1956.

9. Lane, F., "Supersonic Flow Past an Oscillating Cascade with Supersonic Leading Edge Locus," Journal of Aeronautical Sciences, v. 24, p. 65-66, June 1957.

10. Chalkley, H.G., A Study of Supersonic Flow Past Vibrating Panels and Shells, Aeronautical Engineer's Thesis, Naval Postgraduate School, Monterey, CA, 1972.

11. Verdon, J.M. and McCune, J.E., "Unsteady Supersonic Cascade in Subsonic Axial Flow," AIAA Journal, v. 13, no. 2, p. 193-201, February 1975.

12. Verdon, J.M., "Further Developments in the Aerodynamic Analysis of Unsteady Supersonic Cascades, Parts 1 and 2," ASME Papers 77-GT-44 and 77-GT-45, December 1976.

13. Nagashima, T. and Whitehead, D.S., "Aerodynamic Forces and Moments for Vibrating Supersonic Cascade Blades," University of Cambridge Department of Engineering Report CUED/A – TURBO/TR59, 1974.

14. Goldstein, M.E., "Cascade with Supersonic Leading-Edge Locus," AIAA Journal, v. 13, no. 8, p. 1117-1118, August 1975.

15. Kurosaka, M., "On the Issue of Resonance in an Unsteady Supersonic Cascade," AIAA Journal, v. 13, no. 11, p. 1514-1516, November 1975.

16. Brix, C.W., A Study of Supersonic Flow Past Vibrating Shells and Cascades, Aeronautical Engineer's Thesis, Naval Postgraduate School, Monterey, Ca., 1973.

17. Bell, J.K., Theoretical Investigation of the Flutter Characteristics of Supersonic Cascades with Subsonic Leading-Edge Locus, Aeronautical Engineer's Thesis, Naval Postgraduate School, Monterey, CA., 1975.

18. Sauer, R., "Elementare Theorie des langsam schwingenden Uberschallflugels," ZAMP, p. 248-253, 1950.

19. Adamczyk, J.J., Verbal and Written Communications with LCDR J.A. Strada, USN of May 1977.

20. Carrier, G.F., "The Oscillating Wedge in a Supersonic Stream," Journal of Aeronautical Sciences, v. 16, no. 3, p. 150-152, March 1949.

21. Van Dyke, M.D., "Supersonic Flow Past Oscillating Aerofoils Including Nonlinear Thickness Effects," NACA Technical Note 2982, July 1953.

22. Van Dyke, M.D., "On Supersonic Flow Past an Oscillating Wedge," Quarterly of Applied Mathematics, v. 11, no. 3, p. 360-363, October 1953.

23. Teipel, I., "Die Berechnung instationarer Luftkrafte im schallnahen Bereich," Journal de Mecanique, v. 4, no. 3, p. 335-360, September 1965.

24. Teipel, I., "Die Kopfwelle an einem schwingenden Profil," DVL no. 65-30, July 1965.

25. Fleeter, S. and Riffel, R.E., "An Experimental Investigation of the Unsteady Aerodynamics of a Controlled Oscillating MCA Airfoil Cascade," Detroit Diesel Allison EDR 9028, December 1976.

26. Landahl, M.T., Unsteady Transonic Flow, p. 110-113, Pergamon Press, 1961.

27. Liepmann, H.W. and Roshko, A., Elements of Gas Dynamics, p. 110, Wiley, 1967.

28. Samoylovich, G.S., "Unsteady Flow Around and Aeroelastic Vibration in Turbomachine Cascades," U.S. Dept. of Commerce Foreign Technology Division AD 721 959, Wright-Patterson AFB, Ohio, 23 February 1971.

29. Owczarek, J.A., Fundamentals of Gas Dynamics, p. 370, International Textbook Company, 1968.

30. Ferri, A., Elements of Aerodynamics of Supersonic Flows, p. 126-127, MacMillan, 1949.

INITIAL DISTRIBUTION LIST

		No. Copies
1.	Defense Documentation Center Cameron Station Alexandria, Virginia 22314	2
2.	Library, Code 0142 Naval Postgraduate School Monterey, California 93940	2
3.	Department Chairman, Code 67 Department of Aeronautics Naval Postgraduate School Monterey, California 93940	1
4.	Professor M. F. Platzer, Code 67P1 Department of Aeronautics Naval Postgraduate School Monterey, California 93940	15
5.	Professor D. J. Collins, Code 67Co Department of Aeronautics Naval Postgraduate School Monterey, California 93940	1
6.	Professor L. V. Schmidt, Code 67Sx Department of Aeronautics Naval Postgraduate School Monterey, California 93940	1
7.	Distinguished Professor F. D. Faulkner Department of Mathematics, Code 53Fa Naval Postgraduate School Monterey, California 93940	1
8.	Distinguished Professor A. E. Fuhs, Code 69 Department of Mechanical Engineering Naval Postgraduate School Monterey, California 93940	1
9.	Dr. H. J. Mueller, Code AIR-310 Naval Air Systems Command Washington, D.C. 20360	1
10.	Dr. John J. Adamczyk Compressor Branch NASA Lewis Research Center Cleveland, Ohio 44135	1

No. Copies

11. Dr. S. Fleeter — 1
Supervisor, Cascade and Flow Systems
Detroit Diesel Allison
Division of General Motors Corporation
Indianapolis, Indiana 46206

12. LCDR Josephy Anthony Strada, USN — 2
SAMSO/YEUP, P.O. Box 92960
Worldway Postal Center
Los Angeles, California 90009